Defense Nuclear Agency
Alexandria, VA 22310-3398

DNA-TR-90-9

# Propagation of RF Signals Through Structured Ionization
## The General Model

Roger A. Dana
Mission Research Corporation
P.O. Drawer 719
Santa Barbara, CA 93102-0719

March 1991

Technical Report

CONTRACT No. DNA 001-87-C-0169

Destroy this report when it is no longer needed. Do not return to sender.

PLEASE NOTIFY THE DEFENSE NUCLEAR AGENCY, ATTN: CSTI, 6801 TELEGRAPH ROAD, ALEXANDRIA, VA 22310-3398, IF YOUR ADDRESS IS INCORRECT, IF YOU WISH IT DELETED FROM THE DISTRIBUTION LIST, OR IF THE ADDRESSEE IS NO LONGER EMPLOYED BY YOUR ORGANIZATION.

# DISTRIBUTION LIST UPDATE

This mailer is provided to enable DNA to maintain current distribution lists for reports. We would appreciate your providing the requested information.

- ☐ Add the individual listed to your distribution list.
- ☐ Delete the cited organization/individual.
- ☐ Change of address.

*NOTE:*
*Please return the mailing label from the document so that any additions, changes, corrections or deletions can be made more easily.*

NAME: _____

ORGANIZATION: _____

| OLD ADDRESS | CURRENT ADDRESS |
|---|---|
| _____ | _____ |
| _____ | _____ |
| _____ | _____ |

TELEPHONE NUMBER: (___) _____

SUBJECT AREA(s) OF INTEREST:

_____

_____

_____

DNA OR OTHER GOVERNMENT CONTRACT NUMBER: _____

CERTIFICATION OF NEED-TO-KNOW BY GOVERNMENT SPONSOR (if other than DNA):

SPONSORING ORGANIZATION: _____

CONTRACTING OFFICER OR REPRESENTATIVE: _____

SIGNATURE: _____

CUT HERE AND RETURN

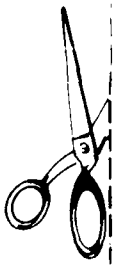

Director
Defense Nuclear Agency
ATTN: TITL
Washington, DC 20305-1000

Director
Defense Nuclear Agency
ATTN: TITL
Washington, DC 20305-1000

# REPORT DOCUMENTATION PAGE

*Form Approved*
*OMB No. 0704.0188*



| 1. AGENCY USE ONLY *(Leave blank)* | 2. REPORT DATE | 3. REPORT TYPE AND DATES COVERED |
|---|---|---|
| | 910301 | Technical 890101 - 891231 |

**4. TITLE AND SUBTITLE**
Propagation of RF Signals Through Structured Ionization
The General Model

**5. FUNDING NUMBERS**
C - DNA 001-87-C-0169
PE - 62715H
PR - RB
TA - RB
WU - DH039580

**6. AUTHOR(s)**
Roger A. Dana

**7. PERFORMING ORGANIZATION NAME(S) AND ADDRESS(ES)**
Mission Research Corporation
P.O. Drawer 719
Santa Barbara, CA 93102-0719

**8. PERFORMING ORGANIZATION REPORT NUMBER**
MRC-R-1262R

**9. SPONSORING/MONITORING AGENCY NAME(S) AND ADDRESS(ES)**
Defense Nuclear Agency
6801 Telegraph Road
Alexandria, VA 22310-3398
RAAE/Ullrich

**10. SPONSORING/MONITORING AGENCY REPORT NUMBER**
DNA-TR-90-9

**11. SUPPLEMENTARY NOTES**
This work was sponsored by the Defense Nuclear Agency under RDT&E RMC codes B4662D RB RB OP140 RAAE 3200E 25904D, B4662D RB RB EA104 RAAE 3200A 25904D, B4662D RB RB 00140 RAAE 3220A 25904D.

**12a. DISTRIBUTION/AVAILABILITY STATEMENT**
Approved for public release; distribution is unlimited.

**12b. DISTRIBUTION CODE**

**13. ABSTRACT** *(Maximum 200 words)*

Design and evaluation of radio frequency (RF) systems that must operate through ionospheric disturbances requires an accurate channel model. Such a model can be used to construct realizations of the received signal for use in digital simulations of transionospheric communications links and radars or hardware channel simulators. This report presents a review of RF propagation through structured ionization, starting with Maxwell's equations and ending with the two-position, two-frequency, two-time mutual coherence function of the received signal. The derivation of the mutual coherence function requires a model for the temporal and spatial variations of the electron density fluctuations in the ionosphere. Under Taylor's frozen-in hypothesis, the electron density fluctuations are described as a rigid structure that drifts past the line-of-sight. In the fully turbulent case, the spatial and temporal fluctuations of the electron density are uncorrelated. Reality should lie somewhere between these two limiting models. A new general model which varies smoothly between the frozen-in and turbulent models is presented in this report, and an efficient channel simulation technique for the general model is described. Examples are given which illustrate the effects on the received signal of the variation from the turbulent to frozen-in models, and the effects of antennas with arbitrary sizes and pointing angles.

| 14. SUBJECT TERMS | | 15. NUMBER OF PAGES |
|---|---|---|
| Scintillation | Ionospheric RF Propagation | 110 |
| Antennas | Channel Model | 16. PRICE CODE |

| 17. Security CLASSIFICATION OF REPORT | 18. Security CLASSIFICATION OF THIS PAGE | 19. Security CLASSIFICATION OF ABSTRACT | 20. LIMITATION OF ABSTRACT |
|---|---|---|---|
| UNCLASSIFIED | UNCLASSIFIED | UNCLASSIFIED | SAR |

NSN 7540-01-280-5500

Standard Form 298 (Rev. 2-89)
Prescribed by ANSI Std. 239-18
298-102

CLASSIFIED BY:
N/A Since Unclassified

DECLASSIFY ON:
N/A Since Unclassified

## PREFACE

The author is indebted to Dr. Leon A. Wittwer of the Defense Nuclear Agency and to Dr. Scott Frasier of Mission Research Corporation for many helpful discussions regarding this work. Special thanks go to Allen H. Michelet of MRC and Major Lee W. Schrock of DNA, who assisted in reviewing and proofreading this report.

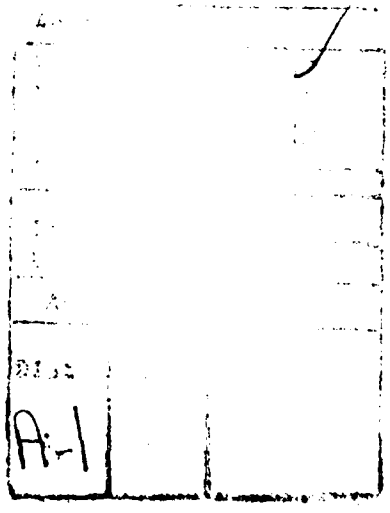

## CONVERSION TABLE

Conversion factors for U.S. Customary to metric (SI) units of measurement

| MULTIPLY → | BY → | TO GET |
|---|---|---|
| TO GET ← | BY ← | DIVIDE |

| | | |
|---|---|---|
| angstrom | 1.000000 x E -10 | meters (m) |
| atmosphere (normal) | 1.01325 x E +2 | kilo pascal (kPa) |
| bar | 1.000000 x E +2 | kilo pascal (kPa) |
| barn | 1.000000 x E -28 | meter$^2$ (m$^2$) |
| British thermal unit (thermochemical) | 1.054350 x E +3 | joule (J) |
| calorie (thermochemical) | 4.184000 | joule (J) |
| cal (thermochemical) / cm$^2$ | 4.184000 x E -2 | mega joule/m$^2$ (MJ/m$^2$) |
| curie | 3.700000 x E +1 | *giga becquerel (GBq) |
| degree (angle) | 1.745329 x E -2 | radian (rad) |
| degree Farenheit | $t_K = (t_F + 459.67)/1.8$ | degree kelvin (K) |
| electron volt | 1.60219 x E -19 | joule (J) |
| erg | 1.000000 x E -7 | joule (J) |
| erg/second | 1.000000 x E -7 | watt (W) |
| foot | 3.048000 x E -1 | meter (m) |
| foot-pound-force | 1.355818 | joule (J) |
| gallon (U.S. liquid) | 3.785412 x E -3 | meter$^3$ (m$^3$) |
| inch | 2.540000 x E -2 | meter (m) |
| jerk | 1.000000 x E +9 | joule (J) |
| joule/kilogram (J/kg) (radiation dose absorbed) | 1.000000 | Gray (Gy) |
| kilotons | 4.183 | terajoules |
| kip (1000 lbf) | 4.448222 x E +3 | newton (N) |
| kip/inch$^2$ (ksi) | 6.894757 x E +3 | kilo pascal (kPa) |
| ktap | 1.000000 x E +2 | newton-second/m$^2$ (N-s/m$^2$) |
| micron | 1.000000 x E -6 | meter (m) |
| mil | 2.540000 x E -5 | meter (m) |
| mile (international) | 1.609344 x E +3 | meter (m) |
| ounce | 2.834952 x E -2 | kilogram (kg) |
| pound-force (lbs avoirdupois) | 4.448222 | newton (N) |
| pound-force inch | 1.129848 x E -1 | newton-meter (N m) |
| pound-force/inch | 1.751268 x E +2 | newton/meter (N/m) |
| pound-force/foot$^2$ | 4.788026 x E -2 | kilo pascal (kPa) |
| pound-force/inch$^2$ (psi) | 6.894757 | kilo pascal (kPa) |
| pound-mass (lbm avoirdupois) | 4.535924 x E -1 | kilogram (kg) |
| pound-mass-foot$^2$ (moment of inertia) | 4.214011 x E -2 | kilogram-meter$^2$ (kg m$^2$) |
| pound-mass/foot$^3$ | 1.601846 x E +1 | kilogram/meter$^3$ (kg/m$^3$) |
| rad (radiation dose absorbed) | 1.000000 x E -2 | **Gray (Gy) |
| roentgen | 2.579760 x E -4 | coulomb/kilogram (C/kg) |
| shake | 1.000000 x E -8 | second (s) |
| slug | 1.459390 x E +1 | kilogram (kg) |
| torr (mm Hg, 0° C) | 1.333220 x E -1 | kilo pascal (kPa) |

*The becquerel (Bq) is the SI unit of radioactivity; 1 Bq = 1 event/s.
**The Gray (Gy) is the SI unit of absorbed radiation.

# TABLE OF CONTENTS

## TABLE OF CONTENTS (Continued)

## TABLE OF CONTENTS (Continued)

# LIST OF ILLUSTRATIONS

# SECTION 1
# INTRODUCTION

Satellite communications systems that utilize transionospheric propagation links may be subject to severe performance degradation when the ionosphere is highly disturbed by high altitude nuclear explosions [*Arendt and Soicher* 1964; *King and Fleming* 1980] or by chemical releases [*Davis et al.* 1974; *Wolcott et al.* 1978]. During these events, the increased electron concentrations and the irregular structure of the ionization can lead to intense Rayleigh signal scintillation at the radio frequencies (RF) used for satellite communication links and space radars.

Under severe scintillation conditions, the signal incident at the receiver can vary randomly in amplitude, phase, time-of-arrival, and angle-of-arrival. If all frequency components of the signal vary essentially identically with time, the propagation channel is referred to as nonselective or flat fading. When the scintillations exhibit statistical decorrelation at different frequencies within the signal bandwidth, the channel is referred to as frequency selective. Frequency selective scintillations are therefore encountered when the signal bandwidth exceeds the frequency selective bandwidth of the channel. When the scintillations exhibit statistical decorrelation across the face of an aperture antenna, the channel may also be referred to as spatially selective. Spatially selective scintillations are therefore encountered when the antenna aperture size exceeds the decorrelation distance of the incident signal.

Under conditions where the signal is spatially selective, the antenna beamwidth is smaller than the angle-of-arrival fluctuations and the effect of the antenna is to attenuate the incident signal that is arriving at off-boresight angles. In the spatial domain, the incident electric field is somewhat decorrelated across the face of the antenna. The induced voltages in the antenna then do not add coherently as they would for an incident plane wave, resulting in a loss in the gain of the antenna. Because of this angular filtering or spatial selectivity, the second-order statistics of the signal at the output of the antenna will be different than those of the incident signal.

The effects of antennas on signals that have propagated through randomly ionized media have been reported by *Wittwer* [1982], *Knepp* [1985], and *Dana* [1986]. This report is an extension of the latter reference, and its purpose is to describe the general model for temporal fluctuations that has recently been developed by Dr. Leon A. Wittwer of the Defense Nuclear Agency. A review of the basic theory of RF propagation through random media is presented, and the channel simulation technique for the general model is described.

The starting point is the generalized power spectral density (GPSD). The first part of this report is a review of the derivation of the GPSD. The intent of this review is to give the reader an understanding of the underlying physics that are contained in the GPSD and an understanding of the assumptions used to calculate the GPSD. The first part of this review follows *Tatarskii* [1971, §64-65]. The discussion of the general model is new in this report.

The derivation of the GPSD starts with Maxwell's equations from which the parabolic wave equation is derived. The parabolic wave equation can be solved to give

the received electric field for a specific electron density distribution in the ionosphere. However, the electron density distribution is a random process so the received electric field is also a random process. The parabolic wave equation is therefore used to derive an equation for the two-position, two-frequency, two-time mutual coherence function of the electric field, $\Gamma(\delta\mathbf{r},\delta\omega,\delta t)$. The solution of the differential equation for $\Gamma$, which is also a solution of Maxwell's equations, then provides a description of the second-order statistics of the received electric field. The Fourier transform of the mutual coherence function is the GPSD of the received signal.

Once the GPSD is obtained for the general model, it is used to compute the mean power, decorrelation time, and frequency selective bandwidth of the signal out of anisotropic antennas with arbitrary pointing angles relative to the line-of-sight. These results are taken from *Frasier* [1988]. Several examples are given that illustrate the general model and the effects of antenna pointing.

In Section 4 an analytical/numerical technique is described that is used to generate realizations of the impulse response function of the signal after propagation through randomly ionized media and reception by multiple antennas. The statistical realizations of the signal at the outputs of multiple antennas are assumed to have Rayleigh amplitude statistics and are therefore valid under strong-scattering conditions. The spatial and frequency correlation properties of the realizations are given by the mutual coherence function. These realizations of the impulse response function are then used to construct the received signal and may be used to exercise simulations of transionospheric communications links or space radars.

# SECTION 2
# THEORY

The starting point for this discussion of the general model is the generalized power spectral density (GPSD). This section presents a review of the derivation of the GPSD and discusses the physics that are contained in this important function.

In deriving the GPSD, two key approximations are usually made about the spatial and temporal electron density fluctuations that cause the scattering in the ionosphere. The first of these is the delta-layer approximation which requires that the scattering occur in an infinitesimally thin layer normal to the line-of-sight. This approximation has been relaxed in the calculations of *Wittwer* [1982] and *Knepp* [1983] and has been found to result in small errors in the GPSD provided that the propagation parameters (frequency selective bandwidth, decorrelation time and decorrelation distance) that characterize the channel are properly specified. The delta-layer approximation is not, in general, adequate to calculate the propagation parameters.

The second approximation that is usually made is Taylor's frozen-in hypothesis which treats the ionization fluctuations or striations as rigid "frozen-in" structures that drift across the line-of-sight. Under this model there is strong coupling between the spatial and temporal variations of the random electric field that is incident at the plane of the receiver. *Wittwer* [1988] has recently proposed a "general model" that smoothly varies between the frozen-in model and a turbulent model where the temporal and spatial ionization fluctuations are uncorrelated. The GPSD for the general model will be calculated in this section.

An analytic solution is obtained in this section for the two-position, two-frequency, two-time mutual coherence function $\Gamma(\delta\mathbf{r},\delta\omega,\delta t)$ of the complex electric field incident on the plane of the receiving antenna. This solution is valid for arbitrary line-of-sight geometries relative to the ionization structures in the ionosphere that cause the scattering of the RF wave. The mutual coherence function then provides the basis for the antenna aperture effects calculations and for the statistical signal generation techniques discussed in subsequent sections of this report. The Fourier transform of the mutual coherence function is the GPSD of the received signal.

## 2.1 PARABOLIC WAVE EQUATION.

Consider a monochromatic spherical wave with an electric field $\mathbf{E}(\mathbf{r},\omega,t)$ which is a function of position $\mathbf{r}$, carrier radian frequency $\omega$, and time t. The wave originates from a transmitter located at $\mathbf{r} = (0,0,-z_t)$ and propagates in free space in the positive z direction until it is incident on an irregularly ionized layer which extends from $0 < z < L$ and is infinite in the x-y plane. After emerging from the layer at $z = L$, the wave propagates in free space to a receiver located at $\mathbf{r} = (0,0,z_r)$. This geometry is shown in Figure 1.

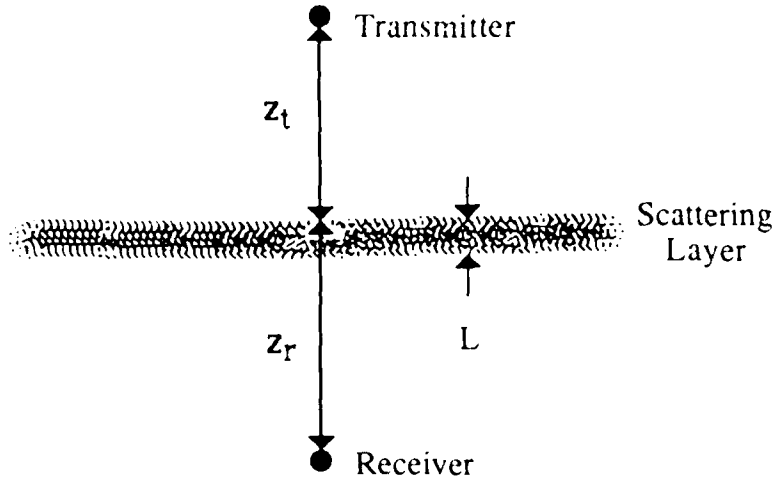


**Figure 1. Propagation geometry.**

The propagation of the wave is governed by Maxwell's equations:

$$\nabla \times \mathcal{E} + \frac{1}{c}\frac{\partial \mathcal{H}}{\partial t} = 0 \qquad \nabla \cdot \mathcal{E} = 0 \tag{1}$$

$$\nabla \times \mathcal{H} - \frac{\varepsilon}{c}\frac{\partial \mathcal{E}}{\partial t} = 0 \qquad \nabla \cdot \mathcal{H} = 0$$

where c is the speed of light in vacuum, $\mathcal{H}$ is the magnetic field, and $\varepsilon$ is the dielectric constant.

The dielectric constant of the propagation medium undergoes random fluctuations with a characteristic frequency which is assumed to be small when compared to the carrier frequency of the wave. With this assumption, the electric and magnetic fields may be written as the product of slowly-varying complex envelopes, denoted **E** and **H**, times exp(iωt):

$$\mathcal{E}(\mathbf{r},\omega,t) = \mathbf{E}(\mathbf{r},\omega,t)\, e^{i\omega t} \tag{2}$$

$$\mathcal{H}(\mathbf{r},\omega,t) = \mathbf{H}(\mathbf{r},\omega,t)\, e^{i\omega t} \ .$$

Inserting these into Maxwell's equations gives

$$\nabla \times \mathbf{E} + ik\mathbf{H} = 0 \tag{3a}$$

$$\nabla \times \mathbf{H} - i\varepsilon k\mathbf{E} = 0 \tag{3b}$$

where $k = \omega/c$ is the wave number of the carrier. After applying the curl operator to Equation 3a and substituting Equation 3b for the $\nabla \times \mathbf{H}$ term, the equation for $\mathbf{E}$ becomes

$$\nabla \times \nabla \times \mathbf{E} - \varepsilon k^2 \mathbf{E} = 0 \ . \tag{4}$$

The vector identity $\nabla \times \nabla \times \mathbf{E} = \nabla(\nabla \cdot \mathbf{E}) - \nabla^2 \mathbf{E}$ reduces the curl curl term in Equation 4 with the result

$$\nabla (\nabla \cdot \mathbf{E}) - \nabla^2 \mathbf{E} - \varepsilon k^2 \mathbf{E} = 0 \ . \tag{5}$$

The $\nabla \cdot \mathbf{E}$ term is reduced by expanding the divergence equation for $\mathbf{E}$:

$$\nabla \cdot \varepsilon \mathbf{E} = \varepsilon \nabla \cdot \mathbf{E} + \mathbf{E} \cdot \nabla \varepsilon = 0 \tag{6}$$

or

$$\nabla \cdot \mathbf{E} = - \mathbf{E} \cdot \nabla (\ln \varepsilon) \ . \tag{7}$$

The wave equation for the complex envelope of the electric field then becomes

$$\nabla^2 \mathbf{E} + \varepsilon k^2 \mathbf{E} + \nabla \left[ \mathbf{E} \cdot \nabla (\ln \varepsilon) \right] = 0 \ . \tag{8}$$

The dielectric constant $\varepsilon$ in a plasma at radio frequencies is given approximately by

$$\varepsilon = 1 - \frac{\omega_p^2}{\omega^2} \tag{9}$$

where the plasma frequency is

$$\omega_p^2 = 4\pi r_e c^2 n_e(\mathbf{r},t) \ . \tag{10}$$

The quantity $r_e$ is the classical electron radius ($r_e = 2.8179 \times 10^{-15}$ m) and $n_e(\mathbf{r},t)$ is the free electron density as a function of position and time. Equation 9 is valid when the carrier frequency is large compared to the plasma frequency. The free electron density is a random variable that will be represented as a mean value plus a random variation:

$$n_e(\mathbf{r},t) = \langle n_e \rangle + \Delta n_e(\mathbf{r},t) \ . \tag{11}$$

The electron density fluctuation $\Delta n_e(\mathbf{r},t)$ is assumed to be a zero mean random process. The term $\varepsilon k^2$ in the wave equation may now be rewritten as

$$\varepsilon k^2 = \langle k \rangle^2 (1 - \varepsilon_1) \tag{12}$$

where

$$\langle k \rangle^2 = \frac{\omega^2}{c^2}\left[1 - \frac{4\pi r_e c^2 \langle n_e \rangle}{\omega^2}\right] \tag{13}$$

and

$$\varepsilon_1 = \left[\frac{\Delta n_e(\mathbf{r},t)}{\langle n_e \rangle}\right]\left[\frac{\langle \omega_p^2 \rangle}{\omega^2 - \langle \omega_p^2 \rangle}\right] . \tag{14}$$

The quantity $\langle \omega_p^2 \rangle$ is the plasma frequency evaluated at the mean electron density.

The magnitude of the gradient term $\nabla(\ln \varepsilon)$ in the wave equation may be estimated as follows:

$$|\nabla(\ln \varepsilon)| = \left|\nabla\left\{\ln\left[1 - \frac{\omega_p^2}{\omega^2}\right]\right\}\right| \approx \frac{4\pi r_e \langle n_e \rangle c^2}{\omega^2}\left|\nabla\left[\frac{\Delta n_e}{\langle n_e \rangle}\right]\right| \approx \frac{\langle \omega_p^2 \rangle}{\omega^2}\frac{1}{L_0} \tag{15}$$

where $L_0$ is the scale size of the electron density fluctuations. As long as $L_0 >> \lambda$, where $\lambda$ is the RF wavelength, the term $\nabla[\mathbf{E}\cdot\nabla(\ln \varepsilon)]$ is small compared to $\varepsilon k^2 \mathbf{E}$ and may be ignored. The steps that follow are therefore only valid when the scale size of the electron density fluctuations is large compared to the carrier wavelength. With this restriction, the wave equation takes the Helmholtz form:

$$\nabla^2 \mathbf{E} + \langle k \rangle^2 (1 - \varepsilon_1)\, \mathbf{E} = 0 . \tag{16}$$

Now consider the complex components of the electric field and let

$$\mathbf{E}(\mathbf{r},\omega,t) = U(\mathbf{r},\omega,t) \exp\left[-\int \langle k(z') \rangle\, dz'\right] . \tag{17}$$

This scalar equation for $\mathbf{E}$ may be used because it is usual for trans-ionospheric RF links to be circularly polarized. It is therefore not necessary to carry out separate calculations for each polarization state. The exponential term in Equation 17 represents the dispersive effects of the smooth plasma and will be discussed later in this section. The electric field envelope U contains the diffractive effects that are of interest under strong-scattering conditions. Substituting Equation 17 for $\mathbf{E}(\mathbf{r},\omega,t)$ in the wave equation gives the following differential equation for U:

$$\nabla_\perp^2 U + \frac{\partial^2 U}{\partial z^2} - 2i\langle k \rangle \frac{\partial U}{\partial z} - \langle k \rangle^2 \varepsilon_1 U = 0 \tag{18}$$

where

$$\nabla_\perp^2 = \frac{\partial^2}{\partial x^2} + \frac{\partial^2}{\partial y^2} . \tag{19}$$

The complex amplitude U varies as the electron density fluctuations. The second derivative $\partial^2 U/\partial z^2$ is then the order of $U/L_0^2$. On the other hand, the term $\langle k \rangle\, \partial U/\partial z$

varies as $U/\lambda L_0$. As long as $\lambda << L_0$, the second derivative is small compared to the first derivative and may be ignored. This is equivalent to neglecting reflected rays and is called the "parabolic" approximation. The parabolic wave equation is then

$$\nabla_\perp^2 U - 2i\langle k\rangle \frac{\partial U}{\partial z} - \langle k\rangle^2 \varepsilon_1 U = 0 \ . \tag{20}$$

It will be seen that this parabolic or small-angle scattering approximation is robust in that it degrades gracefully as the scattering angles get large. The source term $\varepsilon_1 U$ in the parabolic wave equation is a function of frequency and the electron density fluctuations. Different frequencies within a signal bandwidth may therefore propagate differently through the same ionization structure. When this happens, the propagation channel is said to be frequency selective.

## 2.2 TRANSPORT EQUATION.

A partial differential equation for the two-position, two-frequency, two-time mutual coherence function is derived from the parabolic wave equation in this section. This transport equation is derived using the Novikov theorem which requires that the electron density fluctuations be normally distributed. However, *Lee and Jokipii* [1975a] give an alternative derivation that relaxes this assumption.

### 2.2.1 First Form of the Transport Equation.

The two-position, two-frequency, two-time mutual coherence function is defined in a plane normal to the line-of-sight as

$$\Gamma = \langle U(\rho_1,z,\omega_1,t_1)\ U^*(\rho_2,z,\omega_2,t_2)\rangle \tag{21}$$

where $\rho$ is a two-dimensional position vector in the plane normal to the line-of-sight.

In order to obtain an equation for $\Gamma$, the parabolic wave equation for $U(\rho_1,z,\omega_1,t_1)$ is multiplied by $U^*(\rho_2,z,\omega_2,t_2)$. This results in the following equation:

$$\frac{1}{k_1}\nabla_{\perp 1}^2 U(\rho_1,z,\omega_1,t_1)U^*(\rho_2,z,\omega_2,t_2) - 2i\frac{\partial U(\rho_1,z,\omega_1,t_1)}{\partial z}U^*(\rho_2,z,\omega_2,t_2)$$

$$- k_1\,\varepsilon_1(\rho_1,z,\omega_1,t_1)\ U(\rho_1,z,\omega_1,t_1)\ U^*(\rho_2,z,\omega_2,t_2) = 0 \tag{22a}$$

where $k_j$ is given by Equation 13 evaluated at frequency $\omega_j$, $\varepsilon_1(\rho_j,z,\omega_j,t_j)$ is given by Equation 14, and the Laplacian is given by Equation 19 evaluated at $\rho_j$. A similar equation can be written down by interchanging the subscripts 1 and 2 and by taking the complex conjugate with the result:

$$\frac{1}{k_2}\nabla_{\perp 2}^2 U^*(\rho_2,z,\omega_2,t_2)U(\rho_1,z,\omega_1,t_1) + 2i\frac{\partial U^*(\rho_2,z,\omega_2,t_2)}{\partial z}U(\rho_1,z,\omega_1,t_1)$$

$$- k_2\,\varepsilon_1(\rho_2,z,\omega_2,t_2)\ U^*(\rho_2,z,\omega_2,t_2)\ U(\rho_1,z,\omega_1,t_1) = 0 \ . \tag{22b}$$

Upon subtracting Equation 22b from Equation 22a and taking the expectation value, the equation for $\Gamma$ is

$$\frac{1}{k_1}\nabla_{\perp 1}^2\,\Gamma - \frac{1}{k_2}\nabla_{\perp 2}^2\,\Gamma - 2i\,\frac{\partial \Gamma}{\partial z}$$

$$- k_1 \langle \varepsilon_1(\rho_1,z,\omega_1,t_1)\, U(\rho_1,z,\omega_1,t_1)\, U^*(\rho_2,z,\omega_2,t_2)\rangle \qquad (23)$$

$$+ k_2 \langle \varepsilon_1(\rho_2,z,\omega_2,t_2)\, U^*(\rho_2,z,\omega_2,t_2)\, U(\rho_1,z,\omega_1,t_1)\rangle = 0 \ .$$

The expectation of the two source terms in this equation must be carefully evaluated. They involve the product of $UU^*$ and $\varepsilon_1$ where $\varepsilon_1$ is proportional to the fluctuations in the electron density. However, the electric field complex envelope U is also a function of the electron density fluctuations that are encountered along the propagation path. Therefore U and $\varepsilon_1$ are correlated.

### 2.2.2 Novikov Theorem.

The Novikov theorem is used to evaluate the source terms in Equation 23. This theorem is proven in *Tatarskii* [1971, §65] and *Ishimaru* [1978, pp. 457-458]. The theorem states that

$$\langle f_1(\mathbf{R}) f_2(f_1)\rangle = \int \langle f_1(\mathbf{R}) f_1(\mathbf{R}')\rangle \left\langle \frac{\delta f_2(f_1)}{\delta f_1(\mathbf{R}')} \right\rangle d^n\mathbf{R}' \qquad (24)$$

where $f_1(\mathbf{R})$ is a zero-mean, normally-distributed random function of the n-dimensional vector $\mathbf{R}$, $f_2(f_1)$ is a function of $f_1$, and $\delta f_2/\delta f_1$ is a functional derivative. In applying this theorem, $f_1 = \varepsilon_1$ and $f_2 = UU^*$. The theorem is proven by expanding $f_2(f_1)$ in a Taylor series.

### 2.2.3 Source Terms.

Before proceeding with the evaluation of the source terms, it will be convenient to write $\varepsilon_1$ as the product of a frequency term and a term that varies only with space and time:

$$\varepsilon_1(\rho,z,\omega,t) = \xi(\rho,z,t)\,\beta(\omega) \qquad (25)$$

where

$$\xi(\rho,z,t) = \frac{\Delta n_e(\rho,z,t)}{\langle n_e\rangle} \qquad (26)$$

is a random function of the electron density fluctuations and

$$\beta(\omega) = \frac{\langle \omega_p^2\rangle}{\omega^2 - \langle \omega_p^2\rangle} \qquad (27)$$

is a deterministic function of frequency and the mean free electron density.

For the first source term in Equation 23 a straightforward application of the Novikov theorem yields:

$$S_1 = k_1\beta(\omega_1)\,\langle\xi(\rho_1,z,t_1)\,U(\rho_1,z,\omega_1,t_1)\,U^*(\rho_2,z,\omega_2,t_2)\rangle \tag{28}$$

$$= k_1\,\beta(\omega_1)\int_{-\infty}^{\infty}dz'\int_{-\infty}^{\infty}d^2\rho'\int_{-\infty}^{\infty}dt'\,\langle\xi(\rho_1,z,t_1)\xi(\rho',z',t')\rangle$$

$$\times\left\langle\frac{\delta U(\rho_1,z,\omega_1,t_1)}{\delta\xi(\rho',z',t')}\,U^*(\rho_2,z,\omega_2,t_2) + U(\rho_1,z,\omega_1,t_1)\,\frac{\delta U^*(\rho_2,z,\omega_2,t_2)}{\delta\xi(\rho',z',t')}\right\rangle .$$

At this point the electron density fluctuations are assumed to be stationary and delta-correlated along the z axis. This Markov assumption has the mathematical form

$$\langle\xi(\rho,z,t)\xi(\rho',z',t')\rangle = \delta(z-z')\,A\xi(\rho-\rho',t-t') \tag{29}$$

where $\delta(\cdot)$ is the Dirac delta function. The structure function $A\xi(\rho-\rho',t-t')$ is the autocorrelation function of the electron density fluctuations. The Markov assumption is discussed in some detail by *Tatarskii* [1971, §64] and is based on the fact that fluctuations in the dielectric constant in the direction of propagation have little effect on the transverse fluctuation characteristics of the electric field. It is the fluctuations of the dielectric constant transverse to the direction of propagation that dominate the scattering and the transverse fluctuations of the electric field.

Under the assumption of small-angle scattering for which the parabolic wave equation is valid, the component of the electric field traveling in the backward direction will be negligible compared to the component traveling in the forward direction. The electric field $U(\rho,z,\omega,t)$ may then be assumed to depend on $\xi(\rho',z',t')$ only for $z' < z$ (i.e. the electric field does not depend on electron density irregularities that have not yet been encountered along the forward propagation path). Also, $U(\rho,z,\omega,t)$ depends on $\xi(\rho',z',t')$ only for $t' < t$ (i.e. the electric field does not depend on irregularities that have not yet occurred). Thus $\delta U(\rho,z,\omega,t)/\delta\xi(\rho',z',t')$ is equal to 0 for $z' > z$ and for $t' > t$.

The source function $S_1$ may now be rewritten as

$$S_1 = k_1\beta_1\int_{-\infty}^{z}dz'\,\delta(z-z')\int_{-\infty}^{\infty}d^2\rho'\int_{-\infty}^{t}dt'\,A\xi(\rho_1-\rho',t_1-t')\;\times \tag{30}$$

$$\left\langle\frac{\delta U(\rho_1,z,\omega_1,t_1)}{\delta\xi(\rho',z',t')}\,U^*(\rho_2,z,\omega_2,t_2) + U(\rho_1,z,\omega_1,t_1)\,\frac{\delta U^*(\rho_2,z,\omega_2,t_2)}{\delta\xi(\rho',z',t')}\right\rangle$$

where $\beta_j$ is given by Equation 27 evaluated at $\omega_j$. Recalling that

$$\int_{-\infty}^{x} \delta(x'-x)\, dx' = \frac{1}{2} , \tag{31}$$

the source term is further reduced to

$$S_1 = \frac{k_1\beta_1}{2} \int_{-\infty}^{\infty} d^2\rho' \int_{-\infty}^{t} dt'\, A\xi(\rho_1-\rho',t_1-t') \times \tag{32}$$

$$\left\langle \frac{\delta U(\rho_1,z,\omega_1,t_1)}{\delta\xi(\rho',z,t')}\, U^*(\rho_2,z,\omega_2,t_2) + U(\rho_1,z,\omega_1,t_1)\, \frac{\delta U^*(\rho_2,z,\omega_2,t_2)}{\delta\xi(\rho',z,t')} \right\rangle .$$

The parabolic wave equation is used to evaluate the functional derivatives $\delta U/\delta\xi$. Integrating this equation from $-\infty$ to z results in

$$\int_{-\infty}^{z} \nabla_\perp^2\, U(\rho,z'',\omega,t)\, dz'' - 2i\langle k\rangle\, [U(\rho,z,\omega,t) - U_0(\rho,\omega)] - \tag{33}$$

$$\langle k\rangle^2\, \beta(\omega) \int_{-\infty}^{z} \xi(\rho,z'',t)\, U(\rho,z'',\omega,t)\, dz'' = 0$$

where $U_0(\rho,\omega)$ is the transmitted signal. After applying the operator $\delta/\delta\xi(\rho',z',t')$, where $-\infty < z' < z$ and $-\infty < t' < t$, and noting that

$$\frac{\delta\xi(\rho,z,t)}{\delta\xi(\rho',z',t')} = \delta(z-z')\, \delta(\rho-\rho')\, \delta(t-t') , \tag{34}$$

Equation 33 becomes

$$2i\langle k\rangle \frac{\delta U(\rho,z,\omega,t)}{\delta\xi(\rho',z',t')} + \langle k\rangle^2\, \beta(\omega)\, \delta(\rho-\rho')\, \delta(t-t')\, U(\rho,z,\omega,t)$$

$$+ \int_{z'}^{z} \left[ \langle k\rangle^2\beta(\omega)\xi(\rho,z'',t) - \nabla_\perp^2 \right] \frac{\delta U(\rho,z'',\omega,t)}{\delta\xi(\rho',z',t')}\, dz'' = 0 . \tag{35}$$

The lower limit of the integral in this equation is z' because $\delta U(\rho,z,\omega,t)/\delta\xi(\rho',z',t')$ is zero for $z < z'$. Because the source term contains factors of the form $\delta U(\rho,z,\omega,t)/\delta\xi(\rho',z,t')$, z' is set equal to z in Equation 35 with the result

$$\frac{\delta U(\rho,z,\omega,t)}{\delta\xi(\rho',z,t')} = \frac{i\langle k\rangle\beta(\omega)}{2}\, \delta(\rho-\rho')\, \delta(t-t')\, U(\rho,z,\omega,t) . \tag{36}$$

After substituting this into Equation 32, the source term becomes

$$S_1 = \int_{-\infty}^{\infty} d^2\rho' \int_{-\infty}^{\infty} dt' \, A\xi(\rho_1-\rho',t_1-t') \, \Gamma$$

$$\times \left[ \frac{ik_1\beta_1^2}{4} \delta(\rho_1-\rho') \, \delta(t_1-t') - \frac{ik_2\beta_1\beta_2}{4} \delta(\rho_2-\rho') \, \delta(t_2-t') \right] \tag{37}$$

$$= \frac{ik_1\beta_1^2}{4} A\xi(\mathbf{0},0) \, \Gamma - \frac{ik_2\beta_1\beta_2}{4} A\xi(\rho_1-\rho_2,t_1-t_2) \, \Gamma \ .$$

A similar expression may be written down for the second source term in Equation 23:

$$S_2 = k_2\beta(\omega_2) \langle \xi(\rho_2,z,t_2) \, U(\rho_1,z,\omega_1,t_1) \, U^*(\rho_2,z,\omega_2,t_2) \rangle \tag{38}$$

$$= \frac{ik_1\beta_1\beta_2}{4} A\xi(\rho_1-\rho_2,t_1-t_2) \, \Gamma - \frac{ik_2\beta_2^2}{4} A\xi(\mathbf{0},0) \, \Gamma \ .$$

### 2.2.4 Second Form of Transport Equation.

The transport equation for the mutual coherence function is now given by combining Equations 37 and 38 with 23 with the result

$$\frac{\partial\Gamma}{\partial z} + \frac{i}{2}\left[ \frac{1}{k_1}\nabla_{\perp 1}^2 - \frac{1}{k_2}\nabla_{\perp 2}^2 \right] \Gamma \tag{39}$$

$$- \frac{1}{8}\left[ 2k_1k_2\beta_1\beta_2 \, A\xi(\rho_1-\rho_2,t_1-t_2) - (k_1^2\beta_1^2 + k_2^2\beta_2^2) \, A_0 \right] \Gamma = 0$$

where $A_0 = A\xi(\mathbf{0},0)$.

The differential equation for $\Gamma$ will be solved by first letting $\Gamma$ equal $\Gamma_0\Gamma_1$ where $\Gamma_0$ is the free space solution to the transport equation. The well-known solution of the wave equation for the electric field in free space (Eqn. 18 with $\varepsilon_1 = 0$) may be written down directly. The Fresnel approximation that $z >> |\rho|$ is then used to expand the electric field and the free space solution $\Gamma_0$ is computed. The quantity $\Gamma_0$ contains the $1/z^2$ term that partly determines the mean power at the receiver. The next step is to derive a differential equation for $\Gamma_1$ from Equation 39 and the free space solution. It is the mutual coherence function $\Gamma_1$ that determines the second-order statistics of the received signal.

2.2.4.1 Free Space Solution $\Gamma_0$. In free space and for spherical geometry, the complex envelope of the electric field is

$$\mathbf{E} = \mathbf{E}_0 \frac{\exp(-ik|\mathbf{r}|)}{|\mathbf{r}|} \ . \tag{40}$$

It is easy to verify that this is a solution of the wave equation with $\varepsilon_1$ set to zero. Under the assumption of small-angle scattering, $z^2 >> x^2 + y^2$ in the region of interest and $|\mathbf{r}|$ may be expanded as

$$|\mathbf{r}| = \sqrt{x^2 + y^2 + z^2} \approx z + \frac{x^2 + y^2}{2z} \quad . \tag{41}$$

With this Fresnel approximation,

$$\mathbf{E} = \frac{\mathbf{E}_0}{z} \exp\left[ - ik \left( z + \frac{x^2 + y^2}{2z} \right) \right] \quad . \tag{42}$$

After recalling that $U = \exp(ikz)\, E$, the free space mutual coherence function is

$$\Gamma_0 = \langle U(\rho_1, z, \omega_1)\, U^*(\rho_2, z, \omega_2) \rangle \tag{43}$$

$$= \frac{1}{z^2} \exp\left[ \frac{ik_1(x_1^2 + y_1^2)}{2z} + \frac{ik_2(x_2^2 + y_2^2)}{2z} \right] \quad .$$

2.2.4.2 Differential Equation for $\Gamma_1$. After substituting $\Gamma = \Gamma_0 \Gamma_1$ into the transport equation and using Equation 43 for the free space solution, the equation for $\Gamma_1$ becomes

$$\frac{\partial \Gamma_1}{\partial z} + \frac{i}{2k_1} \nabla_{\perp 1}^2 \Gamma_1 - \frac{i}{2k_2} \nabla_{\perp 2}^2 \Gamma_1 \tag{44}$$

$$+ \left[ \frac{x_1}{z} \frac{\partial \Gamma_1}{\partial x_1} + \frac{y_1}{z} \frac{\partial \Gamma_1}{\partial y_1} + \frac{x_2}{z} \frac{\partial \Gamma_1}{\partial x_2} + \frac{y_2}{z} \frac{\partial \Gamma_1}{\partial y_2} \right] - S\, \Gamma_1 = 0$$

where the source term is

$$S = \frac{1}{8} \left[ 2k_1 k_2 \beta_1 \beta_2\, A_\xi(\rho_1 - \rho_2, t_1 - t_2) - (k_1^2 \beta_1^2 + k_2^2 \beta_2^2)\, A_0 \right] \quad . \tag{45}$$

In order for $\Gamma_1$ to represent a statistically stationary random process in space, frequency, and time, $\Gamma_1$ must be a function only of the differences $\rho_1 - \rho_2$, $\omega_1 - \omega_2$, and $t_1 - t_2$ . It is therefore useful to transform Equation 44 to sum and difference spatial and frequency coordinates:

$$X = \frac{x_1 + x_2}{2} \qquad Y = \frac{y_1 + y_2}{2}$$

$$\zeta = x_1 - x_2 \qquad \eta = y_1 - y_2$$

$$\nabla_s^2 = \frac{\partial^2}{\partial X^2} + \frac{\partial^2}{\partial Y^2} \qquad \nabla_d^2 = \frac{\partial^2}{\partial \zeta^2} + \frac{\partial^2}{\partial \eta^2} \tag{46}$$

$$\nabla_s \cdot \nabla_d = \frac{\partial^2}{\partial X \partial \zeta} + \frac{\partial^2}{\partial Y \partial \eta}$$

$$k_s = \frac{k_1 + k_2}{2} \qquad k_d = k_1 - k_2 \ .$$

After some manipulations, the equation for $\Gamma_1$ reduces to

$$\frac{\partial \Gamma_1}{\partial z} - \frac{2i}{4k_\xi^2 - k_d^2} \left[ k_d \nabla_d^2 + \frac{k_d}{4} \nabla_s^2 - k_s \nabla_s \cdot \nabla_d \right] \Gamma_1 + \tag{47}$$

$$\frac{1}{z} \left[ X \frac{\partial}{\partial X} + Y \frac{\partial}{\partial Y} + \zeta \frac{\partial}{\partial \zeta} + \eta \frac{\partial}{\partial \eta} \right] \Gamma_1 - S \Gamma_1 = 0 \ .$$

The boundary condition for this equation is that $\Gamma_1$ evaluated at $z = -z_t$ must be equal to unity independent of the other spatial coordinates. Also, the source term S under most conditions is a function only of the difference coordinates. It will therefore be assumed that $\Gamma_1$ is independent of X and Y. However, the source term will be a function of X and Y if the spatial extent of the scattering region is small as, for example, in a barium cloud. The assumption that $\Gamma_1$ is independent of X and Y then requires that the disturbed region in the ionosphere be large compared to the region from which scattered signal energy is received.

The transport equation may be further reduced by noting that the 1/z term, when z is large, will be small compared to the other terms and may be neglected. The transport equation for $\Gamma_1$ then becomes

$$\frac{\partial \Gamma_1}{\partial z} - \frac{2ik_d}{4k_\xi^2 - k_d^2} \nabla_d^2 \Gamma_1 - S \Gamma_1 = 0 \ . \tag{48}$$

## 2.3 DELTA-LAYER APPROXIMATION.

As an RF wave propagates through a thick, irregularly structured ionization layer, the wave first suffers random phase perturbations due to random variations in the index of refraction. As the wave propagates farther, diffractive effects introduce fluctuations in amplitude as well as phase. If the standard deviation $\sigma_\phi$ of the phase fluctuations that are suffered by the wave is large, then the amplitude fluctuations are characterized by a Rayleigh probability distribution when the wave emerges from the layer. The delta-layer approximation assumes that the phase and amplitude fluctuations are imparted on the wave in an infinitesimally thin layer. This assumption is consistent with the Markov assumption made in deriving the differential equation for the mutual coherence function.

An analytic solution for the two-position, two-frequency mutual coherence function has been obtained for plane waves by *Sreenivasiah, Ishimaru, and Horg* [1976] for a thick ionization layer. *Wittwer* [1979] extended this solution to tr at spherical waves. The analytic form of this solution is sufficiently complex, however, that the necessary Fourier transforms required to compute the GPSD cannot be

performed in closed form. The complex analytic form is simplified by the use of the delta-layer approximation to obtain tractable expressions for the mutual coherence function and the GPSD. Wittwer has evaluated the accuracy of the delta-layer approximation as it affects the delay distribution of the received signal and has found that the maximum error is small for transionospheric satellite communication link geometries as long as the parameters of the GPSD are properly selected. *Wittwer* [1979] has derived expressions for the signal parameters of the GPSD that include the effects of a thick scattering layer.

Now a relationship between the electron density fluctuations and the phase variations imposed on the wave may be calculated. The differential phase change of the wave along the propagation path $\ell$ is

$$\frac{d\phi}{d\ell} = r_e \lambda \Delta n_e(\rho,z,t) \quad . \tag{49}$$

Under the assumption of small-angle scattering used to derive the differential equation for $\Gamma_1$, $d/d\ell$ is approximately equal to $d/dz$, and the total phase change of the wave is

$$\phi = r_e\lambda \int \Delta n_e(\rho,z,t)\, dz = r_e\lambda\langle n_e\rangle \int \xi(\rho,z,t)\, dz \quad , \tag{50}$$

integrated through the ionization layer. The autocorrelation function of the phase change is

$$\begin{aligned} \langle\phi(\rho,t)\phi(\rho',t')\rangle &= [r_e\lambda\langle n_e\rangle]^2 \int dz \int dz' \,\langle\xi(\rho,z,t)\xi(\rho',z',t)\rangle \\ &= [r_e\lambda\langle n_e\rangle]^2 \int A\xi(\rho-\rho',t-t')\, dz \\ &= [r_e\lambda\langle n_e\rangle]^2 L_\delta\, A\xi(\rho-\rho',t-t') \end{aligned} \tag{51}$$

where $L_\delta$ is the delta layer thickness. The Markov approximation (Eqn. 29) has been used in evaluating the autocorrelation of $\xi$. However, it is shown in Appendix A that Equation 51 is valid as long as the scattering layer thickness is large compared to the parallel decorrelation distance of the electron density fluctuations. The phase variance imparted on the wave is

$$\sigma_\phi^2 = [r_e\lambda\langle n_e\rangle]^2 L_\delta\, A_0 \quad . \tag{52}$$

The quantity $A_0$ depends on the power spectrum of the electron density fluctuations in the ionosphere. The value of $A_0$ for a three-dimensional $K^{-4}$ *in situ* power spectrum and for the delta-layer approximation is given in Appendix B.

In general, only part of the total phase variance results in the Rayleigh amplitude fluctuations that are described by the GPSD. *Wittwer* [1979, 1980] calls this part the Rayleigh phase variance. The rest of the total phase variance is associated with the mean dispersive effects described by the exponential term of Equation 17. It is the smaller-sized electron density fluctuations that result in diffractive effects and the larger-sized fluctuations that result in dispersive effects. *Wittwer* [1982] describes how the Rayleigh phase variance may be separated from the total phase variance. In the developments that follow, the phase variance in Equation 52 will be assumed to be the Rayleigh phase variance associated with diffractive effects and amplitude fluctuations.

## 2.4 FORMAL SOLUTION OF THE TRANSPORT EQUATION.

Before proceeding with the solution of the transport equation, it is convenient to expand the source term S by making two non-restrictive assumptions. First, it will be assumed that the RF frequencies of interest are large compared to the plasma frequency. Second, it will be assumed that $k_d$ is much smaller than $k_s$. The solution obtained will then be valid for a small range of frequencies around $k_s$ and for frequencies large compared to typical peak ionospheric plasma frequencies of a few hundred MHz. With these assumptions, the source term becomes

$$S = \frac{\langle\omega_p^2\rangle^2}{4c^4k_s^2}[A\xi(\rho,t) - A_0] - \frac{k_d^2\langle\omega_p^2\rangle^2}{8c^4k_s^4}A_0 \tag{53}$$

where it is understood that $\rho$ is a two-dimensional relative position vector in the $\zeta$-$\eta$ plane normal to the line-of-sight, and t is time difference.

The last term in the equation for S is a function of frequency and z but is independent of $\zeta$ and $\eta$. This suggests that another useful factorization is $\Gamma_1 = \Gamma_2\Gamma_3$ where $\Gamma_3$ is independent of $\zeta$ and $\eta$. After making this substitution in the transport equation for $\Gamma_1$ and separating variables, the result is

$$\frac{1}{\Gamma_2}\frac{\partial\Gamma_2}{\partial z} - \frac{ik_d}{2k_s^2}\frac{\nabla_d^2\Gamma_2}{\Gamma_2} - \frac{\langle\omega_p^2\rangle^2}{4c^4k_s^2}[A\xi(\rho,t) - A_0] + \frac{1}{\Gamma_3}\frac{\partial\Gamma_3}{\partial z} + \frac{k_d^2\langle\omega_p^2\rangle^2}{8c^4k_s^4}A_0 = 0 \ . \tag{54}$$

The last two terms of this equation depend only on the spatial variable z. Therefore the sum of these two terms must be separately equal to zero for arbitrary values of the other spatial variables $\zeta$ and $\eta$.

The source term in the $\Gamma_3$ equation is only non-zero within the delta layer. Thus from the transmitter to the delta layer, $\Gamma_3$ is unity. With this boundary condition, the solution of the $\Gamma_3$ equation is

$$\Gamma_3 = \exp\left[-\frac{k_d^2\langle\omega_p^2\rangle^2A_0}{8c^4k_s^4}(z-z_t)\right] \ , z > z_t \ . \tag{55}$$

This term gives the effect of different transit times of different frequencies that results from the frequency dependence of the index of refraction.

Now the equation for $\Gamma_2$ may be solved using the delta-layer approximation. The equation for $\Gamma_2$ is

$$\frac{1}{\Gamma_2}\frac{\partial \Gamma_2}{\partial z} - \frac{ik_d}{2k_s^2}\frac{\nabla_d^2 \Gamma_2}{\Gamma_2} - \frac{\langle \omega_p^2 \rangle^2}{4c^4 k_s^2}\left[A_\xi(\rho,t) - A_0\right] = 0 \ . \tag{56}$$

Within the delta layer, the $k_d$ term is small compared to the source term and may be ignored. This is equivalent to assuming that diffractive effects are not important within the delta layer [*Lee and Jokipii* 1975b]. Integrating Equation 56 through the delta layer gives the value of $\Gamma_2$ at the point where the wave emerges from the delta layer:

$$\Gamma_2 = \exp\left\{ \frac{\langle \omega_p^2 \rangle^2}{4c^4 k_s^2}\left[A_\xi(\rho,t) - A_0\right] \right\} \ . \tag{57}$$

The solution from this point proceeds as follows. Between the delta layer and the receiver, the signal propagates in free space so the equation for $\Gamma_1$ is

$$\frac{\partial \Gamma_1}{\partial z} - \frac{2ik_d}{4k_s^2 - k_d^2}\nabla_d^2 \Gamma_1 = 0 \ . \tag{58}$$

The $\nabla_d^2 \Gamma_1$ term in this equation gives the effects of diffraction on the signal as it propagates from the delta layer to the receiver. The boundary condition is $\Gamma_1 = \Gamma_2 \Gamma_3$ at the point where the wave emerges from the delta layer. This equation is easily solved by taking the Fourier transform from spatial coordinates $\zeta$ and $\eta$ to angular coordinates. First, it is convenient to transform variables to

$$u = \frac{\zeta}{z} \text{ and } v = \frac{\eta}{z} \ . \tag{59}$$

The angular variables $K_u$ and $K_v$ are then independent of z. After the change in variables, the equation for $\Gamma_1$ becomes

$$\frac{\partial \Gamma_1}{\partial z} - \frac{ik_d}{2k_s^2 z^2}\left[\frac{\partial^2}{\partial u^2} + \frac{\partial^2}{\partial v^2}\right]\Gamma_1 = 0 \ . \tag{60}$$

Fourier transform pairs from spatial coordinates $\rho$ in the plane normal to the line-of-sight to angular coordinates $\mathbf{K}_\perp$, from carrier frequency differences $\omega$ to delay $\tau$, and from time differences t to Doppler frequencies $\omega_D$ are defined in this report to be

$$\hat{\Gamma}(\mathbf{K}_\perp) = \int_{-\infty}^{\infty} \exp(-i\mathbf{K}_\perp \cdot \rho)\, \Gamma(\rho)\, d^2\rho \tag{61a}$$

$$\hat{\Gamma}(\tau) = \int_{-\infty}^{\infty} \exp(i\omega\tau)\, \Gamma(\omega)\, \frac{d\omega}{2\pi} \tag{61b}$$

$$\hat{\Gamma}(\omega_D) = \int_{-\infty}^{\infty} \exp(i\omega_D t)\, \Gamma(t)\, dt \tag{61c}$$

and

$$\Gamma(\rho) = \int_{-\infty}^{\infty} \exp(i\mathbf{K}_\perp \cdot \rho)\, \hat{\Gamma}(\mathbf{K}_\perp)\, \frac{d^2K_\perp}{(2\pi)^2} \tag{62a}$$

$$\Gamma(\omega) = \int_{-\infty}^{\infty} \exp(-i\omega\tau)\, \hat{\Gamma}(\tau)\, d\tau \tag{62b}$$

$$\Gamma(t) = \int_{-\infty}^{\infty} \exp(-i\omega_D t)\, \hat{\Gamma}(\omega_D)\, \frac{d\omega_D}{2\pi} \quad . \tag{62c}$$

Upon transforming from u and v to $K_u$ and $K_v$, the equation for $\hat{\Gamma}_1$ is

$$\frac{\partial \hat{\Gamma}_1}{\partial z} - \frac{ik_d}{2k_s^2 z^2}\left(K_u^2 + K_v^2\right)\hat{\Gamma}_1 = 0 \quad . \tag{63}$$

This equation is integrated from $z = z_t + L_\delta$ to $z = z_t + z_r$ which gives

$$\hat{\Gamma}_1(K_u, K_v, z_t+z_r, \omega, t) = \hat{\Gamma}_1(K_u, K_v, z_t+L_\delta, \omega, t) \exp\left[-\frac{ik_d\gamma}{2k_s^2}\left(K_u^2 + K_v^2\right)\right] \tag{64}$$

where

$$\gamma = \int_{z_t+L_\delta}^{z_t+z_r} \frac{dz}{z^2} = \frac{z_r - L_\delta}{(z_t+z_r)(z_t+L_\delta)} \quad . \tag{65}$$

The expression for $\gamma$ may be simplified by setting $L_\delta$ to zero, which is consistent with the delta-layer approximation. Thus $\gamma$ is given by

$$\gamma = \frac{z_r}{z_t(z_t + z_r)} \quad . \tag{66}$$

At this point, a formal solution for the Fourier transform of the two-position, two-frequency, two-time mutual coherence function at the receiver has been computed in terms of the structure function $A\xi(\rho,t) - A_0$. In the next two sections, models for the temporal variation of the structure function and the quadratic approximation for the spatial variation of this function will be discussed.

## 2.5 TEMPORAL VARIATION MODELS FOR $\Delta n_e$.

Under the frozen-in model, the temporal variation of the electron density fluctuations is given by

$$\Delta n_e(\rho,z,t) = \Delta n_e(\rho - vt,z,0) \quad . \tag{67}$$

This equation is valid if the electron density fluctuations with a scale size $L_0$ do not appreciably change their shape within the time required for the structures to drift a distance $L_0$. This is called Taylor's frozen-in hypothesis, and this model has been used in most previous calculations of the mutual coherence function for RF propagation through the ionosphere. Using this model, the structure function A becomes

$$A\xi(\rho,t) = A\xi(\rho - vt,0) \quad . \tag{68}$$

This model is accurate for ionospheric conditions where the ionization has broken up into a single layer of striations aligned with the earth's magnetic field lines.

The frozen-in model may not be valid before striations have formed or when there are multiple scattering layers in the line-of-sight. Under these conditions, a "turbulent model" that decorrelates spatial and temporal variations may be more appropriate.

Dr. Leon A. Wittwer of the Defense Nuclear Agency has recently proposed a more "General Model" for the temporal and spatial behavior of the structure function [*Wittwer* 1988]. In this model it is assumed that the structure function depends on time and space as $\rho - Cvt$, where C is the space-time correlation coefficient of the electron density fluctuations. This model then varies smoothly between the frozen-in model where C is unity and the turbulent model where C is zero.

## 2.6 QUADRATIC PHASE STRUCTURE APPROXIMATION.

As a practical matter, the quadratic phase structure approximation is required to make the exponent in Equation 57 quadratic in the spatial and temporal variables. This gives the resulting mutual coherence function a tractable mathematical form. However, for the small angle, strong-scattering conditions considered in this report, the correlation distance of the signal will be much smaller than the correlation distance of the electron density fluctuations. The mutual coherence function will then be determined primarily by the values of $A\xi(\rho,t) - A_0$ at small values for the space and

time differences, and a Taylor series expansion of $A\xi(\rho,t) - A_0$, keeping only the quadratic terms, will provide a reasonably accurate mutual coherence function.

First consider only the spatial dependence of the structure function, $A\xi(\rho)$. The temporal behavior will be included later. The Taylor series expansion will make the following calculations independent of the functional form of $A\xi(\rho)$ as long as the second derivative of $A\xi(\rho)$ exists for $\rho$ equal to zero. A detailed discussion of $A\xi(\rho)$ will therefore be deferred to Appendix B. However, some generic properties of $A\xi(\rho)$ need to be considered here in order to specify the functional form of the quadratic terms in the Taylor series expansion.

The propagation coordinate systems are shown in Figure 2. The $\hat{z}$ axis is along the line-of-sight and the $\hat{t}$ axis is aligned with the geomagnetic field lines **B** at the elevation of the delta layer. The $\hat{r}$ and $\hat{s}$ axes are in a plane normal to the magnetic field. The penetration angle $\Phi$ is the angle between the $\hat{z}$ axis and the $\hat{t}$ axis. At the receiver, the $\hat{x}$ axis direction is given by the cross product of **B** and the line-of-sight unit vector, $\hat{z}$, and the $\hat{y}$ direction is orthogonal to both $\hat{x}$ and $\hat{z}$.

Now consider the functional form the power spectrum $S\xi(\mathbf{K})$ of the electron density fluctuations in the r-s-t coordinate system. The power spectrum is usually assumed to be a function of the quantity

$$L_r^2K_r^2 + L_s^2K_s^2 + L_t^2K_t^2$$

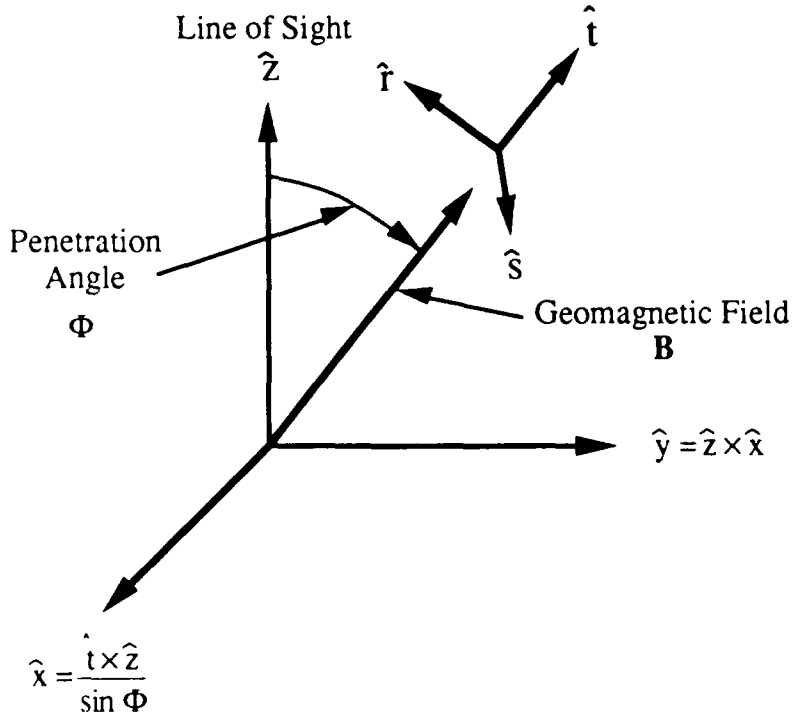


**Figure 2. Propagation coordinate systems.**

where $L_r$ , $L_s$ , and $L_t$ are the scale sizes of the fluctuations in the three directions. The usual assumption that the electron density fluctuations are elongated in the t direction and are symmetric about the t direction will be made. The scale sizes are then

$$L_r = L_s = L_0 \tag{69}$$

$$L_t = q\, L_0$$

where q ($q \geq 1$) is the axial ratio.

The power spectrum $S\xi(\mathbf{K})$ will now be evaluated in the x-y-z coordinate system in order to calculate $A\xi(\rho)$ in this system. The power spectrum in x-y-z coordinates is a function of the quantity [*Wittwer* 1979]

$$L_x^2K_x^2 + L_y^2K_y^2 + L_z^2K_z^2 + 2L_{yz}K_yK_z$$

where

$$L_x = L_0$$

$$L_y = L_0 \sqrt{\cos^2\Phi + q^2\sin^2\Phi} \tag{70}$$

$$L_z = L_0 \sqrt{\sin^2\Phi + q^2\cos^2\Phi}$$

$$L_{yz} = L_0 (q^2\text{-}1) \sin\Phi \cos\Phi$$

The structure function $A\xi(\rho)$ is the two-dimension Fourier transform of the power spectrum $S\xi(\mathbf{K})$:

$$A\xi(\rho) = \int_{-\infty}^{\infty} \exp(i\mathbf{K}_\perp\cdot\rho)\, S\xi(\mathbf{K}_\perp, K_z=0)\, \frac{d^2\mathbf{K}_\perp}{(2\pi)^2} \,. \tag{71}$$

Setting $K_z = 0$ in this equation results in $S\xi(\mathbf{K})$ being a function of

$$L_x^2K_x^2 + L_y^2K_y^2$$

and the structure function being calculated in the plane of the delta layer (i.e. at z = 0). After the Fourier transform is performed, $A\xi(\rho)$ will be a function of the quantity

$$\frac{x^2}{L_x^2} + \frac{y^2}{L_y^2} \,.$$

The quadratic phase structure approximation then takes the form

$$A\xi(\rho) = A_0 \left(1 - A_2 \left(\frac{x^2}{L_x^2} + \frac{y^2}{L_y^2}\right)\right) \,. \tag{72}$$

The coefficient $A_2$ is calculated in Appendix B for a $K^{-4}$ electron density fluctuation spectrum. The coefficient $A_0$ is given in terms of the phase variance by Equation 52.

Under the general model, the temporal variation of the structure function is due to a translation of the spatial coordinates. Equation 72 then becomes

$$A_\xi(\rho,t) = A_0\left[1 - A_2\left(\frac{x^2}{L_x^2} + \frac{y^2}{L_y^2} + \frac{t^2}{T_0^2} - 2\frac{C_{xt}\,x\,t}{L_x T_0} - 2\frac{C_{yt}\,y\,t}{L_y T_0}\right)\right] . \tag{73}$$

The quantity $T_0$ can be thought of as a "decorrelation time" of the electron density fluctuations in the ionosphere. The degree of space-time correlation is determined by the coefficients $C_{xt}$ and $C_{yt}$ .

## 2.7 MUTUAL COHERENCE FUNCTION.

The boundary condition for the mutual coherence function $\Gamma_1$ at the delta layer is given by the product $\Gamma_2\Gamma_3$. Using Equation 52 to relate $A_0$ to the phase variance and then setting the delta layer thickness $L_\delta$ to zero gives the following for $\Gamma_2$ and $\Gamma_3$ at the point where the wave emerges from the delta layer:

$$\Gamma_2 = \exp\left[-\sigma_\phi^2 A_2\left(\frac{x^2}{L_x^2} + \frac{y^2}{L_y^2} + \frac{t^2}{T_0^2} - 2\frac{C_{xt}\,x\,t}{L_x T_0} - 2\frac{C_{yt}\,y\,t}{L_y T_0}\right)\right] \tag{74}$$

and

$$\Gamma_3 = \exp\left[-\frac{1}{2}\left(\frac{\sigma_\phi\omega}{\omega_0}\right)^2\right] \tag{75}$$

where $\omega_0 = ck_s$ is the radian frequency of the carrier.

Upon changing variables in the equation for $\Gamma_2$ to the dimensionless spatial coordinates u and v, performing the Fourier transform to $K_u$ and $K_v$ coordinates, and assuming that the delta layer thickness is zero, the boundary condition for $\hat{\Gamma}_1$ is

$$\hat{\Gamma}_1(K_u,K_v,z_t,\omega,t) = \frac{\pi L_x L_y}{\sigma_\phi^2 A_2 z_t^2}\exp\left[-\sigma_\phi^2 A_2\frac{t^2}{T_0^2} - \frac{\sigma_\phi^2\omega^2}{2\omega_0^2} - \frac{L_x^2K_u^2 + L_y^2K_v^2}{4\sigma_\phi^2 A_2 z_t^2}\right] \tag{76}$$

$$\times\exp\left[-\sigma_\phi^2 A_2\left(C_{xt}^2 + C_{yt}^2\right)\frac{t^2}{T_0^2} - i\,\frac{C_{xt}L_xK_u + C_{yt}L_yK_v}{z_t}\,\frac{t}{T_0}\right]$$

The solution at the plane of the receiver is given by Equation 64 and this boundary condition.

After performing the inverse Fourier transform on the solution $\hat{\Gamma}_1(K_u,K_v,z_t,\omega,t)$ and converting to unnormalized distance units x and y, the two-position, two-frequency, two-time mutual coherence function is

$$\Gamma_1(x,y,\omega,t) = \frac{\exp\left[-\frac{1}{2}\left(\frac{\sigma_\phi\omega}{\omega_0}\right)^2\right]\exp\left[-(1 - C_{xt}^2 - C_{yt}^2)\left(\frac{t}{\tau_0}\right)^2\right]}{\left[1 + i\frac{\omega\Lambda_x}{\omega_{coh}}\right]^{\frac{1}{2}}\left[1 + i\frac{\omega\Lambda_y}{\omega_{coh}}\right]^{\frac{1}{2}}}$$

$$\times \exp\left[-\frac{\left(\frac{x}{\ell_x} - C_{xt}\frac{t}{\tau_0}\right)^2}{1 + i\frac{\omega\Lambda_y}{\omega_{coh}}}\right]\exp\left[-\frac{\left(\frac{y}{\ell_y} - C_{yt}\frac{t}{\tau_0}\right)^2}{1 + i\frac{\omega\Lambda_x}{\omega_{coh}}}\right] \tag{77}$$

where

$$\Lambda_x = \left[\frac{2\ell_x^4}{\ell_x^4 + \ell_y^4}\right]^{\frac{1}{2}} \qquad \Lambda_y = \left[\frac{2\ell_y^4}{\ell_x^4 + \ell_y^4}\right]^{\frac{1}{2}} . \tag{78}$$

The decorrelation distances $\ell_x$ and $\ell_y$ are given by the expressions:

$$\ell_x = \frac{(z_t + z_r)L_x}{z_t\sigma_\phi\sqrt{A_2}} \qquad \ell_y = \frac{(z_t + z_r)L_y}{z_t\sigma_\phi\sqrt{A_2}} , \tag{79}$$

the decorrelation time is given by the expression

$$\tau_0 = \frac{T_0}{\sigma_\phi\sqrt{A_2}} , \tag{80}$$

and the coherence bandwidth $\omega_{coh}$ is given by the expression

$$\omega_{coh} = \frac{\Lambda_y\omega_0^2L_\wedge^2}{2c\sigma_\phi^2A_2}\frac{z_t + z_r}{z_tz_r} . \tag{81}$$

Under the delta-layer approximation, the ratio of the two decorrelation distances is a function of only the penetration angle and the axial ratio and is given by

$$\frac{\ell_y}{\ell_x} = \frac{L_y}{L_x} = \sqrt{\cos^2\Phi + q^2\sin^2\Phi} . \tag{82}$$

The orientation of the x and y axes is usually chosen so that $\ell_x$ is the smaller of the two decorrelation distances. The minimum decorrelation distance is also referred to as $\ell_0$ in the literature. This notation will occasionally be used in this report. Equation 82 is used to calculate $\ell_y$ when only the minimum decorrelation distance is specified.

It will be seen in the next section that the coherence bandwidth is proportional to $2\pi f_0$ where $f_0$ is the frequency selective bandwidth of the signal. It is clear from the form of the mutual coherence function in Equation 77 that the coherence bandwidth could have also been defined by either of the products $\omega_{coh}\Lambda_y$ or $\omega_{coh}\Lambda_x$. The asymmetry factors $\Lambda_x$ and $\Lambda_y$ have been included in the definition of the coherence bandwidth in order to simplify the relationship between $\omega_{coh}$ and $f_0$.

The equations for the decorrelation time, decorrelation distance, and the coherence bandwidth are only valid under the delta-layer approximation and *do not* reflect how these parameters are actually calculated for a given ionospheric disturbance. *Wittwer* [1979] has derived expressions for the decorrelation distance and the coherence bandwidth that are valid for more general scattering layer geometries. It is these more general expressions that are used in signal specifications to calculate these signal parameters.

For satellite communications links, the distance from the ionosphere to the satellite is typically much larger than the distance from the ionosphere to the ground. If the transmitter is on the satellite then $z_t >> z_r$ and if the transmitter is on the ground then $z_t << z_r$ . Because the expressions for the decorrelation distances are not reciprocal in $z_t$ and $z_r$, the values of $\ell_x$ and $\ell_y$ depend on the direction of propagation. However, the expression for the coherence bandwidth is reciprocal in $z_t$ and $z_r$ so $\omega_{coh}$ and the frequency selective bandwidth are independent of the propagation direction. It is interesting to note that the expression for the decorrelation time is independent of the propagation distance, depending only on the "decorrelation time" of the striations and the standard deviation of the phase fluctuations.

The decorrelation distance of the signal as it emerges from the delta layer is approximately equal to $L_0/\sigma_\phi$. Under strong-scattering conditions where $\sigma_\phi >> 1$ , this distance will be much smaller than the electron density fluctuation scale size and the quadratic phase structure approximation conditions are met. Conversely, under weak scattering conditions where $\sigma_\phi \approx 1$, the quadratic phase approximation will give inaccurate results for the mutual coherence function.

Now consider the mutual coherence function for two positions, one frequency and two times:

$$\Gamma_1(x,y,0,t) = \exp\left[ - (1 - C_{xt}^2 - C_{yt}^2) \left(\frac{t}{\tau_0}\right)^2 - \left(\frac{x}{\ell_x} - C_{xt}\frac{t}{\tau_0}\right)^2 - \left(\frac{y}{\ell_y} - C_{yt}\frac{t}{\tau_0}\right)^2 \right] \tag{83}$$

The quantities $\ell_x, \ell_y$, and $\tau_0$ are seen to be the 1/e points of $\Gamma_1(x,0,0,0)$, $\Gamma_1(0,y,0,0)$, and $\Gamma_1(0,0,0,t)$ respectively and are therefore consistent with the usual definitions of decorrelation distance and time.

## 2.8 GENERALIZED POWER SPECTRAL DENSITY.

The generalized power spectral density $S(\mathbf{K}_\perp,\tau,\omega_D)$ of the signal incident on the plane of the receiver is the Fourier transform of the mutual coherence function:

$$S(\mathbf{K}_\perp,\tau,\omega_D) = \int_{-\infty}^{\infty} d^2\rho \int_{-\infty}^{\infty} \frac{d\omega}{2\pi} \int_{-\infty}^{\infty} dt\ \Gamma_1(\rho,\omega,t) \exp\left[-i(\mathbf{K}_\perp\cdot\rho-\omega\tau-\omega_D t)\right] \qquad (84)$$

where angle-of-arrival $\mathbf{K}_\perp$ is the Fourier transform pair of position $\rho$ in the x-y plane, delay $\tau$ is the Fourier transform pair of relative carrier frequency $\omega$, and Doppler frequency $\omega_D$ is the Fourier transform pair of relative time t. The quantity $S(\mathbf{K}_\perp,\tau,\omega_D)(d^2\mathbf{K}_\perp/4\pi^2)d\tau(d\omega_D/2\pi)$ is equal to the mean signal power arriving with angles-of-arrival in the interval $\mathbf{K}_\perp/4\pi^2$ to $(\mathbf{K}_\perp+d^2\mathbf{K}_\perp)/4\pi^2$, with delays relative to a nominal propagation time in the interval $\tau$ to $\tau+d\tau$, and with Doppler frequencies in the interval $\omega_D/2\pi$ to $(\omega_D+ d\omega_D)/2\pi$. The delay dependence of the GPSD is a consequence of the fact that some of the signal energy takes a dog-leg path through the ionosphere from the transmitter to the receiver and arrives later than the signal energy that propagates straight through the ionosphere.

In general, the GPSD can be written as the product of a Doppler spectrum $S_D(\omega_D)$ and an angle-delay spectrum $S_{K\tau}(\mathbf{K}_\perp,\tau)$:

$$S(\mathbf{K}_\perp,\tau,\omega_D) = S_D(\omega_D)\ S_{K\tau}(\mathbf{K}_\perp,\tau)\ . \qquad (85)$$

After performing the integrals indicated in Equation 84, the Doppler spectrum for the general model is

$$S_D(\omega_D) = \frac{\sqrt{\pi}\tau_0}{\sqrt{1 - C_{xt}^2 - C_{yt}^2}} \exp\left[-\frac{(\tau_0\omega_D - C_{xt}K_x\ell_x - C_{yt}K_y\ell_y)^2}{4(1 - C_{xt}^2 - C_{yt}^2)}\right]. \qquad (86)$$

(General Model)

The angle-delay part of the GPSD for the general model is identical to that derived previously for the frozen-in and turbulent models [see, for example, *Dana* 1986]. In terms of the components of $\mathbf{K}_\perp$ ($K_x$ and $K_y$) the angle-delay part of the GPSD is

$$S_{K\tau}(K_x,K_y,\tau) = \left[\frac{\pi}{2}\right]^{\frac{1}{2}} \ell_x\ell_y\,\alpha\omega_{coh} \exp\left[-\frac{K_x^2\ell_x^2}{4} - \frac{K_y^2\ell_y^2}{4}\right]$$

$$\times \exp\left\{-\frac{\alpha^2}{2}\left[\omega_{coh}\tau - \frac{\Lambda_y(K_x^2+K_y^2)\ell_x^2}{4}\right]^2\right\} \qquad (87)$$

where the delay parameter $\alpha$ is defined to be

$$\alpha = \frac{\omega_0}{\sigma_\phi \omega_{coh}} \quad . \tag{88}$$

The components of $\mathbf{K}_\perp$ are related to the scattering angles $\theta_x$ and $\theta_y$ about the x and y axis respectively by the relations

$$K_x = \frac{2\pi \sin(\theta_x)}{\lambda} \tag{89a}$$

$$K_y = \frac{2\pi \sin(\theta_y)}{\lambda} \quad . \tag{89b}$$

It should be noted that the range of delay in Equation 87 is from $-\infty$ to $+\infty$. However, this delay is relative to some nominal propagation time, and the value of the GPSD rapidly approaches zero for decreasing negative values of $\omega_{coh}\tau$. Thus negative values of delay present no real problem with causality.

It is interesting to examine the limits of the general model Doppler spectrum in order to show that this model does indeed encompass both the frozen-in and fully turbulent models. These limits for the Doppler spectra are:

$$\underset{\substack{C_{xt} \to 1 \\ C_{yt} \to 0}}{\text{Limit}} \; S_D(\omega_D) = 2\pi \tau_0 \, \delta(\tau_0 \omega_D - K_x \ell_x) \qquad \text{(Frozen-in Model)} \tag{90}$$

and

$$\underset{\substack{C_{xt} \to 0 \\ C_{yt} \to 0}}{\text{Limit}} \; S_D(\omega_D) = \sqrt{\pi} \, \tau_0 \exp\left[-\frac{\tau_0^2 \omega_D^2}{4}\right] \quad . \qquad \text{(Turbulent Model)} \tag{91}$$

For the frozen-in model, the delta-function relationship between Doppler frequency and $K_x$ is what is obtained by assuming that the random diffraction pattern of the signal is "frozen" and drifts in the x-direction past the receiver. For the turbulent model, the Doppler spectrum is independent of $K_x$ so the temporal and spatial variations in the received signal are also independent. This Gaussian form is the true turbulent Doppler spectrum, as opposed to previous turbulent models that assumed an $\omega_D^{-4}$ Doppler spectrum for mathematical convenience [*Dana* 1986].

The significance of the parameters $\alpha$, $\ell_x$, $\ell_y$, and $\omega_{coh}$ that appear in the angle-delay part of the GPSD will be discussed in the next subsections.

### 2.8.1 Delay Spread and $\alpha$.

The distribution of delayed signal power with a fixed angle-of-arrival, which is given by the second exponential term in Equation 87, has the Gaussian form

$$S_\tau(\tau) = \frac{\alpha\omega_{coh}}{\sqrt{2\pi}} \exp\left[-\frac{\alpha^2\omega_{coh}^2 (\tau - t_p)^2}{2}\right] \tag{92}$$

where $t_p$ is the additional propagation time for signals arriving at the angles $K_x$ and $K_y$. To see this, the expression for $t_p$ is expanded using the definitions for $\ell_x$, $\ell_y$, and $\omega_{coh}$ and the assumption of small-angle scattering to give

$$t_p = \frac{\theta_x^2 + \theta_y^2}{2c} \frac{z_r(z_t + z_r)}{z_t} \quad . \tag{93}$$

The geometry of the scattering in one plane is shown in Figure 3. Clearly, for small-angle scattering, the angle $\theta_t$ at the transmitter is related to the receiver scattering angle $\theta_r$ by the relationship

$$\theta_t = \frac{z_r}{z_t}\theta_r \quad . \tag{94}$$

The difference d between the line-of-sight distance and the scattered path length is given by

$$d = \sqrt{z_r^2 + z_r^2\theta_r} + \sqrt{z_t^2 + z_t^2\theta_t} - (z_r + z_t) \approx \frac{\theta_r^2}{2} \frac{z_r(z_t + z_r)}{z_t} \tag{95}$$

for scattering in one plane only. When scattering about both the x and y axes is taken into account, the total path difference is given by Equation 95 with $\theta_r^2$ replaced by $\theta_x^2+\theta_y^2$. The additional time required for the signal to propagate along the scattered path is just d/c which is equal to $t_p$.

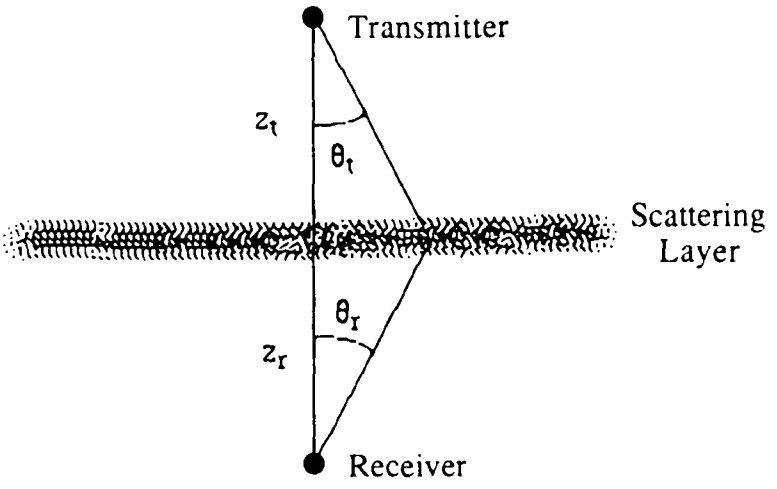


**Figure 3. Scattering geometry.**

For a given value of the coherence bandwidth, larger values of $\alpha$ result in a narrower delay distribution of signal power about the time $t_p$. The delay parameter $\alpha$ is then a measure of the relative importance of diffraction and dispersion with large values of $\alpha$ indicating strong-scattering effects and small values indicating weak scattering or dispersive effects. The strong-scattering limit then requires that the value of $\alpha$ be large.

### 2.8.2 Frequency Selective Bandwidth and $\omega_{coh}$.

The frequency selective bandwidth $f_0$ is an important measure of the effects of scintillation on the propagation of wide bandwidth signals. This quantity is defined as the standard deviation of the time-of-arrival jitter $\sigma_\tau$:

$$f_0 = \frac{1}{2\pi\sigma_\tau} \tag{96}$$

where

$$\sigma_\tau^2 = \langle\tau^2\rangle - \langle\tau\rangle^2 \ . \tag{97}$$

These delay moments can be calculated directly from the angle-delay part of the GPSD using the equation

$$P_0 \langle\tau^n\rangle = \int_{-\infty}^{\infty} \frac{d^2\mathbf{K}_\perp}{(2\pi)^2} \int_{-\infty}^{\infty} d\tau\, \tau^n\, S_{K\tau}(\mathbf{K}_\perp,\tau) \ . \tag{98}$$

It is easy to show that the mean signal power $P_0$ is equal to unity. The first and second moments are easily obtainable in closed form giving the relationship between coherence bandwidth and the frequency selective bandwidth:

$$\omega_{coh} = 2\pi f_0 \left[1 + \frac{1}{\alpha^2}\right]^{\frac{1}{2}} \ . \tag{99}$$

This expression is valid under the quadratic phase structure approximation for which the GPSD is valid. *Yeh and Liu* [1977] have calculated an expression for the time delay jitter keeping both the second and forth order terms in the expansion of the structure function $A_\xi(\rho)$. Their result has more terms in the expression for the time delay jitter. However, the additional terms are significant only when the quadratic approximation for the structure function is invalid and therefore only when the GPSD derived above is also invalid.

The $1+1/\alpha^2$ term in the expression for the coherence bandwidth represents the relative contributions to the time delay jitter from diffraction (1) and dispersion ($1/\alpha^2$). In the limit that $\alpha$ is large, the time delay jitter is determined by diffractive effects alone which should be the case under strong-scattering conditions.

### 2.8.3 Angle-of-Arrival Fluctuations and $\ell_x$ and $\ell_y$.

A key parameter in determining the severity of antenna filtering effects is the standard deviation of the angle-of-arrival fluctuations $\sigma_\theta$ of the electric field incident on an antenna. It is clear that for anisotropic scattering, when $\ell_x$ and $\ell_y$ are unequal, the values of $\sigma_\theta$ for scattering about the x and y axes will differ. The variance of the angle-of-arrival fluctuations about the x-direction is equal to

$$\sigma_{\theta x}^2 = \int_{-\infty}^{\infty} \frac{d^2\mathbf{K}_\perp}{(2\pi)^2} \int_{-\infty}^{\infty} d\tau \left[\frac{\lambda K_x}{2\pi}\right]^2 S_{K\tau}(\mathbf{K}_\perp,\tau) \tag{100}$$

under the small-angle scattering approximation that is required for the GPSD to be valid. A similar expression holds for the angle-of-arrival variance about the y-direction. The standard deviations of the angle-of-arrival fluctuations about the x and y axes are then given by

$$\sigma_{\theta x} = \frac{\lambda}{\sqrt{2}\pi\ell_x} \tag{101a}$$

$$\sigma_{\theta y} = \frac{\lambda}{\sqrt{2}\pi\ell_y} \,. \tag{101b}$$

For small-angle scattering to be a valid assumption, the larger of the two angular standard deviations must be small relative to one radian. Thus the minimum decorrelation distance must be approximately equal to or greater than the RF wavelength $\lambda$. The small angle approximation has been used throughout the derivation of the GPSD, starting with the parabolic wave equation. The resulting expression for the GPSD, however, does not exhibit singular behavior when the angle-of-arrival fluctuations become large and thus the small angle approximation is quite robust.

### 2.8.4 Isotropic Examples.

When the penetration angle is zero the two decorrelation distances are equal ($\ell_x = \ell_y = \ell_0$) and the scattering is isotropic about the line-of-sight. The one-dimensional angle-delay generalized power spectral density is then given by

$$S_{K\tau}(K,\tau) = \int_{-\infty}^{\infty} S_{K\tau}(K_x=K,K_y,\tau)\,\frac{dK_y}{2\pi} \tag{102}$$

$$= \frac{\alpha}{\sqrt{2\pi}}\,\omega_{coh}\ell_0 \exp\left[\frac{1}{2\alpha^2} - \omega_{coh}\tau\right] F\left[\frac{1}{\sqrt{2}\alpha} + \frac{\alpha}{\sqrt{2}}\left(\frac{K^2\ell_0^2}{4} - \omega_{coh}\tau\right)\right]$$

where Wittwer's F function is defined as

$$F(z) = \exp(-z^2) \int_{-\infty}^{\infty} \exp(-t^4 - 2t^2 z)\, dt \quad . \tag{103}$$

*Wittwer* [1980] has developed a polynomial expansion for this integral that is accurate to within one percent. This function may also be written in terms of $K_{1/4}$ and $I_{1/4}$ Bessel functions.

A three-dimensional plot of the isotropic one-dimension angle-delay GPSD is shown in Figure 4. This plot shows the mean received power as a function of normalized angle $K\ell_0$ and normalized delay $\omega_{coh}\tau$. The vertical axis is linear with arbitrary units. The value of $\alpha$ is 4 for this figure so consequently the quantity $\omega_{coh}$ is essentially equal to $2\pi f_0$.

It can be seen that the power arriving at large angles is also the power arriving at long delays. The power arriving at long delays thus has higher spatial frequency components than power arriving at short delays. When there is strong space-time correlation (i.e. when $\sqrt{C_{xt}^2 + C_{yt}^2}$ is approximately equal to unity) these higher spatial frequency components correspond to higher Doppler frequency components. The signal arriving at long delays then varies more rapidly in time than the signal arriving at short delays.

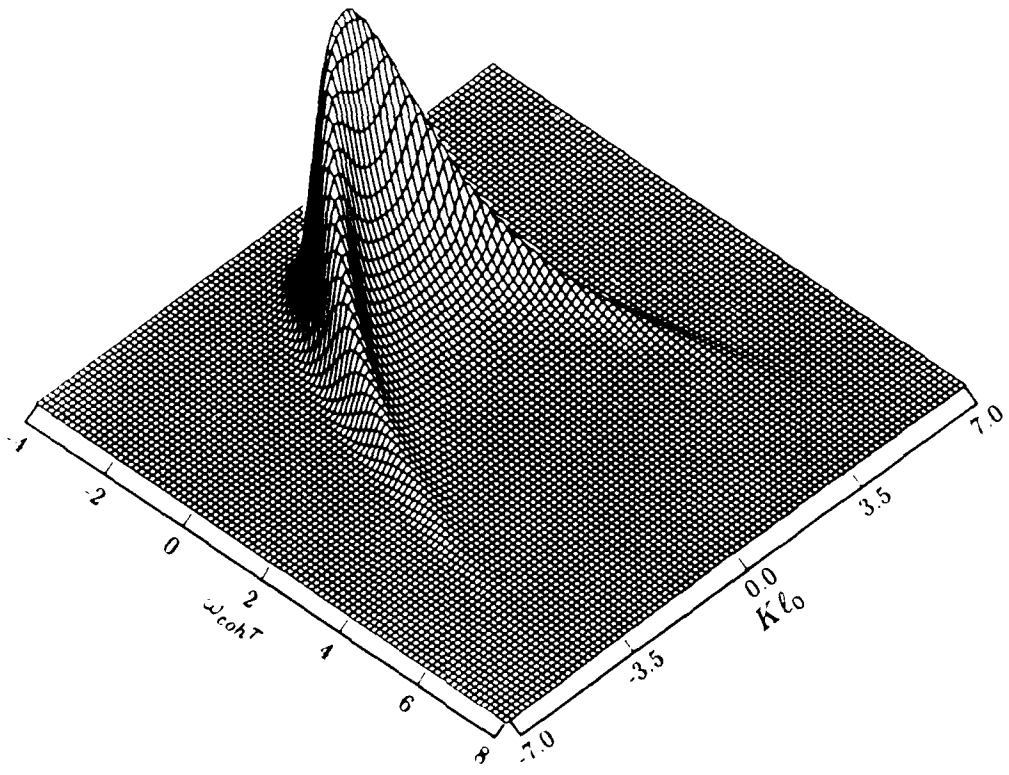


**Figure 4. Angle-delay generalized power spectral density.**

Another view of the GPSD can be obtained by considering the delay-Doppler scattering function

$$S_{\tau D}(\tau,\omega_D) = \int_{-\infty}^{\infty} \frac{dK_x}{2\pi} \int_{-\infty}^{\infty} \frac{dK_y}{2\pi} S(K_x,K_y,\tau,\omega_D) \ . \tag{104a}$$

For both the frozen-in and turbulent models the scattering function is readily evaluated for isotropic scattering with the results:

$$S_{\tau D}(\tau,\omega_D) = \left[\frac{\alpha}{\sqrt{2}\pi}\right]^{\frac{1}{2}} \omega_{coh}\tau_0 \exp\left[\frac{1}{2\alpha^2} - \omega_{coh}\tau\right] F\left[\frac{1}{\sqrt{2}\alpha} + \frac{\alpha}{\sqrt{2}}\left(\frac{\omega_D^2\tau_0^2}{4} - \omega_{coh}\tau\right)\right]$$

(Frozen-in Model) (104b)

$$S_{\tau D}(\tau,\omega_D) = \sqrt{\pi}\,\tau_0 \exp\left[-\frac{\omega_D^2\tau_0^2}{4}\right] \frac{\omega_{coh}}{2} \exp\left[\frac{1}{2\alpha^2} - \omega_{coh}\tau\right] \operatorname{erfc}\left[\frac{1}{\sqrt{2}\alpha} - \frac{\alpha\omega_{coh}\tau}{\sqrt{2}}\right]$$

(Turbulent Model) (104c)

where erfc (·) is the complementary error function. It is clear from the form of Equation 104c that the turbulent model scattering function is separable into a function of Doppler frequency times a function of delay. This is not the case for the frozen-in model.

For the general model the scattering function can be written in the form

$$S_{\tau D}(\tau,\omega_D) = \left[\frac{\alpha}{\sqrt{2}(1 - C_{xt}^2)}\right]^{\frac{1}{2}} \omega_{coh}\tau_0 \exp\left[\frac{1}{2\alpha^2} - \omega_{coh}\tau\right] \tag{104d}$$

$$\times\, \ell_0 \int_{-\infty}^{\infty} \exp\left[-\frac{(\tau_0\omega_D - C_{xt}K_y\ell_0)^2}{4(1 - C_{xt}^2)}\right] F\left[\frac{1}{\sqrt{2}\alpha} + \frac{\alpha}{\sqrt{2}}\left(\frac{K_y^2\ell_0^2}{4} - \omega_{coh}\tau\right)\right] \frac{dK_y}{2\pi}$$

(General Model)

assuming that $C_{yt}$ is zero. The remaining integral in Equation 104d is easily evaluated numerically.

A comparison of the scattering functions for the frozen-in and turbulent models is shown in Figure 5. The frozen-in scattering function is just a reproduction of Figure 4 with normalized angle $K\ell_0$ replaced with normalized Doppler frequency $\tau_0\omega_D$. This is a consequence of the delta-function relationship between angle and Doppler frequency for the frozen-in model. For this model the signal at long delays has correspondingly large Doppler shifts, and a wing-like structure is seen in the

scattering function. The turbulent model scattering function does not exhibit these Doppler wings because the Doppler spectrum is the same at all delays.

Both functions have exactly the same power density at each delay. The difference in appearance of the figures is due to the fact that the turbulent model signal at long delay is more spread out in Doppler frequency and is therefore less obvious.

A progression of scattering functions for the general model is shown in Figure 6. The space-time correlation coefficient $C_{xt}$ varies from 0.99 for the scattering function in the upper left to 0.7 for the scattering function in the lower right. The scattering function for $C_{xt}$ equal to 0.99 is essentially identical to that for the frozen-in model, and the scattering function for $C_{xt}$ equal to 0.7 is essentially identical to that for the turbulent model. For intermediate values of $C_{xt}$, the scattering functions still exhibit Doppler wings but the wings have broader Doppler spectra as $C_{xt}$ decreases.

### 2.8.5 Diffraction Limited Form of the GPSD.

Under the strong-scattering conditions in the ionosphere that cause signal scintillation at radio frequencies, diffractive effects dominate dispersive effects. In this case the value of $\alpha$ in the GPSD is large. In the limit that $\alpha$ approaches infinity, the angle-delay part of the GPSD becomes

$$S_{K\tau}(K_x,K_y,\tau) = \pi \ell_x \ell_y \omega_{coh} \exp\left[ - \frac{K_x^2 \ell_x^2}{4} - \frac{K_y^2 \ell_y^2}{4} \right]$$

$$\times \delta\left[ \omega_{coh}\tau - \frac{\Lambda_y (K_x^2 + K_y^2) \ell_x^2}{4} \right] \qquad (105)$$

The range of delay in this equation is from 0 to $+\infty$ due to the fact that the second term in the delta function is positive.

This geometric optics limit results in a delta-function relationship between angle and delay. The delta function in this equation can be used to associate the signal with a particular angle-of-arrival to a specific delay. This association is used to develop efficient channel simulation techniques.

### 2.8.6 Orthogonalized Form of the GPSD Used in Channel Modelling.

Once the diffraction limit of the GPSD has been taken, the delta-function relationship in Equation 104 can be used to relate angles-of-arrival to delay. The GPSD used in channel modelling can then be integrated over delay producing an angular-Doppler form, denoted $S_{KD}$. After some rearrangement of terms this form of the GPSD is

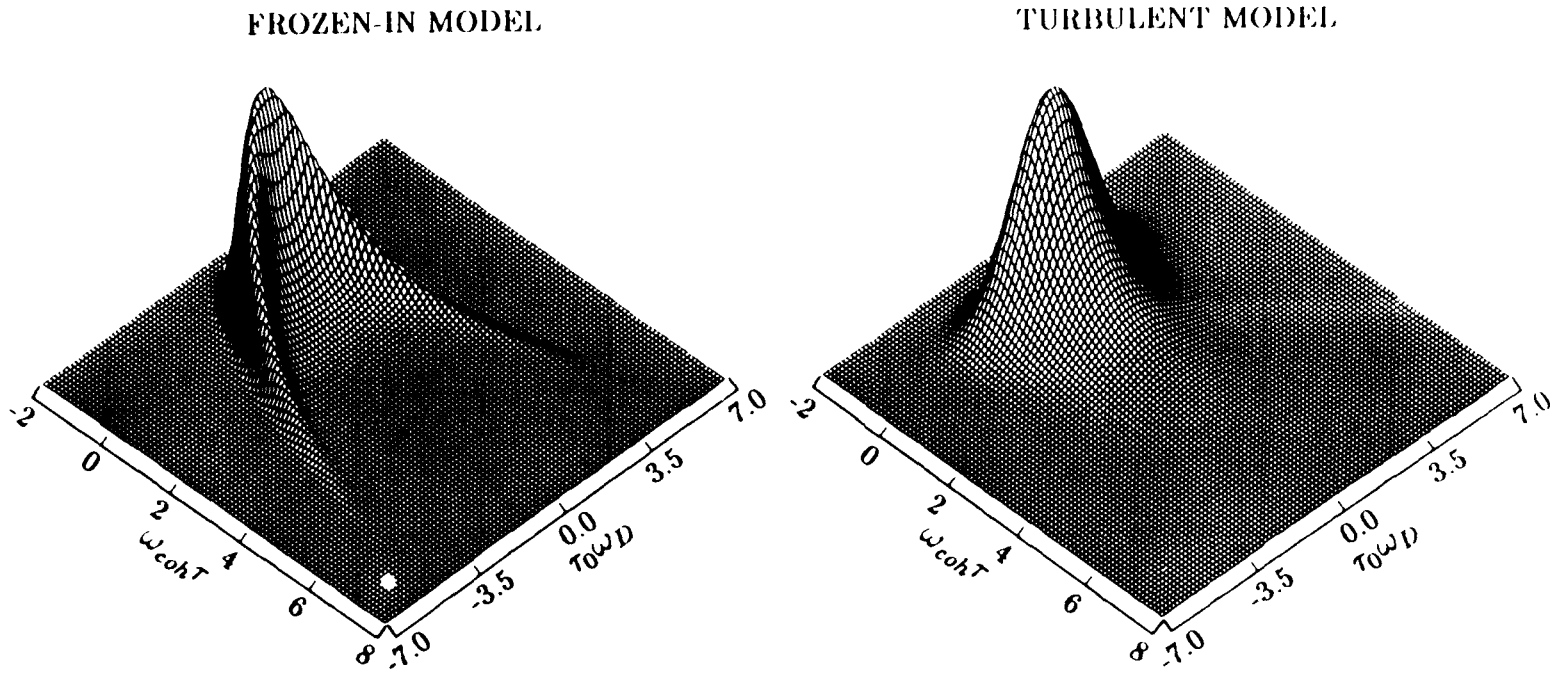


**Figure 5. Comparison of scattering functions for the frozen-in and turbulent models.**

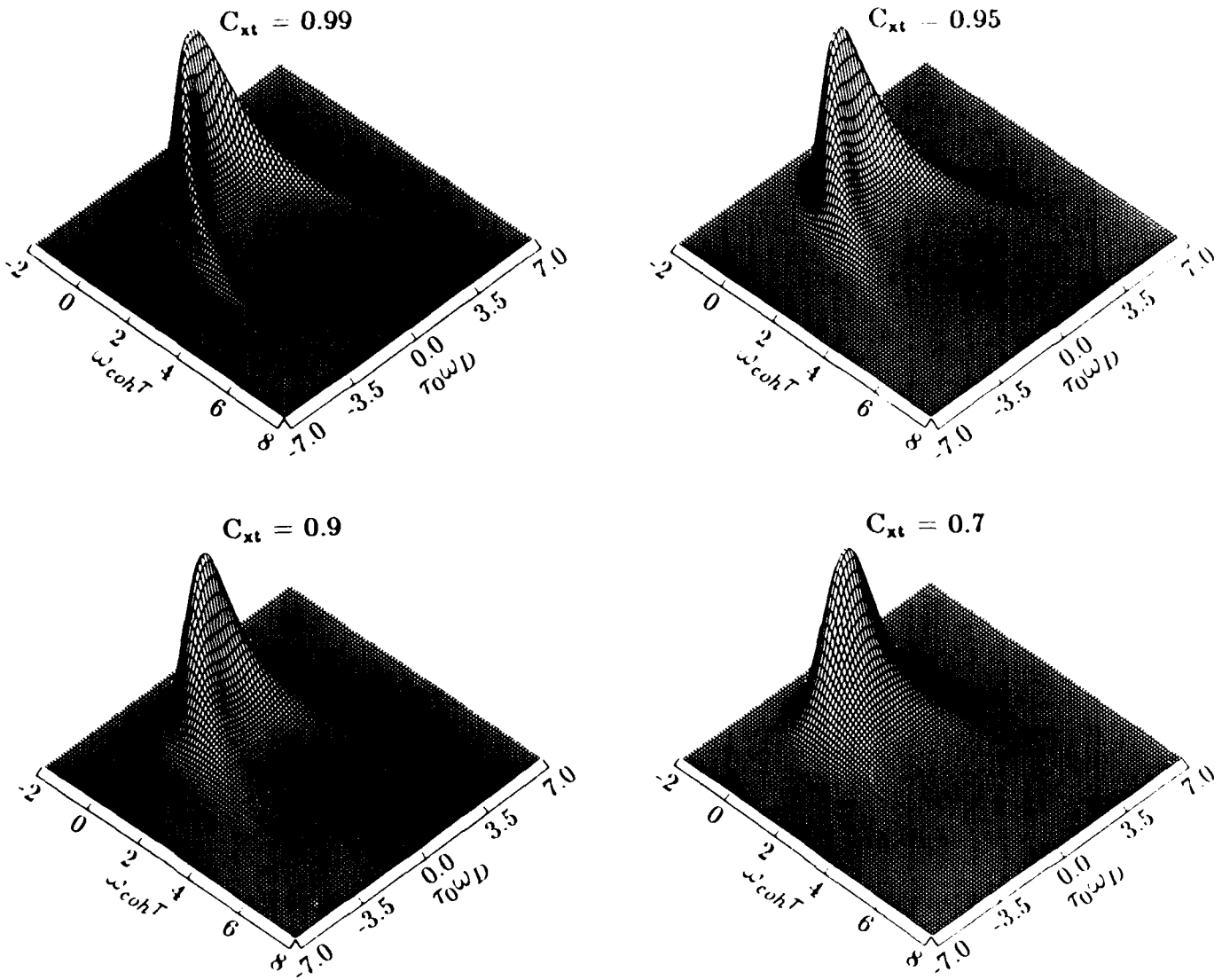


**Figure 6. Scattering functions for the general model.**

$$S_{KD}(K_x,K_y,\omega_D) = \int_0^\infty S(K_x,K_y,\tau,\omega_D)\, d\tau \tag{106}$$

$$= \frac{\pi^{3/2}\ell_x\ell_y\tau_0}{\sqrt{1 - C_{xt}^2 - C_{yt}^2}} \exp\left[-\frac{\tau_0^2\omega_D^2}{4}\right]$$

$$\times \exp\left[-\frac{(K_x\ell_x - C_{xt}\tau_0\omega_D)^2(1 - C_{yt}^2) + (K_y\ell_y - C_{yt}\tau_0\omega_D)^2(1 - C_{xt}^2)}{4(1 - C_{xt}^2 - C_{yt}^2)}\right]$$

$$\times \exp\left[-\frac{2C_{xt}C_{yt}(K_x\ell_x - C_{xt}\tau_0\omega_D)(K_y\ell_y - C_{yt}\tau_0\omega_D)}{4(1 - C_{xt}^2 - C_{yt}^2)}\right].$$

This form of the GPSD shows that, aside from the leading exponential factor, the effect of Doppler frequency is to shift the GPSD in $K_x$-$K_y$ space. Thus it is possible to evaluate Equation 106 for zero Doppler frequency and then to shift the zero point of $K_x$-$K_y$ coordinate system to obtain the GPSD for non-zero Doppler frequencies.

Equation 106 does present a problem due to its $K_x$-$K_y$ cross term. This term makes the evaluation of the signal power in each $K_x$-$K_y$ grid cell computationally difficult and therefore time consuming. Of course a simple rotation can be used to eliminate this term. Thus consider a new coordinate system, $K_p$-$K_q$, where

$$K_p = K_x\cos\vartheta + K_y\sin\vartheta \tag{107}$$

$$K_q = -K_x\sin\vartheta + K_y\cos\vartheta\ .$$

The rotation angle $\vartheta$ between the $K_x$-$K_y$ and $K_p$-$K_q$ coordinate system is chosen to eliminate the $K_p$-$K_q$ cross term. This choice results in the following expression for the tangent of the rotation angle:

$$\tan(2\vartheta) = \frac{2C_{xt}C_{yt}\ell_x\ell_y}{\ell_x^2(1 - C_{xt}^2) - \ell_y^2(1 - C_{yt}^2)}\ . \tag{108}$$

After a little algebra it can be shown that the angular-Doppler GPSD in the $K_p$-$K_q$ coordinate system is

$$S_{KD}(K_p,K_q,\omega_D) = \sqrt{\pi}\tau_0 \exp\left[-\frac{\tau_0^2\omega_D^2}{4}\right] \tag{109}$$

$$\times \frac{\sqrt{\pi}\ell_p}{\sqrt{1 - C_{pt}^2}} \exp\left[-\frac{(K_p\ell_p - C_{pt}\tau_0\omega_D)^2}{4(1 - C_{pt}^2)}\right] \frac{\sqrt{\pi}\ell_q}{\sqrt{1 - C_{qt}^2}} \exp\left[-\frac{(K_q\ell_q - C_{qt}\tau_0\omega_D)^2}{4(1 - C_{qt}^2)}\right]$$

when the following definitions are used:

$$\frac{1}{\ell_p^2} = \frac{\cos^2\vartheta}{\ell_x^2} + \frac{\sin^2\vartheta}{\ell_y^2} \tag{110a}$$

$$\frac{1}{\ell_q^2} = \frac{\sin^2\vartheta}{\ell_x^2} + \frac{\cos^2\vartheta}{\ell_y^2} \tag{110b}$$

$$\frac{C_{pt}}{\ell_p} = \frac{\cos\vartheta\, C_{xt}}{\ell_x} + \frac{\sin\vartheta\, C_{yt}}{\ell_y} \tag{111a}$$

$$\frac{C_{qt}}{\ell_q} = -\frac{\sin\vartheta\, C_{xt}}{\ell_x} + \frac{\cos\vartheta\, C_{yt}}{\ell_y} \quad . \tag{111b}$$

Two key features of the channel modelling technique developed for the general model are the evaluation of the signal power in this rotated coordinate system using simple error functions, and the use of the Doppler shifting property of the GPSD.

## 2.9 IMPULSE RESPONSE FUNCTION AND ANTENNA EFFECTS.

The channel impulse response function of the signal incident on the plane of the receiver and the impulse response function of the signal at the output of an aperture antenna will be discussed in this subsection.

### 2.9.1 Channel Impulse Response function.

Consider a solution $U(\rho,\omega,t)$ to the parabolic wave equation in the plane of the receiver. The dependence of U on propagation distance z has been suppressed because subsequently we will always consider U in the plane of the receiving aperture. The parabolic wave equation solution represents the random effects due to the fluctuating ionosphere on the incident electric field at position $\rho$ and time t from a transmitted monochromatic wave with angular frequency $\omega$. The channel impulse response function of the signal in the receiver plane is [*Knepp and Wittwer* 1984]

$$h(\rho,\tau,t) = \int_{-\infty}^{\infty} U(\rho,\omega+\omega_0,t) \exp\left[i\langle\theta_T(\omega)\rangle + i\omega\tau\right] \frac{d\omega}{2\pi} \tag{112}$$

where $\langle\theta_T(\omega)\rangle$ is the dispersive contribution to the impulse response function resulting from the total electron content (TEC). The impulse response function $h(\rho,\tau,t)$ is defined to be the received signal at time $t + \tau$ and position $\rho$ from a transmitted impulse at time t minus the nominal propagation time (the nominal propagation time is usually set equal to zero).

The term $\exp[i\langle\theta_T(\omega)\rangle]$ in Equation 112 is the transfer function of a smooth ionized plasma and is equal to the exponential term in Equation 17. Thus the smooth plasma transfer function is

$$\langle \theta_T(\omega) \rangle = - \int_{-z_t}^{z_r} \langle k(z) \rangle \, dz = - \frac{\omega}{c} \int_{-z_t}^{z_r} \left[ 1 - \frac{\langle \omega_p^2(z) \rangle}{\omega^2} \right]^{\frac{1}{2}} dz \quad . \tag{113}$$

Because the smooth plasma or dispersive effects represented by $\exp[i\langle \theta_T(\omega) \rangle]$ and the fluctuating plasma effects represented by $U(\rho, z_r, \omega, t)$ appear as the product, it is possible to separately consider these two effects. The dispersive effects will be considered in the next subsection.

If the transmitted signal is a modulated waveform $m_t(t)$, then the signal complex voltage incident on the plane of the receiver is the convolution of the transmitted modulation and the channel impulse response function:

$$u(\rho, t) = \int_{-\infty}^{\infty} m_t(t-\tau) \, h(\rho, \tau, t-\tau) \, d\tau \quad . \tag{114}$$

It is clear from the form of this equation that received signal at time t and delay $\tau$ corresponds to transmitted modulation at time $t - \tau$. The third argument of h in the equation is $t - \tau$ because modulation transmitted at earlier times transits the channel at earlier times. It is generally assumed that the channel varies slowly in time relative to the delay spread of the signal, and $h(\rho, \tau, t-\tau)$ is set equal to $h(\rho, \tau, t)$ in Equation 114. This is strictly true only if the product $f_0\tau_0$ is large. However, the product $f_0\tau_0$ will generally be large under conditions where RF signals can propagate through the ionosphere.

If the delay spread of the impulse response function is larger than the modulation period of $m_t(t)$, then the convolution in Equation 114 will encompass multiple modulation periods. As a result the received signal will contain information from multiple modulation periods. In communications systems this phenomenon is referred to as intersymbol interference.

### 2.9.2 Dispersive Effects.

When the dispersive term $\langle \theta_T(\omega) \rangle$ is expanded in a Taylor series about the carrier radian frequency the result is

$$\langle \theta_T(\omega) \rangle = \langle \theta_T(\omega_0) \rangle - (\omega - \omega_0) \langle \theta_T'(\omega_0) \rangle + \frac{(\omega - \omega_0)^2}{2} \langle \theta_T''(\omega_0) \rangle + \cdots \tag{115}$$

where the first three coefficients in the expansion are

$$\langle \theta_T(\omega_0) \rangle = -\frac{\omega_0}{c} \int_{-z_t}^{z_r} \left[ 1 - \frac{\langle \omega_p^2(z) \rangle}{\omega_0^2} \right]^{\frac{1}{2}} dz \tag{116a}$$

$$\langle \theta_T'(\omega_0) \rangle = \frac{1}{c} \int_{-z_t}^{z_r} \left[ 1 - \frac{\langle \omega_p^2(z) \rangle}{\omega_0^2} \right]^{-\frac{1}{2}} dz \tag{116b}$$

$$\langle \theta_T''(\omega_0) \rangle = -\frac{1}{c} \int_{-z_t}^{z_r} \frac{\langle \omega_p^2(z) \rangle}{\omega_0^3} \left[ 1 - \frac{\langle \omega_p^2(z) \rangle}{\omega_0^2} \right]^{-\frac{3}{2}} dz \quad . \tag{116c}$$

These equations may be expanded using the assumption that the carrier frequency is much larger than the plasma frequency with the results:

$$\langle \theta_T(\omega_0) \rangle \approx -\frac{2\pi R}{\lambda} + \lambda r_e N_T \tag{117a}$$

$$\langle \theta_T'(\omega_0) \rangle \approx \frac{R}{c} + \frac{\lambda^2 r_e N_T}{2\pi c} \tag{117b}$$

$$\langle \theta_T''(\omega_0) \rangle \approx -\frac{\lambda^3 r_e N_T}{2\pi^2 c^2} \tag{117c}$$

where the free space range R and total electron content $N_T$ are given by

$$R = z_t + z_r \tag{118}$$

and

$$N_T = \int_{-z_t}^{z_r} \langle n_e(z) \rangle \, dz \quad . \tag{119}$$

The first terms in Equations 117a and 117b are simply the free space phase shift and propagation time which are proportional to the line-of-sight distance R. The terms proportional to $N_T$ in Equations 117 represent the phase shift, group delay and dispersion due to the mean ionization.

The Doppler shift $f_D$ of the incident signal due to range and TEC dynamics is

$$f_D = \frac{1}{2\pi}\frac{d\langle\theta_T(\omega_0)\rangle}{dt} \approx -\frac{1}{\lambda}\frac{dR}{dt} + \frac{\lambda r_e}{2\pi}\frac{dN_T}{dt} \quad . \tag{120}$$

Note that increasing TEC (positive $dN_T/dt$) increases both the propagation time and the Doppler shift whereas increasing R (positive dR/dt) increases the propagation time but decreases the Doppler shift.

### 2.9.3 Antenna Aperture Effects.

The voltage at the output of an aperture antenna is the spatial convolution of the incident voltage and the aperture weighting function, $A(\rho)$. The received voltage for an antenna located at $\rho_0$ and pointing in the $\mathbf{K}_0$ direction is given by

$$U_A(\rho_0,\omega,t) = \int_{-\infty}^{\infty} U(\rho,\omega,t)\, A(\rho_0-\rho) \exp\left[i\mathbf{K}_0\cdot(\rho_0-\rho)\right] d^2\rho \tag{121}$$

where the subscript A denotes the voltage at the output of the antenna. The z dependence of $U_A$ has been suppressed because it is understood that this voltage is at the plane of the receiver. It is assumed that the aperture weighting function is independent of frequency. This is generally true for a range of frequencies about the carrier frequency that is larger than the signal bandwidth.

In order to relate the GPSD of $U_A$ to the GPSD of the incident signal, the two-position, two-frequency, two-time mutual coherence function of $U_A$ is required. The mutual coherence function of the signal out of the antenna is

$$\Gamma_A(\rho,\omega,t) = \langle U_A(\rho_1,\omega_1,t_1)U_A^*(\rho_2,\omega_2,t_2)\rangle \tag{122}$$

$$= \int_{-\infty}^{\infty} d^2\rho' \int_{-\infty}^{\infty} d^2\rho'' \langle U(\rho',\omega_1,t_1)U^*(\rho'',\omega_2,t_2)\rangle$$

$$\times\ A(\rho'-\rho_1)A^*(\rho''-\rho_2) \exp\left[i\mathbf{K}_0\cdot(\rho_1 - \rho' - \rho_2 + \rho'')\right] \quad .$$

For statistically stationary processes the expectation of $U_AU_A^*$ must be a function only of the differences $\rho = \rho_1 - \rho_2$, $\omega = \omega_1 - \omega_2$, and $t = t_1 - t_2$, and the expectation of $UU^*$ in the integrand must be a function only of the differences $\rho' - \rho''$, $\omega$, and t.

The aperture weighting function can be written in terms of the voltage beam pattern $g(\mathbf{K}_\perp)$ using the Fourier transform relationship

$$A(\rho) = \int_{-\infty}^{\infty} g(\mathbf{K}_\perp) \exp\left(i\mathbf{K}_\perp\cdot\rho\right) \frac{d^2\mathbf{K}_\perp}{(2\pi)^2} \quad . \tag{123}$$

Upon substituting this equation for both aperture weighting functions in the expression for the mutual coherence function, changing variables from $\rho'$ to $\mathbf{r} = \rho' - \rho''$, and changing the order of integration, Equation 122 becomes

$$\Gamma_A(\rho,\omega,t) = \exp(i\mathbf{K}_0\cdot\rho) \int_{-\infty}^{\infty} d^2\mathbf{r}\, \Gamma(\mathbf{r},\omega,t) \exp(-i\mathbf{K}_0\cdot\mathbf{r}) \tag{124}$$

$$\times \int_{-\infty}^{\infty} \frac{d^2K'}{(2\pi)^2}\, g(\mathbf{K}') \exp[i\mathbf{K}'\cdot(\rho_1 - \mathbf{r})] \int_{-\infty}^{\infty} \frac{d^2K''}{(2\pi)^2}\, g^*(\mathbf{K}'') \exp(-i\mathbf{K}''\cdot\rho_2)$$

$$\times \int_{-\infty}^{\infty} d^2\rho''\, \exp[i(\mathbf{K}'' - \mathbf{K}')\cdot\rho''] \ .$$

The last integral in this expression is equal to $(2\pi)^2\, \delta(\mathbf{K}''-\mathbf{K}')$, and the $\mathbf{K}''$ integral may be performed directly. Another change in the order of integration yields

$$\Gamma_A(\rho,\omega,t) = \exp(i\mathbf{K}_0\cdot\rho) \int_{-\infty}^{\infty} \frac{d^2K'}{(2\pi)^2}\, G(\mathbf{K}') \exp(i\mathbf{K}'\cdot\rho) \tag{125}$$

$$\times \int_{-\infty}^{\infty} d^2\mathbf{r}\, \Gamma(\mathbf{r},\omega,t) \exp[-i(\mathbf{K}' + \mathbf{K}_0)\cdot\mathbf{r}] \ .$$

The quantity

$$G(\mathbf{K}) = g(\mathbf{K})g^*(\mathbf{K}) \tag{126}$$

is the power beam pattern of the antenna.

The mutual coherence function $\Gamma(\mathbf{r},\omega,t)$ of the signal incident on the plane of the antenna that appears in the second integral of Equation 125 is the product of the free space term $\Gamma_0$ (Eqn. 43) and the stochastic term $\Gamma_1$. The free space term may be pulled out of the second integral if it is assumed not to vary over the face of the antenna. This is equivalent to assuming that any deviations from a plane wave in the incident signal are due to scattering effects in the ionosphere and are not due to geometrical effects. After the free space term is pulled out of the integral, $\Gamma_A$ may be assumed to represent only the stochastic fluctuations of the received signal.

Now the GPSD of the signal out of the antenna can be computed by taking the appropriate Fourier transforms (see Equation 84) from $\rho$, $\omega$, and t to $\mathbf{K}_\perp$, $\tau$, and $\omega_D$ respectively. After performing the $\omega$ to $\tau$ and t to $\omega_D$ transforms and rearranging terms, the GPSD at the antenna output is

$$S_A(\mathbf{K}_\perp,\tau,\omega_D) = \int_{-\infty}^{\infty} \frac{d^2\mathbf{K}'}{(2\pi)^2} G(\mathbf{K}') \int_{-\infty}^{\infty} d^2\mathbf{r}\ \hat{\Gamma}(\mathbf{r},\tau,\omega_D) \exp\left[-i(\mathbf{K}'+\mathbf{K}_0)\cdot\mathbf{r}\right]$$

$$\times \int_{-\infty}^{\infty} d^2\rho \exp\left[i(\mathbf{K}'-\mathbf{K}_\perp+\mathbf{K}_0)\cdot\rho\right] . \qquad (127)$$

The last integral in this equation is just $(2\pi)^2\,\delta(\mathbf{K}'-\mathbf{K}_\perp+\mathbf{K}_0)$. Using this delta function to perform the $\mathbf{K}'$ integral results in:

$$S_A(\mathbf{K}_\perp,\tau,\omega_D) = G(\mathbf{K}_\perp-\mathbf{K}_0) \int_{-\infty}^{\infty} d^2\mathbf{r}\ \hat{\Gamma}(\mathbf{r},\tau,\omega_D) \exp(-i\mathbf{K}_\perp\cdot\mathbf{r}) \qquad (128)$$

where the remaining integral in this expression is just $S(\mathbf{K}_\perp,\tau,\omega_D)$. The GPSD of the signal out of the antenna is then

$$S_A(\mathbf{K}_\perp,\tau,\omega_D) = G(\mathbf{K}_\perp-\mathbf{K}_0)\, S(\mathbf{K}_\perp,\tau,\omega_D) . \qquad 129)$$

As expected, the effect of an antenna is to modify the incident power as a function of angle. This result will be used throughout the rest of this report.

The effect of antenna filtering is illustrated in Figure 7 which shows four plots of the GPSD at the outputs of four uniformly-weighted circular antennas (with diameter D) for isotropic scattering ($\ell_x = \ell_y = \ell_0$). The antennas in this example are all pointed along the line-of-sight. The plot in the upper left is the same as in Figure 4 and is for a point antenna ($D << \ell_0$), for which there is no antenna filtering. The other three plots in the figure are for cases where the ratio of the antenna diameter to the decorrelation distance is equal to 1, 2, and 4. As the antenna size increases for a given value of $\ell_0$ or, equivalently, as the decorrelation distance decreases for a given antenna diameter, more of the incident signal with large angles-of-arrival is filtered out of the received signal. The effect of this on the mean received power, frequency selective bandwidth, and decorrelation time of the signal out of the antenna will be discussed next.

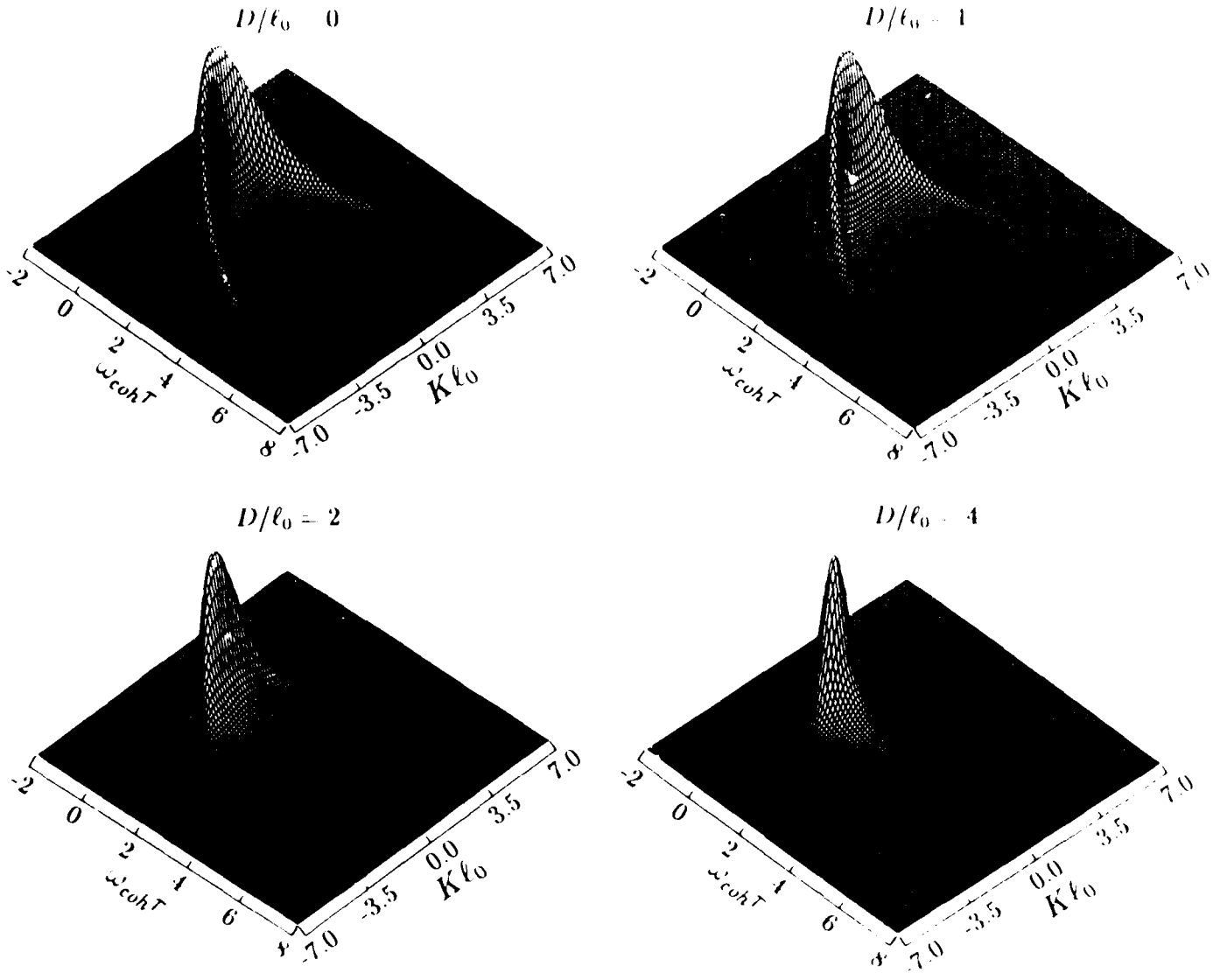


**Figure 7. Generalized power spectra at the outputs of circular antennas.**

# SECTION 3
# ANTENNA FILTERING EFFECTS

An antenna beam pattern acts as an angular filter of the received signal power. Because of this, the mean power, decorrelation time, and frequency selective bandwidth of the signal at the output of an antenna are different than those of the incident signal. The reduction in mean power is a direct consequence of the attenuation of the signal arriving outside of the main beam of the antenna. If the antenna is pointed along the line-of-sight, the signal that is attenuated by the antenna is that with large angles-of-arrival and hence large times-of-arrival. Thus the effect of an antenna pointed along the line-of-sight is to reduce the delay spread of the signal. When the same antenna is pointed away from the line-of-sight, however, its effect on the delay spread of the output signal can be quite different, as will be shown in this section.

Depending on the values of the correlation coefficients $C_{xt}$ and $C_{yt}$, the antenna may also filter the decorrelation time. In the fully turbulent case, the signal at all angles-of-arrival has the same effective decorrelation time, and hence an antenna has no effect on the decorrelation time of the output signal. However in the frozen-in case the effective decorrelation time of the signal varies with angle-of-arrival, and an antenna can strongly filter the decorrelation time. This filtering results in a signal that is more slowly varying at the antenna output than it is on the face of the antenna.

The effects of aperture antennas with arbitrary beamwidths and pointing angles will be considered in this section. The antenna beam patterns for uniformly-weighted circular or rectangular apertures and for Gaussian apertures are described in Section 3.1. Then the filtering equations for mean power, spatial and temporal decorrelation properties, and frequency selective bandwidth of the signal out of a Gaussian antenna with arbitrary beamwidths and pointing angles are given in Section 3.2. Many of these results have been derived previously by *Frasier* [1988] and are just reproduced here.

An example is given in Section 3.3. Here the antenna is assumed to be circular with uniform weighting, and the scattering is assumed to be isotropic ($\ell_x = \ell_y = \ell_0$). The filtering equations for this case are plotted versus the ratio of the antenna diameter to the decorrelation distance for a range of pointing angles. This example illustrates most of the important effects of antenna filtering.

## 3.1 ANTENNA DESCRIPTIONS.

The coordinate systems for the propagation and the antenna are shown in Figure 8. The z axis is along the line-of-sight, and it is assumed that the face of the antenna is in the x-y plane. Note that for a receiving antenna we have reversed the direction of the z axis in the figure from pointing in the direction of propagation to pointing back toward the transmitter. This is done because it is usual for antenna coordinate systems to point out of rather than into an aperture. The beam of the antenna in the figure is pointed away from the line-of-sight in the direction $\mathbf{K}_0$ defined by a pointing direction elevation angle $\Theta_0$ (measured from the $\hat{z}$ axis) and an azimuth angle $\Phi_0$ (measured from the $\hat{u}$ axis). The rotation angle $\Psi$ is the angle between the scattering $\hat{x}$ axis and the antenna $\hat{u}$ axis.

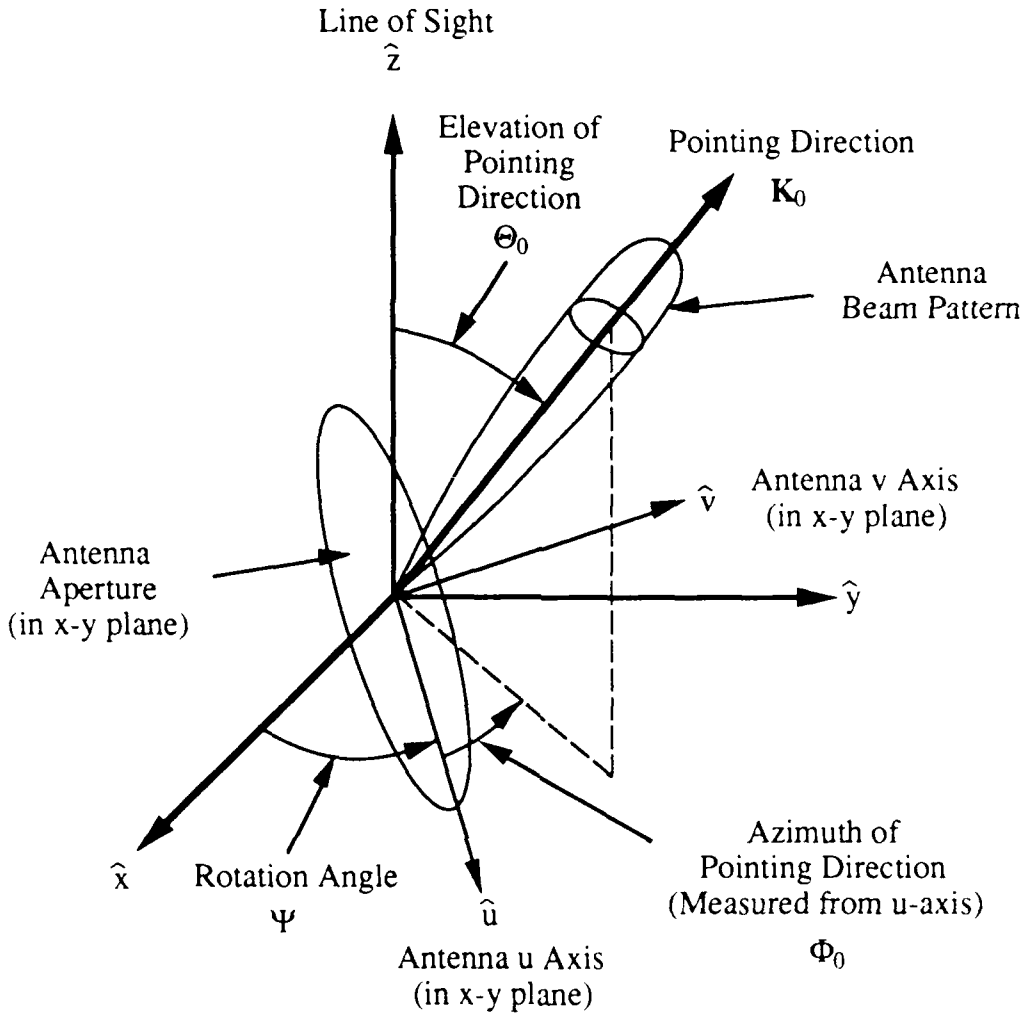


**Figure 8. Propagation and antenna coordinate systems.**

The antenna $(\hat{u}\text{-}\hat{v})$ coordinate system, where $\hat{v}$ is in the x-y plane and is orthogonal to $\hat{u}$, is chosen for convenience in describing the antenna beam pattern. For example, if the antenna is rectangular, the $(\hat{u}\text{-}\hat{v})$ axes should be aligned with the sides of the aperture. It is assumed that the antenna beam pattern is separable in $(\hat{u}\text{-}\hat{v})$ coordinates. Thus the two-dimensional beam pattern $G(\theta_u,\theta_v)$ is approximated by the product $G(\theta_u)G(\theta_v)$ where $\theta_u$ and $\theta_v$ are angles about the u and v axes respectively. In many cases the $\hat{u}$ axis will be parallel to the local earth tangent plane.

In general the face of the antenna will not lie in the x-y plane. However for satellite communications links it is usual for the satellite position to be known accurately through ephemeris data and for an antenna to be dedicated to a single link. Thus it is likely that the angle between the antenna boresight direction and the line-of-sight will be small, and the cosine squared effects of this angle may be ignored. If these angles are not small, then in the developments that follow the antenna size is the projection onto the x-y plane and the antenna beamwidths must include the effects of beam broadening as the beam is pointed away from boresight.

### 3.1.1 Gaussian Beam Profiles.

The antenna beam pattern is assumed to be separable in the u-v coordinate system. The Gaussian antenna beam pattern is then

$$G(K_u,K_v) = \exp\left[-\alpha_u^2(K_u-K_{0u})^2 - \alpha_v^2(K_v-K_{0v})^2\right] \tag{130}$$

where $K_{0u}$ and $K_{0v}$ are components of the pointing vector. The peak gain G(0,0) in this equation has been set to unity because this value is usually included in the calculation of the mean received power. The components of the pointing vector in the u-v plane, $K_{0u}$ and $K_{0v}$, are:

$$K_{0u} = \frac{2\pi}{\lambda}\sin\Theta_0\cos\Phi_0 \tag{131a}$$

$$K_{0v} = \frac{2\pi}{\lambda}\sin\Theta_0\sin\Phi_0 \ . \tag{131b}$$

For either the u or the v direction, the antenna beam pattern for pointing along the line-of-sight can also be written as

$$G(\theta) = \exp\left[-\ln 2\left(\frac{2\theta}{\theta_0}\right)^2\right] \tag{132}$$

where $\theta_0$ is the 3-dB beamwidth (i.e., full width at half maximum). Equating the two patterns gives

$$\alpha_u^2 = \frac{\ln 2\ \lambda^2}{\pi^2\theta_{0u}^2} \tag{133}$$

where $\theta_{0u}$ is the 3-dB beamwidth in the u-direction. A similar expression holds for $\alpha_v^2$ which relates this parameter to the 3-dB beamwidth in the v-direction, $\theta_{0v}$.

### 3.1.2 Uniformly Weighted Circular Apertures.

For a uniformly-weighted circular aperture, the aperture weighting function is

$$A(\rho) = \begin{cases} \frac{1}{a} & \text{if } |\rho| \le \frac{D}{2} \\ 0 & \text{otherwise} \end{cases} \tag{134}$$

where D is the diameter of the circular aperture. The value of a is chosen so that the peak antenna gain is unity. The voltage antenna gain pattern $g(\mathbf{K}_\perp)$ is related to the aperture distribution function by the Fourier transform

$$g(\mathbf{K}_\perp) = \int_{-\infty}^{\infty} \exp(-i\mathbf{K}_\perp \cdot \rho)\, A(\rho)\, d^2\rho \quad . \tag{135}$$

With $\rho$ confined to the plane of the aperture, the dot product $\mathbf{K}_\perp \cdot \rho$ is

$$\mathbf{K}_\perp \cdot \rho = kr \sin\theta \sin\varphi \tag{136}$$

where $\theta$ is the angle from the normal to the aperture, $\varphi$ is the azimuth angle, $k = 2\pi/\lambda$, and $r = |\rho|$. The Fourier transform then becomes

$$g(\theta) = \frac{1}{a} \int_0^{D/2} dr\; r \int_{-\pi}^{\pi} d\varphi \exp(-ikr \sin\theta \sin\varphi) \quad . \tag{137}$$

Performing the indicated integrals results in the well known form for the power beam pattern

$$G(\theta) = g(\theta)g^*(\theta) = \frac{4J_1^2[\pi(D/\lambda)\sin\theta]}{[\pi(D/\lambda)\sin\theta]^2} \tag{138}$$

where $J_1$ is the Bessel function, and where $G(0) = 1$ when the value of a is chosen to be the area of the aperture, $\pi D^2/4$.

The 3-dB (full width at half maximum) beamwidth [i.e. $G(\theta_0/2) = 1/2$] is given by solving the equation

$$\frac{4J_1^2(x)}{x^2} = \frac{1}{2} \tag{139}$$

with the result $x = 1.616340$. Assuming that the beamwidth is small so $\sin(\theta_0/2) \approx \theta_0/2$, the beamwidth in terms of the diameter D is

$$\theta_0 = 1.02899 \frac{\lambda}{D} \text{ radians} \quad . \tag{140}$$

If the uniformly-weighted circular antenna beam pattern is approximated by a Gaussian pattern with the same 3-dB beamwidth, then the $\alpha$ coefficients that appear in Equation 129 are

$$\alpha_u^2 = \alpha_v^2 = \frac{(\ln 2)D^2}{(1.02899\pi)^2} \quad . \tag{141}$$

### 3.1.3 Uniformly Weighted Rectangular Apertures.

For uniformly-weighted rectangular apertures, the aperture weighting function is

$$A(u,v) = \begin{cases} \frac{1}{a} & \text{if } |u| \le \frac{D_u}{2} \text{ and } |v| \le \frac{D_v}{2} \\ 0 & \text{otherwise} \end{cases} \tag{142}$$

where $D_u$ and $D_v$ are the lengths of the aperture in the u and v directions respectively. In this case, the Fourier transform indicated in Equation 135 gives the result

$$G(\theta_u,\theta_v) = G(\theta_u)\, G(\theta_v) \tag{143}$$

where $G(\theta_u)$ has the familiar $\sin^2(x)/x^2$ form:

$$G(\theta_u) = \frac{\sin^2 [\pi(D_u/\lambda)\sin\theta\xi]}{[\pi(D_u/\lambda)\sin\theta_u]^2} \quad . \tag{144}$$

A similar expression holds for $G(\theta_v)$. The normalization a of the aperture weighting function is just the area $D_uD_v$ of the rectangular antenna. The 3-dB beamwidth is given by solving the equation

$$\frac{\sin^2(x)}{x^2} = \frac{1}{2} \tag{145}$$

with the result x = 1.391557. The u and v beamwidths in terms of the antenna sizes $D_u$ and $D_v$ are then given by

$$\theta_{0u} = 0.885893\,\frac{\lambda}{D_u} \qquad \theta_{0v} = 0.885893\,\frac{\lambda}{D_v} \qquad \text{(radians)} \tag{146}$$

assuming that $\sin(\theta_0/2) \approx \theta_0/2$. If this beam pattern is approximated by a Gaussian pattern with the same 3-dB beamwidth, the $\alpha$ coefficients that appear in Equation 130 are

$$\alpha_u^2 = \frac{(\ln 2)D_u^2}{(0.885893\pi)^2} \qquad \alpha_v^2 = \frac{(\ln 2)D_v^2}{(0.885893\pi)^2} \quad . \tag{147}$$

## 3.2 FILTERING EQUATIONS.

The filtering equations relate the statistics of the signal at the outputs of one or more antennas to the statistics of the signal incident on the antennas. The statistics that are considered in this section are the mean power, frequency selective bandwidth, decorrelation distances, and decorrelation time of the signal out of an antenna and the cross correlation of the signals out of two separate antennas. Gaussian beam patterns will be assumed for mathematical convenience. An elegant derivation of most of the equations given in this section may be found in *Frasier* [1988].

The severity of the filtering effects is determined by the relative size of the standard deviation of the angle-of-arrival fluctuations $\sigma_\theta$ and the antenna beamwidths. When $\sigma_\theta$ is small compared to the antenna beamwidths, the signal arrives essentially at the peak of the beam pattern, if the pointing error is small, and the filtering effects are small. However, if $\sigma_\theta$ is large compared to the beamwidths, much of the signal arrives at angles outside of the main lobe of the antenna beam pattern and the filtering effects are large. Equivalently, large values of the ratio $\sigma_\theta/\theta_0$ correspond to situations where the decorrelation distance of the incident signal is small compared to the antenna size and the incident electric field as seen by the aperture is no longer a plane wave. In this situation, the induced voltages across the face of the aperture do not add coherently when summed together by the antenna with a loss in signal power as a result.

In the next subsections, expressions will be presented for the mean power, frequency selective bandwidth, decorrelation time, and decorrelation distances of the signal at the output of an antenna. Clearly the numerical value of these quantities must be independent of the choice of coordinate systems (e.g., x-y or u-v coordinates) and *Frasier* [1988] has derived expression for these quantities which are coordinate-system independent. However evaluation of the filtering equations requires a choice of coordinate systems, and the x-y systems will be used here.

Before presenting the filtering equations, it is convenient to define some quantities that are common to all these equations:

$$Q_x = 1 + \frac{4\alpha_u^2}{\ell_x^2}\cos^2\Psi + \frac{4\alpha_v^2}{\ell_x^2}\sin^2\Psi \tag{148}$$

$$Q_y = 1 + \frac{4\alpha_u^2}{\ell_y^2}\sin^2\Psi + \frac{4\alpha_v^2}{\ell_y^2}\cos^2\Psi \tag{149}$$

$$Q_{xy} = \frac{4(\alpha_u^2 - \alpha_v^2)}{\ell_x \ell_y}\cos\Psi \sin\Psi \tag{150}$$

$$Q_0 = \sqrt{Q_x Q_y - Q_{xy}^2}\ . \tag{151}$$

The components of the pointing vector in the x-y coordinate system are also required and are obtained from their form in the u-v coordinate system (Eqn. 131) using a simple rotation:

$$K_{0x} = \frac{2\pi}{\lambda}\sin\Theta_0 \cos(\Phi_0+\Psi) \tag{152a}$$

$$K_{0y} = \frac{2\pi}{\lambda}\sin\Theta_0 \sin(\Phi_0+\Psi)\ . \tag{152b}$$

### 3.2.1 Scattering Loss.

The mean power of the signal out of an antenna is calculated using the expression:

$$P_A = \int_{-\infty}^{\infty} \frac{d^2\mathbf{K}_\perp}{(2\pi)^2} \int_{-\infty}^{\infty} d\tau \int_{-\infty}^{\infty} \frac{d\omega_D}{2\pi} G(\mathbf{K}_\perp - \mathbf{K}_0)\, S(\mathbf{K}_\perp, \tau, \omega_D) \tag{153}$$

which gives the result

$$P_A = \frac{1}{Q_0} \exp\left[ - \left(1 - \frac{Q_y}{Q_0^2}\right) \frac{K_{0x}^2 \ell_x^2}{4} - \left(1 - \frac{Q_x}{Q_0^2}\right) \frac{K_{0y}^2 \ell_y^2}{4} - \frac{Q_{xy}}{2Q_0^2} K_{0x} \ell_x K_{0y} \ell_y \right] . \tag{154}$$

The first term in this equation, $1/Q_0$, is just the mean received power when the antenna is pointed along the line-of-sight.

In the limit that both decorrelation distances are large relative to the size of the antenna only the exponential term in the expression for $P_A$ differs from unity, and the expression for the mean received power reduces to

$$\underset{\substack{\ell_x \to \infty \\ \ell_y \to \infty}}{\text{Limit}} P_A = \exp\left[-\left(\alpha_u^2 K_{0u}^2 + \alpha_v^2 K_{0v}^2\right)\right] \tag{155}$$

which is equal to the antenna beam gain in the direction of the line-of-sight.

The scattering loss of the antenna in decibels is

$$L_S\,(\text{dB}) = -10 \log_{10}(P_A) . \tag{156}$$

This loss therefore includes both the loss in the mean received power due to scintillation and the loss due to the fact that the antenna may be pointed away from the line-of-sight.

### 3.2.2 Frequency Selective Bandwidth.

The frequency selective bandwidth is defined in Section 2.8.2 in terms of the time delay jitter of the signal. At the output of an antenna, these moments are given by

$$P_A\langle\tau^n\rangle = \int_{-\infty}^{\infty} \frac{d^2\mathbf{K}_\perp}{(2\pi)^2} \int_{-\infty}^{\infty} d\tau\, \tau^n \int_{-\infty}^{\infty} \frac{d\omega_D}{2\pi} G(\mathbf{K}_\perp - \mathbf{K}_0)\, S(\mathbf{K}_\perp, \tau, \omega_D) . \tag{157}$$

Straightforward evaluation of the indicated integrals for n equal to 1 and 2 is indeed a formidable algebraic task. However *Frasier* [1988] gives surprisingly simple-appearing expressions for $\sigma_\tau$ and the antenna-filtered value of the frequency selective bandwidth, $f_A$, which are independent of the choice of the coordinate system. In terms

of the notation used in this report, the expression for $f_A$ is somewhat more complicated and is

$$\frac{f_A}{f_0} = \frac{\left[\frac{\ell_x^4+\ell_y^4}{\ell_x^2\ell_y^2}\right]^{\frac{1}{2}} Q_0^2}{\left[\frac{\ell_x^2 Q_x^2}{\ell_y^2} + \frac{\ell_y^2 Q_y^2}{\ell_x^2} + 2Q_{xy}^2 + P\right]^{\frac{1}{2}}} \tag{158}$$

where the term P gives the effects of antenna pointing. This pointing angle term may be written as:

$$P = P_x K_{0x}^2 \ell_x^2 + P_y K_{0y}^2 \ell_y^2 + P_{xy} K_{0x} \ell_x^2 K_{0y} \ell_y^2 \tag{159}$$

where

$$P_x = 2Q_{xy}^2(1-Q_x) + \frac{Q_y \ell_y^2 (Q_0^2-Q_y)^2}{Q_0^2 \ell_x^2} + \frac{Q_x Q_{xy}^2 \ell_x^2}{Q_0^2 \ell_y^2} \tag{160a}$$

$$P_y = 2Q_{xy}^2(1-Q_y) + \frac{Q_x \ell_x^2 (Q_0^2-Q_x)^2}{Q_0^2 \ell_y^2} + \frac{Q_y Q_{xy}^2 \ell_y^2}{Q_0^2 \ell_x^2} \tag{160b}$$

$$P_{xy} = Q_{xy}\left[(Q_x-1)(1-Q_y) - Q_{xy}^2 + \frac{Q_x \ell_x^2 (Q_0^2-Q_x)}{Q_0^2 \ell_y^2} + \frac{Q_y \ell_y^2 (Q_0^2-Q_y)}{Q_0^2 \ell_x^2}\right] . \tag{160c}$$

### 3.2.3 Decorrelation Time.

The temporal coherence function of the signal out of an antenna is given by

$$P_A \Gamma_A(t) = \int_{-\infty}^{\infty} \frac{d\mathbf{K}_\perp}{(2\pi)^2} \int_{-\infty}^{\infty} d\tau \int_{-\infty}^{\infty} \frac{d\omega_D}{2\pi} \exp(-i\omega_D t)\, S_A(K_x, K_y, \tau, \omega_D) . \tag{161}$$

In general, the temporal coherence function is complex when the pointing angle is non-zero because antenna pointing results in a mean Doppler shift of the output signal. The antenna-filtered decorrelation time $\tau_A$ is then calculated by finding the 1/e point of $|\Gamma_A(t)|$ with the result

$$\frac{\tau_A}{\tau_0} = \frac{1}{\left[1 - C_{xt}^2 - C_{yt}^2 + \frac{C_{xt}^2 Q_y + C_{yt}^2 Q_x - 2C_{xt}C_{yt}Q_{xy}}{Q_0^2}\right]^{\frac{1}{2}}} . \tag{162}$$

In the turbulent limit (i.e., $C_{xt} = 0$ and $C_{yt} = 0$),

$$\frac{\tau_A}{\tau_0} = 1 \qquad \text{(Turbulent Model)} \tag{163}$$

and in the frozen-in limit (i.e., $C_{xt} = 1$ and $C_{yt} = 0$)

$$\frac{\tau_A}{\tau_0} = \frac{Q_0}{\sqrt{Q_y}} . \qquad \text{(Frozen-in Model)} \qquad (164)$$

It is interesting to note that the antenna-filtered decorrelation time is not explicitly dependent on pointing angle, but does depend on the ratio of the antenna beamwidth and the standard deviation of the angular scattering through the Q factors. Of course as a phased array antenna beam is scanned away from boresight, the effective aperture size will decrease thereby broadening the beamwidth and implicitly changing the value of the filtered decorrelation time.

The mean Doppler shift $\omega_A$ due to antenna pointing is

$$\omega_A = \frac{[C_{xt}(Q_0^2-Q_y)-C_{yt}Q_{xy}]K_{0x}\ell_x - [C_{yt}(Q_0^2-Q_x)-C_{xt}Q_{xy}]K_{0y}\ell_y}{\tau_0 Q_0^2} . \qquad (165)$$

This quantity is clearly equal to zero for the turbulent model. For non-zero values of the space-time correlation coefficients, the mean Doppler shift is proportional to the components of the pointing vector.

### 3.2.4 Decorrelation Distances.

The x-direction decorrelation distance of the signal out of the antenna is given by the 1/e point of $\Gamma_A(x)$ where

$$P_A\Gamma_A(x) = \int_{-\infty}^{\infty}\frac{dK_y}{2\pi}\int_{-\infty}^{\infty}d\tau\int_{-\infty}^{\infty}\frac{d\omega_D}{2\pi}\int_{-\infty}^{\infty}\frac{dK_x}{2\pi}\exp(iK_x x)\, S_A(K_x,K_y,\tau,\omega_D) . \qquad (166)$$

A similar expression holds for $\Gamma_A(y)$. These two expression give the following results for the decorrelation distances $\ell_{Ax}$ and $\ell_{Ay}$ of the signal at the antenna output:

$$\frac{\ell_{Ax}}{\ell_x} = \frac{Q_0}{\sqrt{Q_y}} \qquad (167)$$

$$\frac{\ell_{Ay}}{\ell_y} = \frac{Q_0}{\sqrt{Q_x}} . \qquad (168)$$

The interpretation of these quantities is that $\ell_{Ax}$ and $\ell_{Ay}$ are the distances in the x- or y-direction respectively that the antenna must be instantaneously displaced in order for the normalized cross correlation of the output signal to have a value of 1/e. As was the case for the antenna-filtered decorrelation time, these quantities do not explicitly depend on pointing angle.

## 3.3 ISOTROPIC EXAMPLE.

An isotropic example is presented in this section to illustrate some of the effects of the antenna on the parameters discussed above. For this example, both the angular scattering and the antenna beam pattern will be assumed to be isotropic, so

$$\ell_x = \ell_y = \ell_0 \tag{169}$$

and

$$\alpha_u^2 = \alpha_v^2 = \frac{\ln 2\, \lambda^2}{\pi^2 \theta_0^2} \ . \tag{170}$$

Without further loss of generality, it can be assumed that the antenna is pointed in the x-direction and that the rotation angle is zero. The components of the pointing vector are then given by

$$K_{0x} = \frac{2\pi}{\lambda} \sin \Theta_0 \tag{171a}$$

$$K_{0y} = 0 \ . \tag{171b}$$

With these assumptions the Q factors become

$$Q_x = Q_y = Q = 1 + \frac{4 \ln 2}{\pi \theta_0^2} \frac{\lambda^2}{\ell_0^2} \tag{172a}$$

$$Q_{xy} = 0 \ . \tag{172b}$$

At this point it is convenient to write the antenna beamwidth in terms of the antenna size in order to eliminate the explicit dependence of the Q factors on carrier wavelength:

$$\theta_0 = a_0 \frac{\lambda}{D} \tag{173}$$

where, for uniformly-weighted antennas,

$$a_0 = \begin{cases} 1.02899 & \text{Circular antenna} \\ 0.885893 & \text{Square antenna} \end{cases} \tag{174}$$

The Q factor can then be written as

$$Q = \begin{cases} 1 + 0.265 \dfrac{D^2}{\ell_0^2} & \text{Circular antenna} \\ 1 + 0.358 \dfrac{D^2}{\ell_0^2} & \text{Square antenna} \end{cases} \tag{175}$$

The mean received power for isotropic scattering and an isotropic antenna is

$$P_A = \frac{1}{Q} \exp\left[ - \frac{a_0^2 \pi^2 (Q-1)}{Q} \frac{\Theta_0^2}{\theta_0^2} \frac{\ell_0^2}{D^2} \right] \tag{176}$$

when the pointing angle is assumed to be small compared to one radian so $\sin\Theta_0$ is approximately equal to $\Theta_0$. For a given value of $\ell_0/D$ (i.e., for a fixed value of Q) the effect of antenna pointing, as expected, is to monotonically decrease the mean received power as the antenna beam is pointed farther away from the line-of-sight. In the limit that the decorrelation distance is much larger than the antenna diameter, the Q factor approaches unity and the mean received power is approximately equal to 1/Q independent of pointing angle. In other words, when the angular scattering standard deviation is large compared to the antenna beamwidth and the pointing angle, the mean power is insensitive to the location of the beam peak relative to the line-of-sight.

The scattering loss $L_S$ ($L_S = 1/P_A$) for a uniformly-weighted circular antenna is plotted in Figure 9 versus the ratio $\ell_0/D$ when the pointing angle of the antenna beam is 0, $\theta_0/2$ and $\theta_0$. It is assumed for this example that the beamwidth remains constant as the beam in pointed away from the line-of-sight. When the decorrelation distance is large compared to the antenna diameter, the curves approach the line-of-sight loss of beam (0 dB for a pointing angle equal to zero, 3 dB for a pointing angle equal to one-half beamwidth, and 12 dB for a pointing angle equal to a full beamwidth). When the decorrelation distance is small compared to the antenna diameter, the angle-of-arrival spread of the incident signal is large compared to the beamwidth, so, as mentioned above, the scattering loss is insensitive to pointing angle as long as the pointing angle remains within a few beamwidths of the line-of-sight. Between these two limits, the scattering loss of a beam pointed away from the line-of-sight may actually decrease with decreasing $\ell_0/D$ as the signal is scattered away from the line-of-sight and into the main lobe of the antenna.

The equation for the ratio of the filtered to unfiltered frequency selective bandwidth, $f_A/f_0$, for this isotropic example is

$$\frac{f_A}{f_0} = \left[ \frac{Q^3}{Q + 2a_0^2 \pi^2 (Q-1)^2 \frac{\Theta_0^2}{\theta_0^2} \frac{\ell_0^2}{D^2}} \right]^{\frac{1}{2}} . \tag{177}$$

It is interesting to note that when the pointing angle is zero the ratio $f_A/f_0$ is equal to Q which is also equal to the scattering loss in this case. Figure 10 shows plots of the ratio $f_A/f_0$ as a function of the ratio $\ell_0/D$ for a uniformly-weighted circular antenna and for three pointing angles.

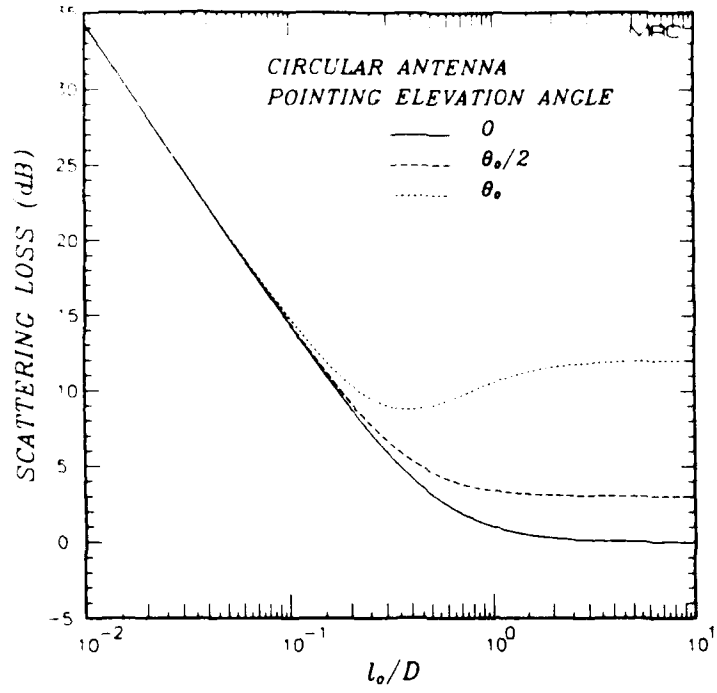


**Figure 9. Scattering loss for a uniformly-weighted circular antenna and isotropic scattering.**

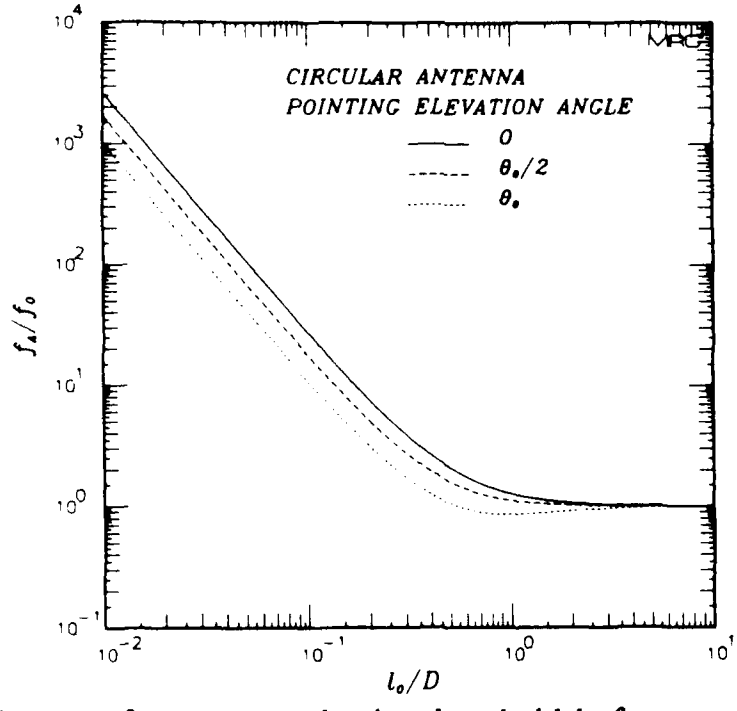


**Figure 10. Filtered frequency selective bandwidth for a uniformly-weighted circular antenna and isotropic scattering.**

For an antenna pointed along the line-of-sight, the potentially beneficial effect of antenna filtering is that the signal which is filtered out is that which arrives at relatively large delays. It is this delayed signal that causes most of the intersymbol interference in the detection and demodulation of wide bandwidth signals. Stated another way, because the antenna filters out much of the delayed signal, and since the frequency selective bandwidth is an inverse measure of the signal delay spread, the filtering increases the frequency selective bandwidth of the output signal relative to that at the antenna input.

Clearly the situation is different if the antenna is pointed away from the line-of-sight. The ratio $f_A/f_0$ is less than unity for non-zero pointing angles and values of $\ell_0/D$ between about 0.1 and 1.0. This implies that the standard deviation of the delay jitter is increased by the antenna. This does not imply however that the antenna is somehow creating more signal power at long delays than is incident on the antenna, as measured by $f_0$. Rather, the antenna pointed away from the line-of-sight is weighting the power at long delays more than that at short delays with the peak weighting occurring at the delay that corresponds to the pointing angle. The result is an increased value of the time delay jitter standard deviation. Thus intersymbol interference effects in the output of an antenna beam may increase as the beam is pointed away from the line-of-sight.

Antenna filtering also affects the decorrelation time of the received signal. For isotropic scattering and an isotropic antenna, the equation for the ratio $\tau_A/\tau_0$ reduces to

$$\frac{\tau_A}{\tau_0} = \frac{\sqrt{Q}}{\sqrt{Q + (C_{xt}^2+C_{yt}^2)(1-Q)}}. \tag{178}$$

This equation is plotted in Figure 11 versus the ratio $\ell_0/D$ for various values of

$$C = \sqrt{C_{xt}^2 + C_{yt}^2}\ . \tag{179}$$

As discussed above, the antenna-filtered value of decorrelation time is not explicitly dependent on the pointing angle. It does depend strongly on the model for the temporal fluctuations. For the turbulent model ($C_{xt}^2 + C_{yt}^2 = 0$), the Doppler spectrum is independent of angle, so the signal arriving at all angles has the same decorrelation time. Hence the filtered value of decorrelation time is equal to that of the incident signal (i.e., $\tau_A/\tau_0 = 1$) for this model. For larger values of $C_{xt}^2 + C_{yt}^2$ there is coupling between the angular spectrum and the Doppler spectrum of the incident signal. The effect of an antenna is to narrow the angular spectrum of the received signal as shown in Figure 7. Thus when $C_{xt}^2 + C_{yt}^2$ is greater than zero the antenna also narrows the Doppler spectrum of the received signal. Because the decorrelation time of the signal is an inverse measure of the width of the Doppler spectrum, the decorrelation time of the signal out of the antenna increases as antenna filtering effects increase. For the frozen-in case, $C_{xt}^2 + C_{yt}^2$ is equal to unity and $\tau_A/\tau_0 = \sqrt{Q}$. This expression gives the upper limit of the antenna-filtered decorrelation time.

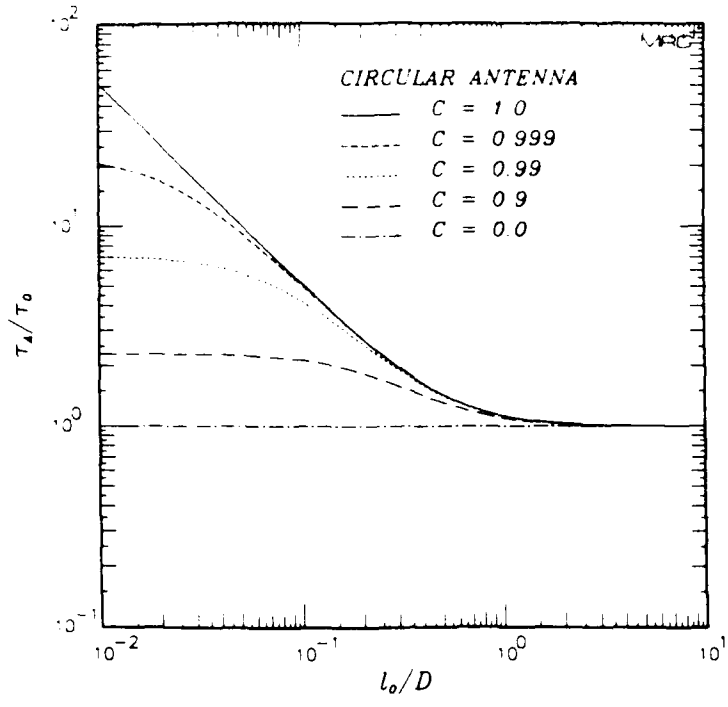


**Figure 11. Filtered decorrelation time for a uniformly-weighted circular antenna and isotropic scattering.**

The corresponding mean Doppler shift is

$$\omega_A = \frac{2\pi a_0 C_{xt}(Q-1)}{\tau_0 Q} \frac{\Theta_0}{\theta_0} \frac{\ell_0}{D} \quad . \tag{180}$$

The normalized mean Doppler shift due to antenna pointing, $\tau_0\omega_A/C_{xt}$, is plotted in Figure 12 versus the ratio $\ell_0/D$.

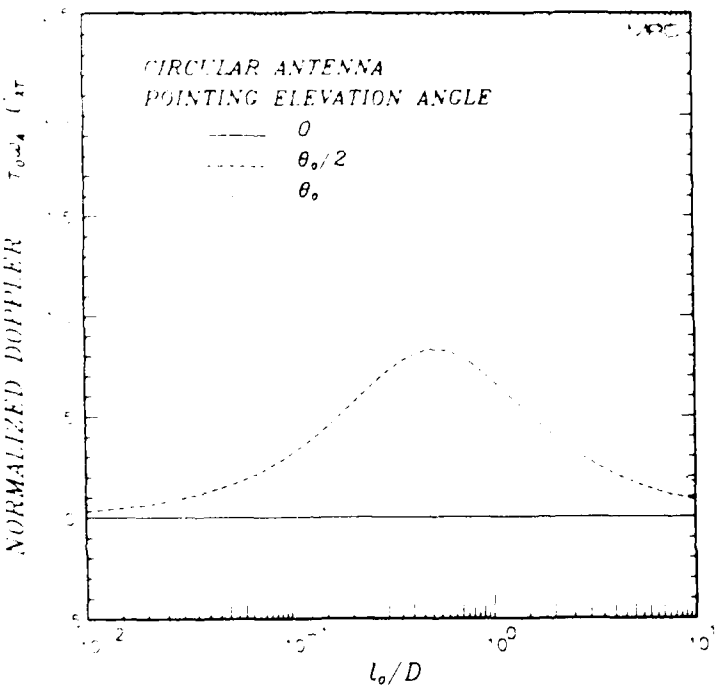


Figure 12. Normalized mean Doppler shift due to antenna pointing for a uniformly-weighted circular antenna and isotropic scattering.

# SECTION 4
# CHANNEL SIMULATION

A statistical channel simulation technique is described in this section that allows realizations of the impulse response functions to be generated at the outputs of multiple antennas with spatial and temporal correlation properties given by the GPSD and with Rayleigh amplitude statistics. Realizations generated with this technique represent only the diffractive part of the received voltage, and they are valid only under strong-scattering conditions where the GPSD is valid and where Rayleigh statistics apply. Under these conditions, however, they represent a solution of Maxwell's equations for propagation of RF waves through randomly structured ionization.

The channel simulation technique for the General Model that is described here was developed by Dr. Leon A. Wittwer of the Defense Nuclear Agency (DNA), and has been implemented in the channel model Fortran code ACIRF (*A*ntenna/*C*hannel *I*mpulse *R*esponse *F*unction) written by the author and Dr. Wittwer. This code is available to qualified users through DNA.

The basic formalism used to generate statistical realizations of the channel impulse response function without antenna effects explicitly included was first developed by *Wittwer* [1980] for isotropic irregularities. *Knepp* [1983] extended the technique to the case of elongated irregularities. (The elongated case corresponds to a 90 degree penetration angle and to an infinite axial ratio.) The channel simulation technique was further generalized by *Dana* [1986] to include the effects of general anisotropic scattering and multiple antennas.

## 4.1 IMPULSE RESPONSE FUNCTION.

A key assumption used to generate realizations of the channel impulse response function is that the channel is statistically stationary (in the wide sense) in space, frequency, and time. As a consequence, the impulse response function is delta correlated in angle, delay, and Doppler frequency. This allows the impulse response function to be generated from white Gaussian noise in the angle, delay, and Doppler frequency domains, and then Fourier transformed to the space and time domains. If necessary for a particular application, the Fourier transform from delay to frequency may be performed to obtain the channel transfer function.

The impulse response function at the output of an aperture antenna located at $\rho_0$ and pointed in direction $\mathbf{K}_0$ is given by taking the Fourier transform of the wave equation solution $U_A(\rho_0,\omega,t)$ (Eqn. 121) from the frequency domain to the delay domain with the result:

$$h_A(\rho_0,\tau,t) = \int_{-\infty}^{\infty} h(\rho,\tau,t)\, A(\rho-\rho_0) \exp\left[i\mathbf{K}_0\cdot(\rho-\rho_0)\right] d^2\rho \ . \qquad (181)$$

This equation represents the spatial convolution of the aperture weighting function and the impulse response function $h(\rho,\tau,t)$ of the signal incident on the face of the aperture.

The channel simulation technique depends on writing $h(\rho,\tau,t)$ in terms of Fourier transforms from angle to space and from Doppler frequency to time. In order to show that Equation 181 can be written in this form, first consider writing $h(\rho,\tau,t)$ in terms of its Fourier transforms:

$$h(\rho,\tau,t) = \int_{-\infty}^{\infty} \frac{d^2\mathbf{K}_\perp}{(2\pi)^2} \int_{-\infty}^{\infty} \frac{d\omega_D}{2\pi} \exp\left[i(\mathbf{K}_\perp \cdot \rho - \omega_D t)\right] \hat{h}(\mathbf{K}_\perp,\tau,\omega_D) \ . \qquad (182)$$

Equation 123 gives the aperture weighting function $A(\rho-\rho_0)$ in terms of its Fourier transform and the antenna voltage pattern $g(\mathbf{K}_\perp)$. Substituting these expressions into Equation 181 and doing the usual change in the order of integration to produce a delta function results in

$$h_A(\rho_0,\tau,t) = \int_{-\infty}^{\infty} \frac{d^2\mathbf{K}_\perp}{(2\pi)^2} \int_{-\infty}^{\infty} \frac{d\omega_D}{2\pi} \exp\left[i(\mathbf{K}_\perp \cdot \rho_0 - \omega_D t)\right] g(\mathbf{K}_\perp - \mathbf{K}_0) \hat{h}(\mathbf{K}_\perp,\tau,\omega_D) \ . \qquad (183)$$

This equation is used to generate realizations of the impulse response function by first generating random samples of $\hat{h}(\mathbf{K}_\perp,\tau,\omega_D)$ and then performing the indicated Fourier transforms. Because of the assumption of a statistically stationary channel, $\hat{h}(\mathbf{K}_\perp,\tau,\omega_D)$ must be delta correlated in angle, delay, and Doppler frequency:

$$\langle \hat{h}(\mathbf{K}_\perp,\tau,\omega_D) \hat{h}^*(\mathbf{K}',\tau',\omega_D') \rangle = S(\mathbf{K}_\perp,\tau,\omega_D)\, \delta(\mathbf{K}_\perp - \mathbf{K}')\, \delta(\tau-\tau')\, \delta(\omega_D - \omega_D') \qquad (184)$$

The first-order amplitude statistics of the complex quantity $h(\rho,\tau,t)$ are Rayleigh which is a consequence of the central limit theorem. That is, $h(\rho,\tau,t)$ represents the summation of many scattered waves travelling in slightly different directions. Thus the two orthogonal components of $h(\rho,\tau,t)$ (either the in-phase and quadrature-phase components or, in the notation used in this report, the real and imaginary parts) are independent, zero mean, normally-distributed random variables. Consequently the resulting amplitude is Rayleigh distributed, and the resulting phase is uniformly distributed. Equation 181 indicates that $h_A(\rho,\tau,t)$ is the summation or integration of weighted values of $h(\rho,\tau,t)$ and is therefore also Rayleigh distributed (i.e. the sum of normally-distributed random variables is itself normally distributed). Strictly speaking the statistics of $\hat{h}(\mathbf{K}_\perp,\tau,\omega_D)$ could be almost anything that obeys Equation 184, and the central limit theorem could be invoked to argue that $h(\rho,\tau,t)$ and $h_A(\rho,\tau,t)$ are zero-mean, normally-distributed complex quantities. Indeed, multiple phase screen techniques can be used to generate Rayleigh-distributed realizations of $h(\rho,\tau,t)$ starting with just random phase perturbations of an electric field. However, such faith in the central limit theorem is not necessary if $\hat{h}(\mathbf{K}_\perp,\tau,\omega_D)$ starts out as a zero-mean, normally-distributed complex quantity. This allows many fewer points to be used in performing discrete Fourier transforms from angle to space than would otherwise be required to guarantee Rayleigh statistics.

## 4.2 GENERATION OF REALIZATIONS.

The first step necessary to generate realizations of the impulse response function is the evaluation of the GPSD on an angular $K_x$-$K_y$ grid. Once the power in the angular grid cells has been obtained, these quantities are used to construct random samples of the angular spectrum of the signal. The delta-function relationship between angle and delay (Eqn. 105) is used to relate an annulus in the $K_x$-$K_y$ grid to specific delay bins, and the translation properties of the GPSD seen in Equation 105 are used to relate specific angles to Doppler bins. The random angular spectrum is then multiplied by the antenna beam pattern, and a two-dimensional discrete Fourier transform (DFT) is performed to the antenna phase center location. A final Fourier transform from the Doppler frequency domain produces the impulse response function as a function of time and delay. Examples of such realizations are presented in Section 5.

Before launching into a detailed discussion of the channel simulation technique, it is useful to consider the consequences of the shifting property of the angle-Doppler GPSD (Eqns. 106 or 109).

### 4.2.1 Computationally Efficient form of the Impulse Response Function.

The angle-Doppler GPSD in Equation 106 contains terms of the form $K_x \ell_x - C_{xt}\tau_0\omega_D$ and $K_y \ell_y - C_{yt}\tau_0\omega_D$. Thus, except for the leading Gaussian term in Equation 106, the mean signal power at a non-zero Doppler frequency can be obtained from the GPSD evaluated at zero Doppler frequency and shifted in angle by the appropriate amount. This fact is used to reduce the computations necessary to generate realizations of the impulse response function.

To see the consequences of the shifting property, consider the impulse response function given by Equation 183 which is the basis of the channel simulation technique. In continuous notation and using the delta-function relationship between angle and delay, the random angle-Doppler-delay spectrum of the signal may be written as

$$\hat{h}(\mathbf{K}_\perp,\tau,\omega_D) = \begin{cases} \xi_N(\mathbf{K}_\perp,\omega_D)\sqrt{S_{KD}(\mathbf{K}_\perp,\omega_D)} & \text{if } \tau = \dfrac{\Lambda_y(K_x^2+K_y^2)\ell_x^2}{4\omega_{coh}} \\ 0 & \text{otherwise} \end{cases} \tag{185}$$

where $\xi_N(\mathbf{K}_\perp,\omega_D)$ is white Gaussian noise with unity mean power and with the properties

$$\langle \xi_N(\mathbf{K}_\perp,\omega_D)\xi_N^*(\mathbf{K}',\omega_D')\rangle = \delta(\mathbf{K}_\perp-\mathbf{K}')\,\delta(\omega_D-\omega_D') \tag{186a}$$

$$\langle \xi_N(\mathbf{K}_\perp,\omega_D)\xi_N(\mathbf{K}',\omega_D')\rangle = 0\ . \tag{186b}$$

Now the key point to be made here is that the angle-Doppler GPSD, $S_{KD}(K_x,K_y,\omega_D)$, may be written in the form

$$S_{KD}(K_x,K_y,\omega_D) = S_D(\omega_D)\, S_{KC}(K_x - C_{xt}\tau_0\omega_D/\ell_x, K_y - C_{yt}\tau_0\omega_D/\ell_y) \tag{187}$$

where

$$S_D(\omega_D) = \sqrt{\pi}\tau_0 \exp\left[-\frac{\tau_0^2\omega_D^2}{4}\right] \tag{188}$$

and where

$$S_{KC}(K_x,K_y) = \frac{\pi \ell_x \ell_y}{\sqrt{1 - C_{xt}^2 - C_{yt}^2}} \times \exp\left[-\frac{K_x^2\ell_x^2(1 - C_{yt}^2) + K_y^2\ell_y^2(1 - C_{xt}^2) + 2C_{xt}C_{yt}K_x\ell_xK_y\ell_y}{4(1 - C_{xt}^2 - C_{yt}^2)}\right]. \tag{189}$$

After inserting these expressions into Equation 183, the impulse response function is

$$h_A(\rho_0,\tau,t) = \int_{-\infty}^{\infty}\frac{dK_x}{2\pi}\int_{-\infty}^{\infty}\frac{dK_y}{2\pi}\int_{-\infty}^{\infty}\frac{d\omega_D}{2\pi}\exp\left[i(K_xx_0+K_yy_0-\omega_Dt)\right] \times g(K_x-K_{0x},K_y-K_{0y})\,\xi_N(K_x,K_y,\omega_D) \times \sqrt{S_D(\omega_D)\, S_{KC}(K_x - C_{xt}\tau_0\omega_D/\ell_x, K_y - C_{yt}\tau_0\omega_D/\ell_y)} \tag{190}$$

where $\rho_0 = (x_0,y_0)$. Of course the delta-function relationship between angle and delay still holds although it is not shown explicitly in this equation. The problem with this expression as written is that $S_{KC}$ must be recomputed for each new Doppler frequency, which is time consuming.

However $S_{KC}$ can be evaluated once at zero Doppler frequency and shifted for non-zero frequencies. In a digital simulation this shift is most efficiently done in discrete steps. Thus let

$$C_{xt}\tau_0\omega_D = m_x\Delta K_x\ell_x + \varepsilon_x\ell_x \tag{191a}$$

$$C_{yt}\tau_0\omega_D = m_y\Delta K_y\ell_y + \varepsilon_y\ell_y \tag{191b}$$

where $\Delta K_x$ and $\Delta K_y$ are the angular grid cell sizes that will be used to numerically evaluate Equation 190,

$$m_x = \text{int}\left[\frac{C_{xt}\tau_0\omega_D}{\ell_x\Delta K_x}\right] \tag{192a}$$

$$m_y = \text{int}\left[\frac{C_{yt}\tau_0\omega_D}{\ell_y\Delta K_y}\right], \tag{192b}$$

and $\varepsilon_x$ and $\varepsilon_y$ are the residuals after the discrete shifts. The function int [·] denotes the integer part of the argument. Now define a shifted angle-Doppler GPSD, denoted $S_{KS}$:

$$S_{KS}(K_x,K_y) = S_{KC}(K_x - C_{xt}\tau_0\omega_D/\ell_x, K_y - C_{yt}\tau_0\omega_D/\ell_y) \ . \tag{193}$$

After substituting this into the equation for the impulse response function and changing angular variables to

$$K_x' = K_x - \varepsilon_x \tag{194a}$$

$$K_y' = K_y - \varepsilon_y \ , \tag{194b}$$

Equation 190 becomes

$$h_A(\rho_0,\tau,t) = \int_{-\infty}^{\infty}\frac{dK_x'}{2\pi}\int_{-\infty}^{\infty}\frac{dK_y'}{2\pi}\int_{-\infty}^{\infty}\frac{d\omega_D}{2\pi}\exp\{i[(K_x'+\varepsilon_x)x_0+(K_y'+\varepsilon_y)y_0-\omega_D t]\} \tag{195}$$

$$\times\ g(K_x'+\varepsilon_x-K_{0x},K_y'+\varepsilon_y-K_{0y})\,\xi_N(K_x'+\varepsilon_x,K_y'+\varepsilon_y,\omega_D)\sqrt{S_D(\omega_D)\,S_{KS}(K_x',K_y')} \ .$$

We have ignored the residual shift in the arguments of $S_{KS}$ so this function is the result of a discrete shift of the function $S_{KC}$. Equation 195, in discrete form, is used to generate the impulse response functions at the outputs of multiple antennas.

### 4.2.2 Discrete Evaluation of the GPSD.

The first step in generating the impulse response function at the output of an antenna is the evaluation of the GPSD on a discrete $K_x$-$K_y$-$\omega_D$ grid. The delta-function relationship between angle and delay is used to relate signal components within an angular annulus to a particular delay bin. Thus at this point it is not necessary to explicitly include delay, and the GPSD can be integrated over this variable. In order to assure conservation of energy (or, more correctly, to conserve signal power), the GPSD is integrated over each $K_x$-$K_y$-$\omega_D$ grid cell, and that power is assigned to the center point of the cell. A procedure for efficiently performing the three-dimensional integral is described in this subsection.

The two-dimensional angular and Doppler grids are defined by the equations

$$K_x = k_x\Delta K_x \qquad (-N_x/2 \le k_x \le N_x/2-1) \tag{196a}$$

$$K_y = k_y\Delta K_y \qquad (-N_y/2 \le k_y \le N_y/2-1) \tag{196b}$$

$$\omega_D = m_D\Delta\omega_D \qquad (-N_D/2 \le m_D \le N_D/2-1) \ . \tag{196c}$$

The requirements on the grid cell sizes $\Delta K_x$, $\Delta K_y$, and $\Delta\omega_D$ and on the number of grid cells $N_x$, $N_y$, and $N_D$ will be discussed later.

$$E_A(k_x,k_y,m_D) = \int_{(k_x-1/2)\Delta K_x}^{(k_x+1/2)\Delta K_x} \frac{dK_x}{2\pi} \int_{(k_y-1/2)\Delta K_y}^{(k_y+1/2)\Delta K_y} \frac{dK_y}{2\pi} \int_{(m_D-1/2)\Delta\omega_D}^{(m_D+1/2)\Delta\omega_D} \frac{d\omega_D}{2\pi} S_A(K_x,K_y,\omega_D) \tag{197}$$

Equation 197 is completely general, but it implies that the triple integral must be computed and stored separately for each antenna with different beamwidths or pointing angles. If, however, it is assumed that the antenna beam pattern is constant across a $K_x$-$K_y$-$\omega_D$ grid cell, then this equation can be approximated by

$$E_A(k_x,k_y,m_D) = G(k_x\Delta K_x - K_{0x}, k_y\Delta K_y - K_{0y})\, E_{KD}(k_x,k_y,m_D) \tag{198}$$

where $E_{KD}(k_x,k_y,m_D)$ is the incident signal power in the $K_x$-$K_y$-$\omega_D$ grid cell. The accuracy of this approximation is addressed in Appendix C where it is shown to conserve energy (or power) to within a small fraction of a percent.

In order to produce an efficient channel model, the quantity $E_{KD}(k_x,k_y,m_D)$ must be readily evaluated. Therein lies a major problem of the general model. Straightforward evaluation of $E_{KD}$ requires a closed-form expression for the triple integral:

$$E_{KD}(k_x,k_y,m_D) = \int_{(k_x-1/2)\Delta K_x}^{(k_x+1/2)\Delta K_x} \frac{dK_x}{2\pi} \int_{(k_y-1/2)\Delta K_y}^{(k_y+1/2)\Delta K_y} \frac{dK_y}{2\pi} \int_{(m_D-1/2)\Delta\omega_D}^{(m_D+1/2)\Delta\omega_D} \frac{d\omega_D}{2\pi} S_{KD}(K_x,K_y,\omega_D) \tag{199}$$

where the integrand is given by Equation 106. It is clear that the $K_x$-$K_y$ and angle-Doppler cross terms in the expression for $S_{KD}(K_x,K_y,\omega_D)$ do not allow a simple closed form expression for $E_{KD}$ in the general case, although such expressions can be obtained in the frozen-in and turbulent limits.

Two "tricks" are used to efficiently evaluate Equation 199. The first trick is to take advantage of the translational properties of the GPSD described in the previous subsection. The power in a $K_x$-$K_y$-$\omega_D$ grid cell is

$$E_{KD}(k_x,k_y,m_D) = \int_{(m_D-1/2)\Delta\omega_D}^{(m_D+1/2)\Delta\omega_D} \frac{d\omega_D}{2\pi} S_D(\omega_D) \tag{200}$$

$$\times \int_{(k_x-1/2)\Delta K_x}^{(k_x+1/2)\Delta K_x} \frac{dK_x}{2\pi} \int_{(k_y-1/2)\Delta K_y}^{(k_y+1/2)\Delta K_y} \frac{dK_y}{2\pi} S_{KC}(K_x - C_{xt}\tau_0\omega_D/\ell_x, K_y - C_{yt}\tau_0\omega_D/\ell_y) .$$

The key to simplifying this expression is to note that the Doppler grid cell size is relatively small because of the large number of Doppler samples that are required to produce a long time realization. Thus it can be assumed that $S_{KC}$ is constant over a Doppler cell, and Equation 200 reduces to

$$E_{KD}(k_x,k_y,m_D) = E_D(m_D)\, E_{KC}(k_x-m_x,k_y-m_y) \tag{201}$$

where

$$E_D(m_D) = \frac{1}{2}\left\{\text{erfc}\left[\frac{(m_D-1/2)\tau_0\Delta\omega_D}{2}\right] - \text{erfc}\left[\frac{(m_D+1/2)\tau_0\Delta\omega_D}{2}\right]\right\} . \tag{202}$$

The quantity $E_{KC}(k_x-m_x,k_y-m_y)$ is the power in a shifted $K_x$-$K_y$ grid cell. Because of the $K_x$-$K_y$ cross terms in the expression for $S_{KC}$, an easily evaluated closed-form result is still not obtainable for $E_{KC}$.

The second trick used in the channel model technique is to note that a rotation by the angle $\vartheta$ (Eqn. 108) in the $K_x$-$K_y$ plane produces an orthogonal form of the GPSD which does not contain angular cross terms, and is therefore readily integrated. This orthogonalized GPSD is given by Equation 109, which has the following form for its angular part:

$$S_{KC}(K_p,K_q) = \frac{\pi \ell_p \ell_q}{\sqrt{(1 - C_{pt}^2)(1 - C_{qt}^2)}} \exp\left[- \frac{K_p^2 \ell_p^2}{4(1 - C_{pt}^2)} - \frac{K_q^2 \ell_q^2}{4(1 - C_{qt}^2)}\right] . \tag{203}$$

The signal power in a $K_p$-$K_q$ grid cell, with indices $k_p$ and $k_q$ respectively, is

$$E_{KC}(k_p,k_q) = E_p(k_p)\, E_q(k_q)$$

where

$$E_p(k_p) = \frac{1}{2}\left\{\text{erfc}\left[\frac{(k_p-1/2)\Delta K_p \ell_p}{2\sqrt{1 - C_{pt}^2}}\right] - \text{erfc}\left[\frac{(k_p+1/2)\Delta K_p \ell_p}{2\sqrt{1 - C_{pt}^2}}\right]\right\} . \tag{204}$$

A similar expression holds for $E_q(k_q)$.

Now, $E_{KC}(k_p,k_q)$ can be computed on a fine $K_p$-$K_q$ grid, and the values simply assigned to the $K_x$-$K_y$ grid cell in which they fall. The $K_x$-$K_y$ cell indices are computed as follows:

$$k_x = \text{int}\left[\frac{k_p\Delta K_p\cos\vartheta - k_q\Delta K_q\sin\vartheta}{\Delta K_x}\right] \tag{205a}$$

$$k_y = \text{int}\left[\frac{k_p\Delta K_p\sin\vartheta + k_q\Delta K_q\cos\vartheta}{\Delta K_y}\right] . \tag{205b}$$

The total power in a $K_x$-$K_y$ grid cell is then the sum of all $E_{KC}(k_p,k_q)$ values that fall within the $K_x$-$K_y$ cell. Roughly ten $K_p$-$K_q$ grid cells are required within each $K_x$-$K_y$ cell for this brute-force procedure to work. Thus the $K_p$-$K_q$ cell sizes are determined by the expressions:

$$\Delta K_p = \frac{0.1}{\left[\frac{\cos^2\vartheta}{(\Delta K_x)^2} + \frac{\sin^2\vartheta}{(\Delta K_y)^2}\right]^{\frac{1}{2}}} \tag{206a}$$

$$\Delta K_q = \frac{0.1}{\left[\frac{\sin^2\vartheta}{(\Delta K_x)^2} + \frac{\cos^2\vartheta}{(\Delta K_y)^2}\right]^{\frac{1}{2}}} . \tag{206b}$$

A detailed description of the algorithms used to compute $E_{KC}(k_x-m_x,k_y-m_y)$ and to shift this array for different Doppler frequencies is given in Appendix D.

### 4.2.3 Random Realizations.

The next step in the channel model is to generate a random realization of the angle-Doppler spectrum of the impulse response function and to assign the spectral components to delay bins using the delta-function relationship between angle and delay. Discrete Fourier transforms are then performed to obtain the impulse response function.

4.2.3.1 Assignment of Angular Spectral Components to Delay Bins. The delta-function relationship between angle and delay (Eqn. 105) in the diffraction-limited form of the GPSD is used to assign angular spectral components to discrete delay bins. This form of the GPSD is non-zero only when

$$\tau = \frac{\Lambda_y(K_x^2+K_y^2)\ell_x^2}{4\omega_{coh}} . \tag{207}$$

A straightforward approach to assigning angular spectral components to delay bins is to compute the right-hand side of Equation 207 at the center of each $K_x$-$K_y$ grid cell and to compute the index of the delay bin using

$$j = \frac{\tau}{\Delta\tau} = \frac{\Lambda_y(K_x^2+K_y^2)\ell_x^2}{4\omega_{coh}\Delta\tau} \tag{208}$$

where $\Delta\tau$ is the sample size of the delay bins. The problem with this approach is that when the delay sample size is sufficiently small, the number of angular spectral components that fall within a delay bin may vary substantially from one delay bin to the next producing ragged statistics. A simple solution to this problem is to randomly wiggle the angular grid cell centers before applying Equation 208. This spreads angular spectral components more or less uniformly into any one of several delay bins, and results in better agreement between the ensemble signal power in a delay bin and

the realization power in that bin. The randomly-wiggled angular grid cell centers are computed as

$$K_x = \left[k_x + \xi_{U,x} - \frac{1}{2}\right]\Delta K_x \tag{209a}$$

$$K_y = \left[k_y + \xi_{U,y} - \frac{1}{2}\right]\Delta K_y \tag{209b}$$

where $\xi_{U,x}$ and $\xi_{U,y}$ are independent, uniformly distributed random numbers on the interval [0,1). These wiggled cell centers are then used to compute the corresponding j index of the delay grid.

In this way each angular spectral component is assigned to a unique delay bin. Because the angular spectral components are uncorrelated, this procedure also guarantees that the impulse response function is uncorrelated from one delay bin to another.

4.2.3.2 Discrete Representation of Impulse Response Function. The discrete impulse response function is defined on a discrete time and delay grid defined by the equations:

$$t = n_t\Delta t \qquad (n_t=1, 2, \cdots, N_t) \tag{210a}$$

$$\tau = j\Delta\tau\ . \qquad (j=0, 1, \cdots, N_\tau - 1) \tag{210b}$$

The requirements on the discrete time step $\Delta t$, the number to time steps $N_t$, the delay sample size $\Delta\tau$, and the number of delay bins $N_\tau$ will be given in Section 4.3.

Equation 195 gives the impulse response function in terms of Fourier transforms from the random angle-Doppler spectral components to the time domain at the location of the phase center of each antenna. In discrete form, this equation is

$$\begin{aligned} h_A(j\Delta\tau,n_t\Delta t) = {} & \frac{8\pi^3}{\Delta K_x\Delta K_y\Delta\omega_D\Delta\tau} \sum_{m_D=-N_D/2}^{N_D/2-1} \frac{\Delta\omega_D}{2\pi} \sum_{k_x=-N_x/2}^{N_x/2-1} \frac{\Delta K_x}{2\pi} \sum_{k_y=-N_y/2}^{N_y/2-1} \frac{\Delta K_y}{2\pi} \\ & \times \exp\left\{i[(k_x\Delta K_x+\varepsilon_x)x_0 + (k_y\Delta K_y+\varepsilon_y)y_0 - m_D\Delta\omega_D n_t\Delta t]\right\} \\ & \times g(k_x\Delta K_x+\varepsilon_x-K_{0x}, k_y\Delta K_y+\varepsilon_y-K_{0y})\ \xi_N(k_x,k_y,m_D) \\ & \times \sqrt{E_D(m_D)\ E_{KS}(k_x\Delta K_x, k_y\Delta K_y)}\ . \end{aligned} \tag{211}$$

The normalization factor $(8\pi^3/\Delta K_x\Delta K_y\Delta\omega_D\Delta\tau)$ has been chosen so that $h_A(j\Delta\tau,n_t\Delta t)\Delta\tau$ represents the received signal during the delay interval $j\Delta\tau$ to $(j+1)\Delta\tau$. As the $K_x$ and $K_y$ sums are performed, Equation 208 is used to assign angular spectral components to delay bins. Then the signal components in each delay bin are Fourier transformed from the Doppler domain to the time domain.

The quantity $\xi_N(k_x,k_y,m_D)$ is a complex, zero-mean, Gaussian random variable with the properties

$$\langle \xi_N(a,b,c)\xi_N^*(\alpha,\beta,\gamma)\rangle = \delta_{a,\alpha}\,\delta_{b,\beta}\,\delta_{c,\gamma} \tag{212a}$$

$$\langle \xi_N(a,b,c)\rangle = 0 \tag{212b}$$

$$\langle \xi_N(a,b,c)\xi_N(\alpha,\beta,\gamma)\rangle = 0 \tag{212c}$$

where $\delta_{m,n}$ is the Kronecker delta symbol. A convenient method of generating the complex, zero-mean, Gaussian random numbers is to use the following equation

$$\xi_N = \sqrt{-P_0 \ln(\xi_{U,1})}\,\exp(2\pi i \xi_{U,2}) \tag{213}$$

where $\xi_{U,1}$ and $\xi_{U,2}$ are independent random numbers uniformly distributed on the interval [0,1), and $P_0$ is the mean power of the random samples ($P_0 = \langle \xi_N \xi_N^* \rangle = 1$ for this application).

In comparing the discrete equation for the impulse response function with its continuous-variable analog (Eqn. 195), note that the residual shifts $\varepsilon_x$ and $\varepsilon_y$ may be ignored in the arguments of the random spectral components, $\xi_N$, because shifted white Gaussian noise is still white Gaussian noise.

4.2.3.3 Elimination of the DC Component. As written, the equation for the discrete impulse response function (Eqn. 211) allows a Doppler spectral component with zero-Doppler frequency (i.e. the $m_D = 0$ component). This component will in turn result in a DC component in the time domain realization, which is undesirable, particularly if the DC component is large.

A simple solution to this problem is to set the zero-Doppler frequency component of $\xi_N(k_x,k_x,m_D)$ to zero. Just doing this, however, results in reducing the mean power in the impulse response function by the zero-Doppler frequency power, $E_D(0)$.

This latter problem can be simply solved by allowing the Doppler frequency bins adjacent to zero Doppler to expand in size. Thus the first positive Doppler frequency bin encompasses frequencies 0 to $3\Delta\omega_D/2$ and has power $E_D(1) + E_D(0)/2$. Similarly, the first negative Doppler frequency bin encompasses frequencies 0 to $-3\Delta\omega_D/2$ and has power $E_D(-1) + E_D(0)/2$. All other Doppler frequency bins encompass frequencies $(m_D-1/2)\Delta\omega_D$ to $(m_D+1/2)\Delta\omega_D$ and have power $E_D(m_D)$.

## 4.3 GRIDS.

Angle and Doppler frequency grid sizes are determined by requiring that the angular-Doppler grid encompass a large fraction, say 0.999, of the power in the GPSD of the signal. The 0.001 error must then be allocated between the angular and Doppler parts of the three-dimensional grid. An arbitrary, but intuitively reasonable, allocation is to divide the error equally between the angular and Doppler frequency parts of the

grid and equally between the two angular components. Thus the Doppler grid limits are determined by requiring that the Doppler grid encompass $\sqrt{0.999}$ of the Doppler frequency power, and each angular grid must encompass $(0.999)^{1/4}$ of the angular power

The angular and Doppler frequency power spectra are all Gaussian. Thus each can separately be written in the form

$$S(\kappa) = \sqrt{\pi} \exp\left[-\frac{\kappa^2}{4}\right] \tag{214}$$

where $\kappa$ is a normalized angle or Doppler frequency (i.e. $\kappa$ is equal to $K_x \ell_x$ or $K_y \ell_y$ or $\tau_0 \omega_D$). In order for a $\kappa$ grid to encompass a fraction $\zeta_0$ of the signal power, it must extend from $-\kappa_{max}$ to $+\kappa_{max}$ where

$$\zeta_0 = \int_{-\kappa_{max}}^{\kappa_{max}} S(\kappa)\, d\kappa \ . \tag{215}$$

This equation is easily solved for $\kappa_{max}$ in terms of $\zeta_0$ with the result

$$\kappa_{max} = 2\, \mathrm{erf}^{-1}(\zeta_0) \tag{216}$$

where $\mathrm{erf}^{-1}(\cdot)$ is the inverse error function. If $\zeta_0$ is chosen to be $\sqrt{0.999}$ for the Doppler frequency grid, then

$$\kappa_{D,max} = 2 \times 2.4612 = 4.9224 \ , \tag{217a}$$

and if $\zeta_0$ is chosen to be $(0.999)^{1/4}$ for either angular grid, then

$$\kappa_{K,max} = 2 \times 2.5895 = 5.1790 \ . \tag{217b}$$

A second requirement on the size of the angular, Doppler, and delay grids is that they be defined at the output of the antennas, thereby eliminating areas of the grids that contribute to the signal power incident on the antennas but do not contribute to the power of the output signals because of antenna filtering. Much of the complexity of the algorithms used to determine grid sizes is a result of this requirement, but computing grid sizes in this way results in a substantial reduction in the size of the grids, and therefore in computation time, when antenna filtering effects are large.

The numbers of cells in the angular ($N_x$ and $N_y$), delay ($N_\tau$), and time ($N_t$) grids are inputs to the channel simulation. The delay sample size ($\Delta\tau$) and the number of samples per decorrelation time ($N_0$) are also inputs. From these quantities and the channel and antenna parameters, the angular ($\Delta K_x$ and $\Delta K_y$), Doppler ($\Delta\omega_D$), and time ($\Delta t$) grid cell sizes and the required number of Doppler samples ($N_D$) are computed. Requirements on input grid parameters and consistency checks on computed grid parameters are described in the next subsections.

### 4.3.1 Angular Grid.

Angular grid sizes are determined by the requirement that the fraction $\sqrt{0.999} = 0.9995$ of the signal power after antenna filtering be contained in the two-dimensional angular grid. First consider the $K_x$ grid. Because of the symmetry in the angular grid, the requirements on the $K_y$ grid can then be obtained by analogy.

The $K_x$ power spectrum at the output of an antenna is

$$S_A(K_x) = \int_{-\infty}^{\infty} \frac{dK_y}{2\pi} \int_{-\infty}^{\infty} d\tau \int_{-\infty}^{\infty} \frac{d\omega_D}{2\pi} G(K_x-K_{x0},K_y-K_{y0})\, S(K_x,K_y,\tau,\omega_D) \qquad (218)$$

$$= \frac{\sqrt{\pi}\,\ell_x}{\sqrt{Q_y}} \exp\left[ - \alpha_u^2 K_{0u}^2 - \alpha_v^2 K_{0v}^2 - \frac{Q_0^2}{Q_y} \frac{K_x^2 \ell_x^2}{4} + \left( A_x - \frac{A_y Q_{xy}}{Q_y} \right) \frac{K_x \ell_x}{2} + \frac{A_y^2}{4Q_y} \right]$$

where

$$A_x = (Q_x-1)K_{0x}\ell_x + Q_{xy}K_{0y}\ell_y \qquad (219a)$$

$$A_y = Q_{xy}K_{0x}\ell_x + (Q_y-1)K_{0y}\ell_y \quad . \qquad (219b)$$

The limits of the $K_x$ grid are determined by requiring that

$$\zeta_0 P_A = \int_{-K_{x,max}}^{K_{x,max}} S_A(K_x) \frac{dK_x}{2\pi} \quad . \qquad (220)$$

If the coefficient of the linear $K_x$ term in the exponent of Equation 218 is positive then the lower limit of the integral in Equation 220 can be replaced by $-\infty$. Conversely, if the coefficient is negative then the upper limit can be replaced by $+\infty$. Either way, the result for $\zeta_0$ is

$$\zeta_0 = \frac{1}{2}\left\{ 1 + \mathrm{erf}\left[ \frac{Q_0 K_{x,max}\ell_x}{2\sqrt{Q_y}} - \frac{|A_x Q_y - A_y Q_{xy}|}{2Q_0\sqrt{Q_y}} \right] \right\} \qquad (221)$$

where erf (·) is the error function. Setting $\zeta_0$ equal to $(0.999)^{1/4}$ and solving for $K_{x,max}$ gives the following approximate result:

$$K_{x,max} = \frac{\kappa_{K,max}}{\ell_{Ax}} + \frac{|A_x Q_y - A_y Q_{xy}|}{\ell_{Ax} Q_0 \sqrt{Q_y}} \quad . \qquad (222a)$$

Similarly, the limit of the $K_y$ grid is

$$K_{y,max} = \frac{\kappa_{K,max}}{\ell_{Ay}} + \frac{|A_y Q_x - A_x Q_{xy}|}{\ell_{Ay} Q_0 \sqrt{Q_x}} \quad . \qquad (222b)$$

The first terms in the expressions for $K_{x,max}$ and $K_{y,max}$ give the required extent of the grid when the antenna is pointed along the line-of-sight. The second terms, which are non-zero only when the antenna is pointed away from the line-of-sight, give the amount by which the grid must be extended in order for the grid to encompass the beam.

Clearly, $K_{x,max}$ and $K_{y,max}$ depend on antenna beamwidths and pointing angles because of the A and Q factors. If there are multiple antennas then $K_{x,max}$ and $K_{y,max}$ must be computed for each antenna. The largest values are then used to determine the boundaries of the angular grid.

The angular grid cell sizes can now be computed as

$$\Delta K_x = \frac{2K_{x,max}}{N_x} \tag{223a}$$

$$\Delta K_y = \frac{2K_{y,max}}{N_y} \tag{223b}$$

where the number of grid cells, $N_x$ and $N_y$, are inputs to the channel model.

A reasonable minimum value for the number of $K_x$ or $K_y$ grid cells is 32. However, this number may not be sufficient if there are multiple antennas with different phase center locations. Consider the two antennas with the largest separations, $d_x$ and $d_y$, in the x-y plane. Because the impulse response functions at the outputs of the two antennas are generated by discrete Fourier transforms from the angular domain to the phase center locations of the antenna, the unambiguous distances, $2\pi/\Delta K_x$ and $2\pi/\Delta K_y$, of the DFTs must exceed the maximum antenna separations, say by a factor of 2. This then puts upper limits on $\Delta K_x$ and $\Delta K_y$:

$$\Delta K_x \leq \frac{\pi}{d_x} \tag{224a}$$

$$\Delta K_y \leq \frac{\pi}{d_y} \tag{224b}$$

If these criteria are not met, then $N_x$ and/or $N_y$ must be increased, thereby decreasing $\Delta K_x$ and/or $\Delta K_y$, until they are met. The minimum required values for $N_x$ and $N_y$ can then be written as

$$N_x = \max\left[32, \frac{2d_x K_{x,max}}{\pi}\right] \tag{225a}$$

$$N_y = \max\left[32, \frac{2d_y K_{y,max}}{\pi}\right] \tag{225b}$$

### 4.3.2 Doppler Frequency and Time Grids.

The Doppler frequency grid size is also determined by the requirement that 99.9 percent of the signal power after antenna filtering be contained in the Doppler frequency grid. Thus the antenna-filtered Doppler power spectrum is required. This function is most easily obtained by noting that the temporal coherence function has the form

$$\Gamma_A(t) = P_A \exp\left[ - \frac{t^2}{\tau_A^2} + i\omega_A t \right] . \tag{226}$$

Recall from Section 3.2.3 that $\omega_A$ is the mean Doppler shift due to antenna pointing. The Doppler power spectrum is then given by the equation

$$S_A(\omega_D) = \int_{-\infty}^{\infty} \Gamma_A(t)\, dt = \sqrt{\pi}\, \tau_A\, P_A \exp\left[ - \frac{\tau_A^2\, (\omega_D+\omega_A)^2}{4} \right] . \tag{227}$$

The calculation of the limits on the Doppler frequency grid is exactly analogous to that done for the angular grid. The limits of the $\omega_D$ grid are determined by setting $\zeta_0$ equal $\sqrt{0.999}$ in the equation

$$\zeta_0 P_A = \int_{-\omega_{D,max}}^{\omega_{D,max}} S_A(\omega_D) \frac{d\omega_D}{2\pi} . \tag{228}$$

Solving for $\zeta_0$,

$$\zeta_0 = \frac{1}{2}\left[ 1 + \mathrm{erf}\left[ \frac{\tau_A(\omega_{D,max}-|\omega_A|)}{2} \right] \right] , \tag{229}$$

gives the following approximate result for $\omega_{D,max}$:

$$\omega_{D,max} = \frac{N_{D,max}}{\tau_A} + |\omega_A| . \tag{230}$$

The first term in this expression gives the required maximum Doppler frequency when the antenna is pointed along the line-of-sight, and the second term is the result of the mean Doppler shift effect of antenna pointing. If there are multiple antennas, then $\omega_{D,max}$ must be calculated for each antenna, and the largest value used to determine the Doppler grid size.

At this point the required number of Doppler frequencies $N_D$ is still unspecified. However, because a fast Fourier transform (FFT) will be used to transform from Doppler frequency to time, the time grid requirements may be used to derive the Doppler frequency grid cell size $\Delta\omega_D$ and then the required number of Doppler frequency samples, $N_D$.

Consider the requirements on the time samples. *Dana* [1982, 1988] has shown that at least 10 samples per decorrelation time are required to accurately reproduce the temporal statistics of Rayleigh fading. This is also a DNA requirement on Rayleigh Fading realizations of the impulse response function [*Wittwer* 1980]. The time grid cell size is then

$$\Delta t = \frac{\tau_{A,min}}{N_0} \tag{231}$$

where $N_0$ is the number of samples per decorrelation time ($N_0$ must be greater than or equal to 10), and $\tau_{A,min}$ is the smallest value for all antennas of the filtered decorrelation time.

In addition, DNA requires that there be at least 100 decorrelation times in all realizations of the antenna output impulse response function. Thus,

$$N_t \geq \frac{100\tau_{A,max}}{\Delta t} , \tag{232}$$

where $\tau_{A,max}$ is the largest value for all antennas of the filtered decorrelation time. If this condition is not met then the number of time samples $N_t$ must be increased. It is also necessary that $N_t$ be equal to a power of 2 in order to use an FFT. The minimum value of $N_t$ is then 1024 in order to meet the requirement in Equation 232 with $N_0$ equal to 10.

Because of the FFT relationship between the time and Doppler frequency domains, the Doppler frequency grid cell size is

$$\Delta\omega_D = \frac{2\pi}{N_t\Delta t} . \tag{233}$$

The minimum number of Doppler frequency samples necessary for the grid to encompass the maximum required Doppler frequency is then given by

$$N_D = \frac{2\omega_{D,max}}{\Delta\omega_D} = \frac{N_t\omega_{D,max}\tau_{A,min}}{\pi N_0} . \tag{234}$$

In general, $N_D$ will be smaller than $N_t$ implying that fewer than $N_t$ Doppler frequency samples are required. The Doppler frequency arrays may then be zero-padded to $N_t$ samples before the FFT is performed. If, however, $N_D$ is greater than $N_t$, the implication is that there are too few samples per decorrelation time, and $N_0$ must be increased.

The minimum number of Doppler frequency samples can be computed from Equations 230 and 234. If all antennas are pointed along the line-of-sight, then the minimum value of $N_D$ is

$$N_{D,min} = \frac{\kappa_{D,max}N_t}{\pi N_0} . \tag{235}$$

For realizations with 100 decorrelation times ($N_t/N_0 = 100$), the minimum number of Doppler samples is approximately 150. If antennas are pointed away from the line-of-sight, the required number of Doppler samples will increase beyond 150.

### 4.3.3 Delay Grid.

The delay sample size is usually chosen on the basis of the modulation bandwidth of the transmitted signal, and is therefore not a parameter that is under the direct control of the channel simulation. For example, in a phase-shift keying (PSK) application there must be at least two delay samples per channel symbol in order to accurately simulate the transmitted frequency spectrum. The delay sample size is then generally chosen to be equal to one-half the channel symbol period. In a frequency-shift keying (FSK) application with frequency hopping, the delay sample size is chosen so that the unambiguous frequency bandwidth of the impulse response function, $1/\Delta\tau$, exceeds the hopping bandwidth by some comfortable margin.

The number of delay bins is an input to the channel simulation. The requirement on both $N_\tau$ and $\Delta\tau$ is that the realization delay grid size $N_\tau\Delta\tau$ encompass at least 97.5 percent of the delayed signal power at the outputs of the antennas. A somewhat smaller percentage is used to define the limits of the delay grid than is used to define other grid limits because of the slower decay of signal power with delay than with angle and Doppler frequency (exponential decay with delay versus Gaussian decay with angle and Doppler frequency).

The ensemble signal power in the delay bins is given by the integral

$$P_j = \int_{j\Delta\tau}^{(j+1)\Delta\tau} S_A(\tau)\, d\tau \qquad (236)$$

where $S_A(\tau)$ is the delay power spectral density at the output of an antenna. The general expression for $S_A(\tau)$ is quite complicated when the antenna is pointed away from the line-of-sight, and will not be given here. The reader is referred to *Frasier* [1988] for details on $S_A(\tau)$.

The total signal power in the delay grid,

$$P_{G\tau} = \sum_{j=0}^{N_\tau-1} P_j \ , \qquad (237)$$

must be greater than or equal to $0.975P_A$. If not, then either $N_\tau$ or $\Delta\tau$ or both must be increased.

# SECTION 5
# MATCHED FILTER EXAMPLES

This section presents examples of the received voltage out of a filter matched to a transmitted square pulse. These examples are intended to illustrate the effects of frequency selectivity and antenna filtering on a transionospheric communications link and to illustrate the differences in the structure of the received signal depending on whether the frozen-in, turbulent, or general models are used to generate the impulse response function realizations. The following calculation also illustrates how the received voltage can be constructed from the impulse response function realizations in a digital link simulation. Additional examples for specific system applications may be found in *Bogusch, et. al.* [1981] and in *Bogusch, Guigliano, and Knepp* [1983].

## 5.1 MATCHED FILTER OUTPUT SIGNAL.

The output of a matched filter can be constructed by convolving the impulse response function of the channel and antenna with the combined impulse response function of the transmitter and receiver. A second approach is to construct the combined frequency response of the transmitter, channel, antenna, and receiver and then to Fourier transform that result to obtain the matched-filter output. This latter approach is used for the examples presented in this section.

The starting point is to calculate the channel/antenna transfer function which is the Fourier transform of the impulse response function:

$$H(\omega,t) = \int_{0}^{\infty} h(\tau,t) \exp(-i\omega\tau)\, d\tau \quad . \tag{238}$$

This function represents the response of the channel and antenna at time t to a transmitted sinewave with radian frequency $\omega$.

For a transmitted square pulse with a chip duration $T_c$, the voltage out of the matched filter at time t can be written as

$$u(\tau,t) = \int_{-\infty}^{\infty} M(\omega)\, H(\omega,t) \exp(i\omega\tau)\, \frac{d\omega}{2\pi} \tag{239}$$

where $\tau$ is the time delay of the matched filter relative to the nominal time-of-arrival (i.e. the time-of-arrival under benign propagation conditions). The combined spectrum of the transmitted square pulse and the receiver matched filter is

$$M(\omega) = T_c \frac{\sin^2(\omega T_c/2)}{(\omega T_c/2)^2} \quad . \tag{240}$$

The impulse response function is generated with $N_\tau$ delay samples of size $\Delta\tau$, so the discrete channel/antenna transfer function has an unambiguous frequency response

of $2\pi/\Delta\tau$ radians. If this bandwidth is divided into $N_F$ frequency samples, then the discrete channel/antenna transfer function at time $n_t\Delta t$ is

$$H(k_F\Delta\omega,n_t\Delta t) = \sum_{j=0}^{N_\tau-1} h(j\Delta\tau,n_t\Delta t)\Delta\tau \exp\,[-ij\Delta\tau k_F\Delta\omega] \qquad (241)$$

where $\Delta\omega = 2\pi/(N_F\Delta\tau)$. Recall that the normalization of the impulse response function is such that the factor $\Delta\tau$ following $h(j\Delta\tau,n_t\Delta t)$ must be included. The range of the index $k_F$ in this equation is from $-N_F/2$ to $N_F/2-1$ representing a range of frequencies from $-N_F\Delta\omega/2$ to $(N_F-1)\Delta\omega/2$. Of course the number of frequency samples must be at least as large as the number of delay samples in order for the transfer function to preserve the information contained in the impulse response function. However, if the number of delay samples is chosen to be the minimum number required, then it may be necessary to select the number of frequency samples to be larger than the number of delay samples in order to minimize aliasing (in delay) of the matched-filter output.

The output voltage of the matched filter, as a function of time and relative delay, is then given by

$$u(\tau,n_t\Delta t) = \frac{\Delta\omega T_c}{2\pi} \sum_{k_F=-N_F/2}^{N_F/2-1} \left[\frac{\sin^2(k_F\Delta\omega T_c/2)}{(k_F\Delta\omega T_c/2)^2}\right] H(k_F\Delta\omega,n_t\Delta t) \exp\,(ik_F\Delta\omega\tau)\ . \qquad (242)$$

If the delay samples size $\Delta\tau$ of the realization of the impulse response function is chosen to be $T_c/2$, then $\Delta\omega T_c/2 = 2\pi/N_F$ and $u(\tau,n_t\Delta t)$ represents a signal that is band-limited to the frequency range $-1/T_c$ to $+1/T_c$. Note that the matched-filter output $u(\tau,t)$ is unambiguous in delay over the interval from 0 to $(N_F-1)\Delta\tau$ compared to the delay interval of 0 to $(N_\tau-1)\Delta\tau$ for the original realization.

In the examples that follow, the chip rate $R_c$ is set at 1 MHz, and the random realizations of the impulse response function are generated with a delay sample size of $T_c/2$ ($T_c = 1/R_c$). However, the frequency selective effects depend only on the ratio of the frequency selective bandwidth to the chip rate $f_0/R_c$. For the antenna examples, a uniformly-weighted circular antenna and isotropic scattering are assumed. Antenna effects then depend only on the ratio of the antenna diameter D to the decorrelation distance $\ell_0$ and the antenna pointing angle.

## 5.2 FREQUENCY SELECTIVE EFFECTS.

In a high data rate communications link, the major effect of frequency selective fading is intersymbol interference. Even relatively small amounts of delay spread can catastrophically degrade demodulation performance in such a link using conventional matched-filter detection techniques.

Figure 13 shows examples of the matched-filter output amplitude for three levels of frequency selective propagation disturbances, characterized by the ratio of the frequency selective bandwidth $f_0$ to the chip rate $R_c$. The impulse response functions were generated using the frozen-in model ($C_{xt} = 1.0$ and $C_{yt} = 0$) and a small antenna (i.e. $D << \ell_0$). Each frame in the figure provides a three-dimensional picture of the matched-filter output amplitude for a single transmitted pulse as a function of time delay (abscissa) and time (scale directed into the figure). The total duration of each of the frames is 10 decorrelation times.

In the top frame the frequency selective bandwidth is equal to the chip rate and only a small amount of distortion is evident in the waveform (which is slightly rounded due to band limiting at the first nulls of the signal spectrum). The effect of fading can be seen in this frame as the peak amplitude rises and falls with time. Some minor distortion of the output amplitude is seen but for the most part the signal is contained within the period of one chip. This channel is nearly-flat fading which means that all frequency components within the signal bandwidth propagate essentially the same way through the disturbed ionosphere. There is very little time delay spread beyond one chip in the matched-filter output.

The middle frame in Figure 13 shows the matched-filter output amplitude for the case were $f_0/R_c$ is equal to 0.2. For this smaller value of the frequency selective bandwidth, more of the signal energy is arriving with delays of more than a chip, and there are multiple distinct peaks in the matched-filter output amplitude. It is these structures that can cause delay tracking algorithms to lose lock and that cause intersymbol interference which can degrade demodulation performance.

The bottom frame shows a highly disturbed case where $f_0$ is a tenth of the chip rate. This causes signal energy to be spread over approximately eight chip periods. When a contiguous set of pulses is transmitted, the delay spread of the received signal results in the simultaneous reception of information from about eight previous chips which can produce severe intersymbol interference.

An effect due to the frozen-in model that is evident in Figure 13 is that the signal arriving at long delays varies more rapidly in time than the signal arriving at shorter delays. A comparison of the matched-filter output amplitude generated with the frozen-in, general, and turbulent models is shown in Figure 14 for the case where $f_0/R_c$ is equal to 0.1. The top frame in this figure for the frozen-in model is just a reproduction of the bottom frame in Figure 13. Again 10 decorrelation times of the signal are plotted. The middle frame is a general model realization ($C_{xt} = 0.9$ and $C_{yt} = 0$), and the bottom frame is for the turbulent model ($C_{xt} = C_{yt} = 0$). The difference between the top and bottom frames is that the turbulent model amplitude has the same fading rate at all delays. It can be seen that the general model realization falls somewhere between these two limiting cases.

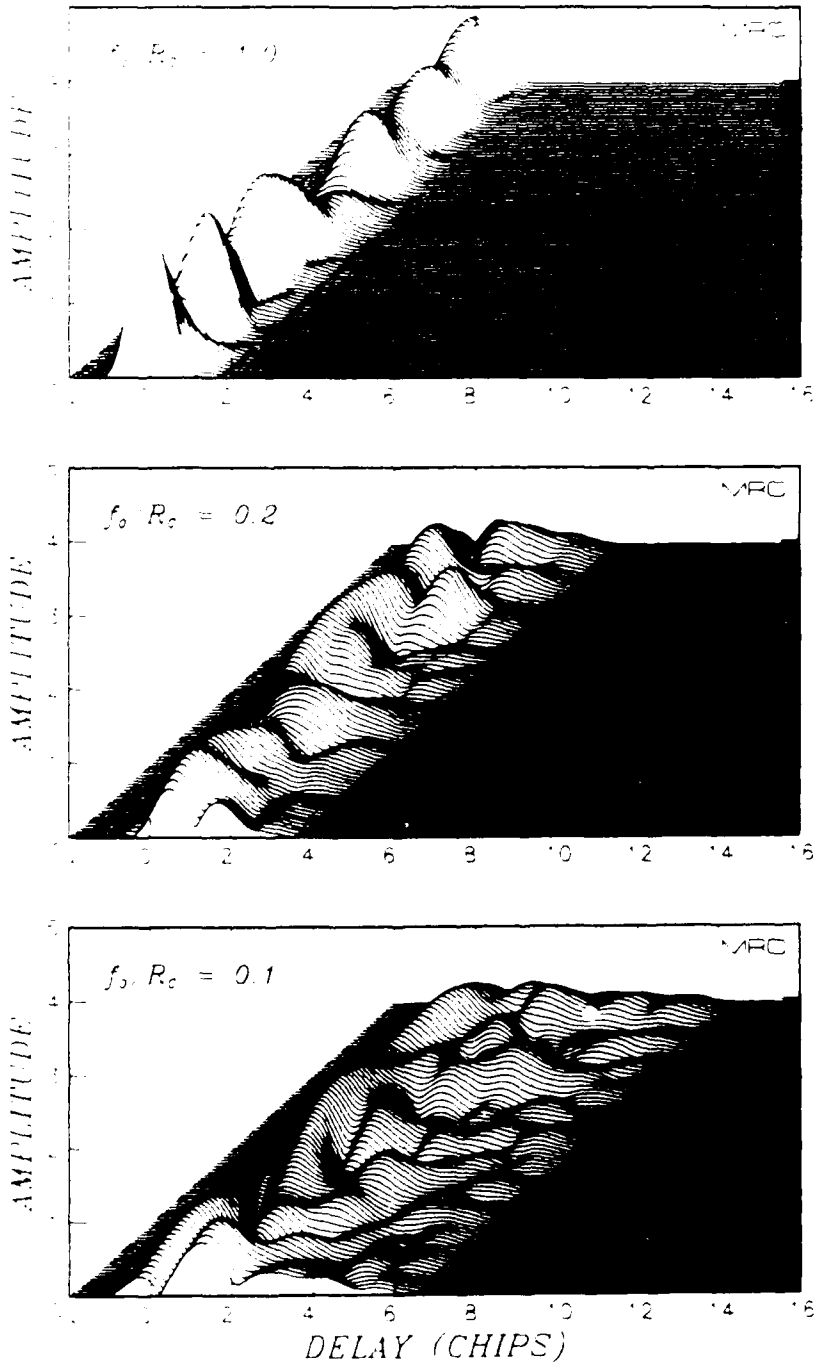


**Figure 13. Effects of frequency selective fading.**

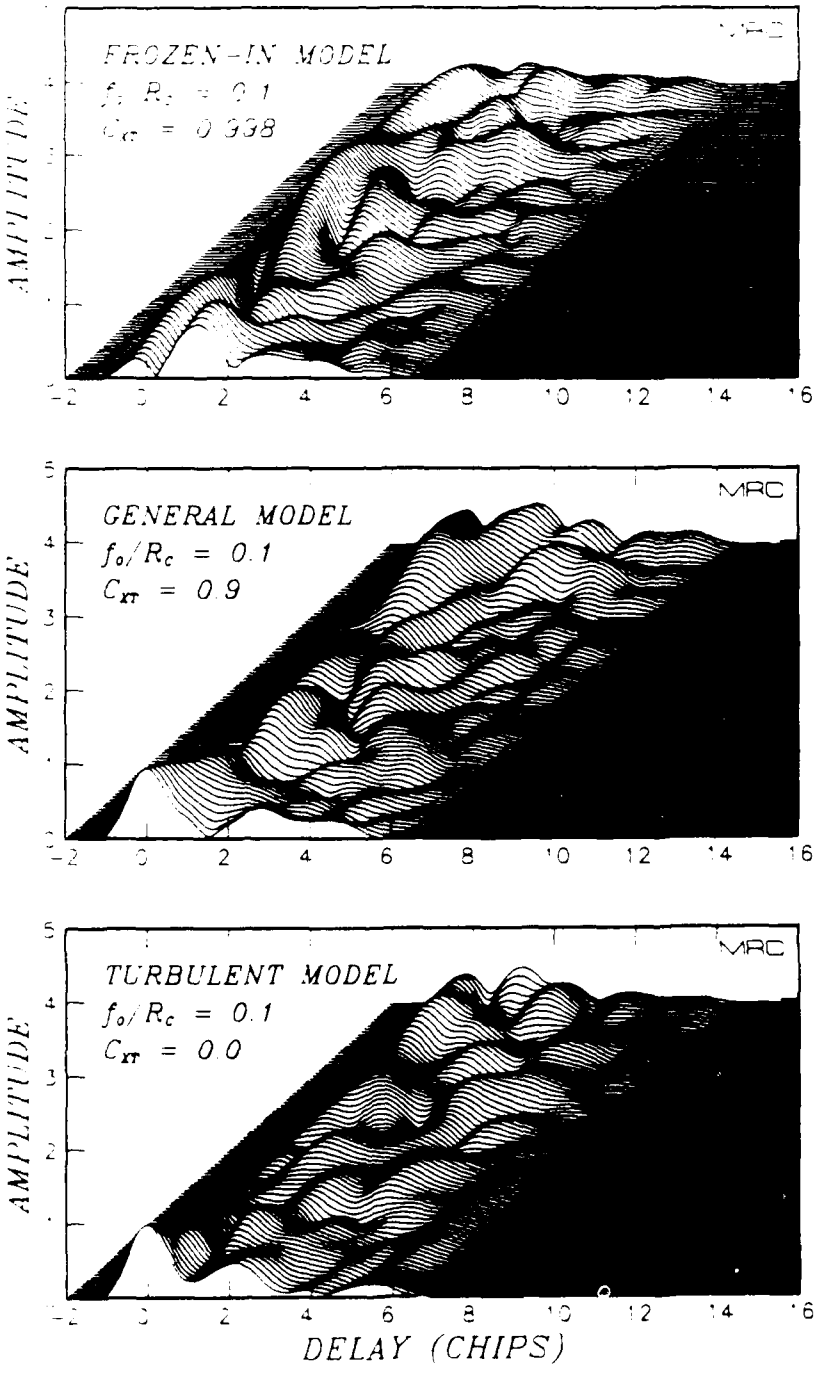


**Figure 14. Comparison of matched filter output amplitude for the frozen-in, general, and turbulent models.**

## 5.3 SPATIALLY SELECTIVE EFFECTS.

Spatially selective effects are important for high data rate communications links that rely on large antennas to achieve sufficient signal-to-noise ratios for low error rate data demodulation. Scattering loss of an antenna is a function of the size of the antenna D relative to the decorrelation distance.

When $\ell_0$ is greater than D, the electric field is highly correlated across the face of the antenna and the full gain of the antenna is realized. However, the antenna may be located at a position where the incident power is in a deep fade. The solution to this problem is to have multiple antennas physically separated by a distance larger than the maximum decorrelation distance. The probability of having all antennas simultaneously experience deep fades in the received power is then substantially reduced.

The problem of spatial selectivity occurs when $\ell_0$ is less than D and the electric field is decorrelated across the face of the antenna. In this case, the induced voltages in the antenna add noncoherently due to the random phase variations in the electric field, and a loss of signal power, or equivalently of antenna gain, is the result. From another perspective, this loss occurs when the angular scattering process responsible for amplitude and phase scintillation and frequency selective effects also causes some of the transmitted signal energy to be scattered out of the antenna beam.

Figure 15 shows examples of the matched-filter output amplitude for three levels of spatially selective propagation disturbance, characterized by the ratio of the antenna size to the decorrelation distance. The ratio of the frequency selective bandwidth to the chip rate rate is 0.1, and the antenna is pointing along the line-of-sight. The top frame is for the case where $\ell_0$ is much greater than D, and is just a reproduction of the bottom frame of Figure 13. The middle frame is for a $\ell_0$/D ratio of 0.5 where the scattering loss is 3.1 dB. The effect of the antenna is to preferentially attenuate the signal energy arriving at large angles and also at large delays and thereby to reduce the delay spread of the output signal. In the bottom frame where $\ell_0$/D is equal to 0.2, the output signal is almost flat with very little delay spread distortion of the matched-filter output. Although this substantially reduces the effects of frequency selective fading, the cost is an 8.8-dB reduction in the average signal power.

Finally, Figure 16 shows examples of the matched-filter output amplitude for three values of the pointing angle $\Theta_0$. The ratio of the frequency selective bandwidth to the chip rate rate is 0.1, and the ratio of decorrelation distance to antenna diameter is 0.5. The top frame for a pointing angle of zero is just a reproduction of the middle frame of Figure 15. The average scattering loss for this case is 3.1 dB. The bottom two frames show the matched-filter output amplitude for pointing angles of one-half beamwidth ($\Theta_0=\theta_0/2$) with a scattering loss of 4.6 dB and one beamwidth ($\Theta_0=\theta_0$) with a scattering loss of 9.2 dB.

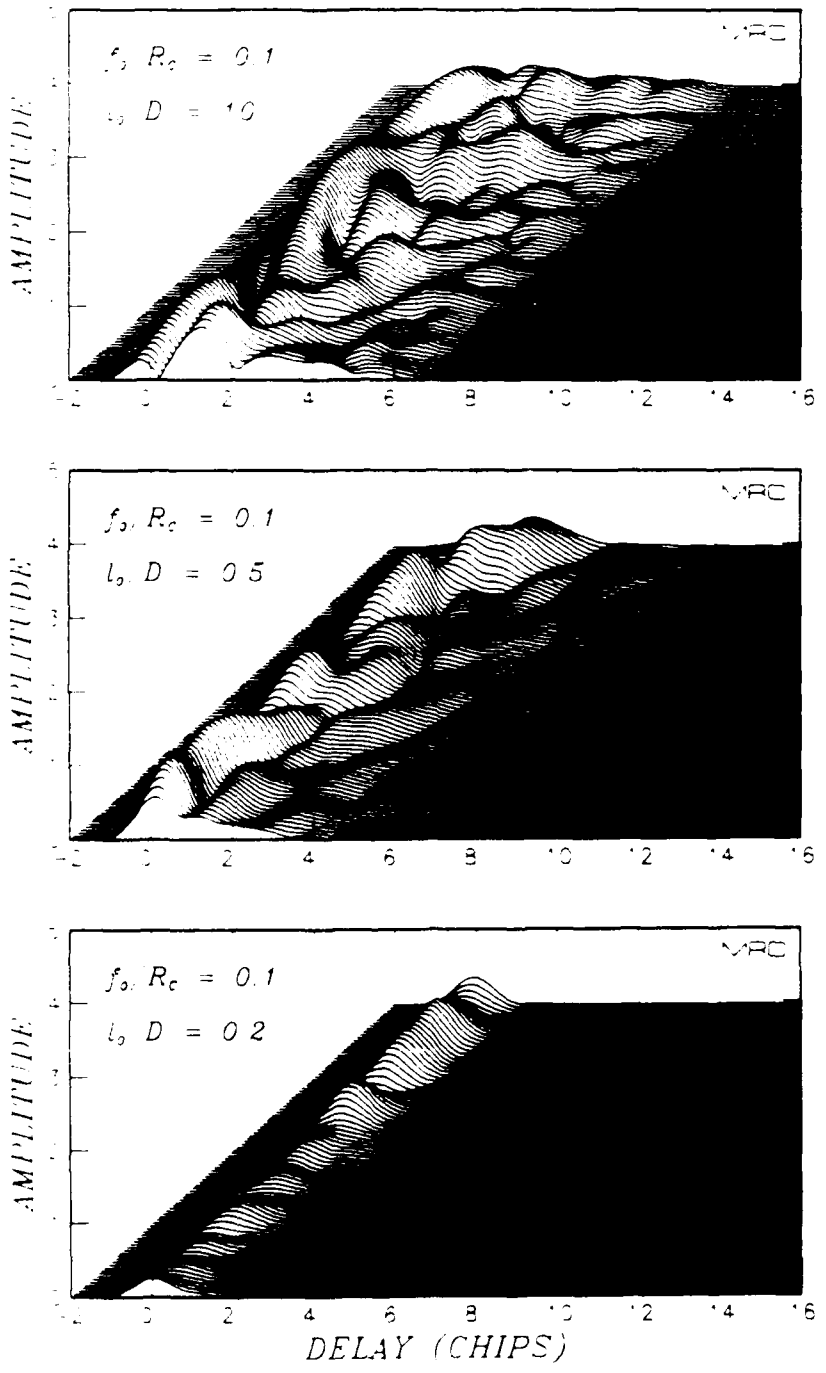


**Figure 15. Effects of spatially selective fading.**

Although the average scattering losses are about the same, the bottom frame of Figure 16 ($\ell_0/D = 0.5$ and $\Theta_0=\theta_0$) and the bottom frame of Figure 15 ($\ell_0/D = 0.2$ and $\Theta_0=0$) are qualitatively quite different. For the case with the pointing angle equal to a beamwidth, the received power is much more spread out in delay compared to the case with zero pointing angle where the signal energy is concentrated near zero delay. This is due to the fact that the antenna pointed away from the line-of-sight has relatively higher gain at large angles and long delays and relatively lower gain at small angles and short delays than does an antenna pointed along the line-of-sight. Thus for an antenna pointed away from the line-of-sight, increased scattering loss does not necessarily result in reduced frequency selective effects.

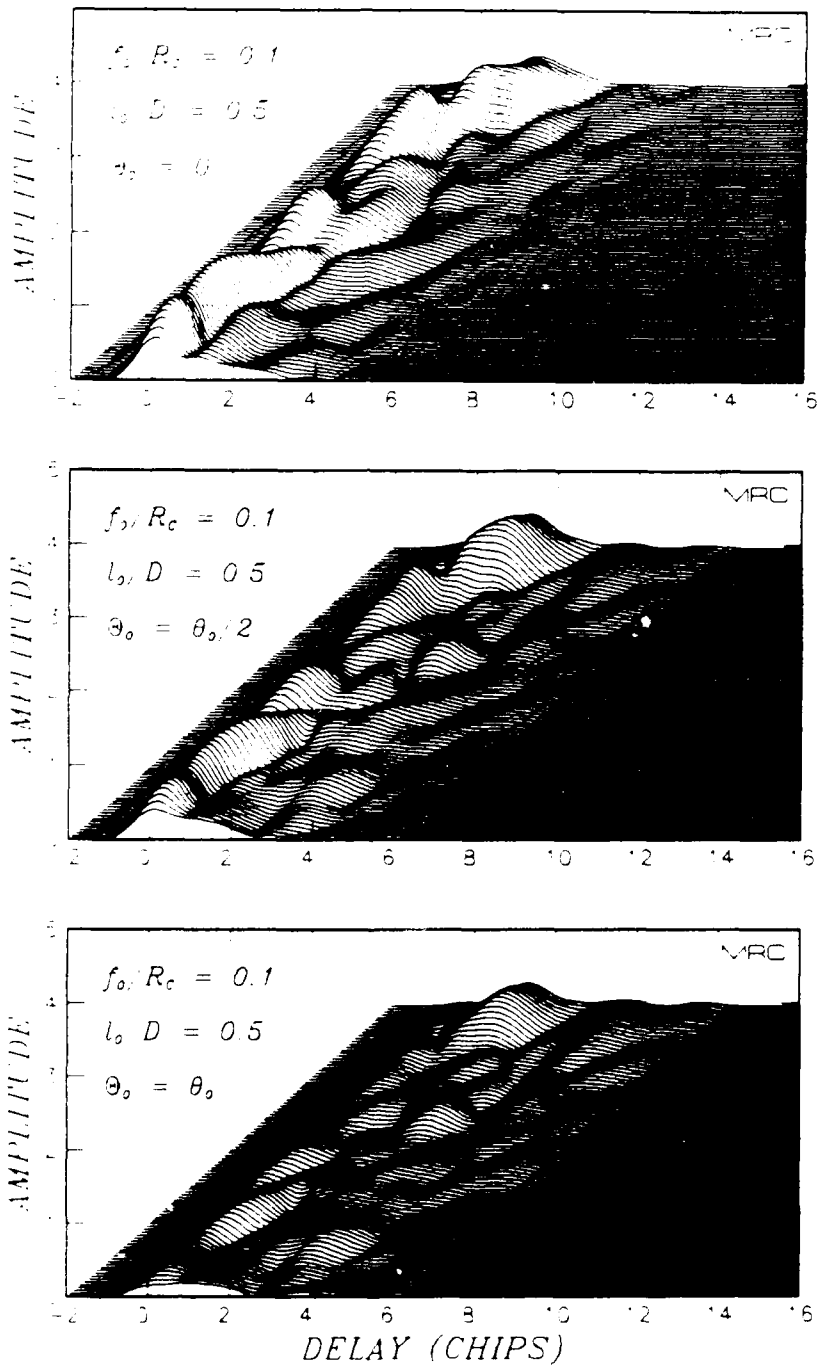


**Figure 16. Effects of beam pointing.**

# SECTION 6
# LIST OF REFERENCES


Arendt, P. R., and H. Soicher, "Effects of Arctic Nuclear Explosions on Satellite Radio Communication," *Proc. IEEE*, Vol. 52, No. 6, pp. 672-676, June 1964.

Bogusch, R. L., F. W. Guigliano, D. L. Knepp, and A. H. Michelet, "Frequency Selective Propagation Effects on Spread-Spectrum Receiver Tracking," *Proc. IEEE*, Vol. 69, No. 7, pp. 787-796, July 1981.

Bogusch, R. L., F. W. Guigliano, and D. L. Knepp, "Frequency Selective Scintillation Effects and Decision Feedback Equalization in High Data-Rate Satellite Links," *Proc. IEEE*, Vol. 71, No. 6, pp. 754-767, June 1983.

Dana, R. A., *Temporal Statistics of Scintillation for Satellite Communication and Radar Systems*, DNA-TR-81-129, MRC-R-692, Mission Research Corporation, April 1982.

Dana, R. A., *Propagation of RF Signals Through Structured Ionization. Theory and Antenna Aperture Effect Applications*, DNA-TR-86-158, MRC-R-976, Mission Research Corporation, May 1986.

Dana, R. A., *Statistics of Sampled Rayleigh Fading*, DNA-TR-89-5, MRC-R-1203, Mission Research Corporation, April 1988.

Davis, T. N., G. J. Romick, E. M. Westcott, R. A. Jeffries, D. M. Kerr, and H. M. Peek, "Observations of the Development of Striations in Large Barium Clouds," *Planet. Space Science*, Vol. 22, p. 67, 1974.

Frasier, S. L., *Antenna-Filtered Scintillation Parameters of Non-Zero Antenna Pointing Angles*, DNA-TR-89-262, MRC-R-1220, Mission Research Corporation, December 1988.

Ishimaru, A., *Wave Propagation and Scattering in Random Media*, Academic Press, New York, 1978.

King, M. A., and P. B. Fleming, "An Overview of the Effects of Nuclear Weapons on Communications Capabilities," *Signal*, pp.59-66, January 1980.

Knepp, D. L., "Analytic Solution for the Two-frequency Mutual Coherence Function for Spherical Wave Propagation," *Radio Science*, Vol. 18, No. 4, pp. 535-549, July 1983.

Knepp, D. L., "Aperture Antenna Effects After Propagation Through Strongly Disturbed Random Media," *IEEE Trans. Antennas Propagat.*, Vol. AP33, No. 10, pp. 1074-1084, October 1985.

Knepp, D. L. and L. A. Wittwer, "Simulation of Wide Bandwidth Signals That Have Propagated Through Random Media," *Radio Science*, Vol. 19, No. 1, pp. 303-318, January 1984.

Lee, L. C., and J. R. Jokipii, "Strong Scintillation in Astrophysics. I. The Markov Approximation, Its Validity and Application to Angular Broadening," *Astrophys. J.*, Vol. 196, No. 3, pp. 695-707, March 1975(a).

Lee, L. C., and J. R. Jokipii, "Strong Scintillation in Astrophysics. II. A Theory of Temporal Broadening of Pulses," *Astrophys. J.*, Vol. 201, No. 2, pp. 532-543, October 1975(b).

Sreenivasiah, I., A. Ishimaru, and S. T. Hong, "Two-Frequency Mutual Coherence Function and Pulse Propagation in a Random Medium: An Analytic Solution to the Plane Wave Case," *Radio Science*, Vol. 11, No. 10, pp. 775-778, October 1976.

Tatarskii, V. I., *The Effects of the Turbulent Atmosphere on Wave Propagation*, translated by Israel Program for Scientific Translations, National Technical Information Service, U.S. Department of Commerce, 1971.

Wittwer, L. A., *Radio Wave Propagation in Structured Ionization for Satellite Applications*, DNA 5304D, Defense Nuclear Agency, January 1979.

Wittwer, L. A., *A Trans-Ionospheric Signal Specification for Satellite $C^3$ Applications*, DNA 5662D, Defense Nuclear Agency, December 1980.

Wittwer, L. A., *Radio Wave Propagation in Structured Ionization for Satellite Applications II*, DNA-IR-82-02, Defense Nuclear Agency, August 1982.

Wittwer, L. A., Private communication, 1988.

Wolcott, J. H., D. J. Simons, T. E. Eastman, and T. J. Fitzgerald, "Characteristics of Late-Time Striations Observed During Operation STRESS," *Effect of the Ionosphere on Space Terrestrial Systems*, edited by J. M. Goodman, pp. 602-613, U. S. Government Printing Office, 1978.

Yeh, K. C. and C. H. Liu, "An Investigation of Temporal Moments of Stochastic Waves," *Radio Science*, Vol. 12, No. 5, pp. 671-680, September 1977.

# APPENDIX A
# PHASE VARIANCE DUE TO ELECTRON DENSITY FLUCTUATIONS

A relationship between the phase variance imparted on the wave as it propagates through the ionization layer and the electron density fluctuations will be derived in this appendix. This relationship is given by Equation 51 which was derived using the Markov approximation. However, it will be shown here that the relationship requires only that the layer thickness be large compared to the decorrelation distance of the electron density fluctuations along the line-of-sight.

It was shown in Section 2 that the total phase change of the wave as it propagates through the ionization layer is

$$\phi = r_e \lambda \langle n_e \rangle \int \xi(\rho,z,t)\, dz \quad . \tag{243}$$

The autocorrelation function of the phase fluctuations is then

$$\langle \phi(\rho,t)\phi(\rho',t') \rangle = (r_e \lambda \langle n_e \rangle)^2 \int_0^L dz \int_0^L dz' \, \langle \xi(\rho,z,t)\xi(\rho',z',t') \rangle \tag{244}$$

where L is the thickness of the scattering layer. For spatially and temporally stationary random electron density fluctuations, the expectation must be a function of the differences $\delta\rho=\rho-\rho'$, $\delta z=z-z'$ and $\delta t=t-t'$ only. Denoting the autocorrelation of $\xi(\rho,z,t)$ by $B_\xi(\delta\rho,\delta z,\delta t)$ and the autocorrelation of $\phi(\rho,t)$ by $B_\phi(\delta\rho,\delta t)$, Equation 244 becomes

$$B_\phi(\delta\rho,\delta t) = (r_e \lambda \langle n_e \rangle)^2 \int_0^L dz \int_0^L dz' \, B_\xi(\delta\rho,\delta z,\delta t) \quad . \tag{245}$$

This double integral may be reduced to a single integral by changing the order of integration with the result

$$B_\phi(\delta\rho,\delta t) = (r_e \lambda \langle n_e \rangle)^2 L \int_{-L}^{L} dz \left(1 - \frac{|z|}{L}\right) B_\xi(\delta\rho,\delta z,\delta t) \quad . \tag{246}$$

If the correlation distance of $B_\xi(\delta\rho,\delta z,\delta t)$ along the z direction is small compared to L, then $B_\xi(\delta\rho,\delta z,\delta t)$ will become small before $|z|/L$ approaches unity in the integral, and the $|z|/L$ term may be ignored. The limits of the integral may then be set to $\pm\infty$ and the integral reduces to

$$B_\phi(\delta\rho,\delta t) = (r_e \lambda \langle n_e \rangle)^2 L \int_{-\infty}^{\infty} dz \, B_\xi(\delta\rho,\delta z,\delta t) \quad . \tag{247}$$

The remaining integral is denoted by $A\xi(\delta\rho,\delta t)$ so the autocorrelation of the phase fluctuations is

$$B_\phi(\delta\rho,\delta t) = (r_e\lambda\langle n_e\rangle)^2 \, L \, A\xi(\delta\rho,\delta t) \ , \tag{248}$$

which is the same as the final expression in Equation 51.

# APPENDIX B
# CHANNEL PARAMETERS FOR $K^{-4}$ ELECTRON DENSITY FLUCTUATIONS

The expansion coefficients $A_0$ and $A_2$ are calculated in this appendix using the quadratic approximation of the structure function $A_\xi(\rho)$ of the electron density fluctuations and using the delta-layer approximation. From these coefficients, the phase variance, decorrelation distance, and the coherence bandwidth of the signal incident on the plane of the receiver are written in terms of physical parameters. However, these channel parameters are computed from a disturbed ionosphere model using the more general formalism of *Wittwer* [1979,1980] which accounts for the finite thickness of the scattering region and other complicating effects. The purpose of this appendix is only to illustrate the dependence of the channel parameters on geometrical and electron density fluctuation parameters.

A power-law form of the PSD for the three-dimensional electron density fluctuations is assumed:

$$S_\xi(\mathbf{K}) = \frac{8\pi^{3/2}\Gamma(n)L_r L_s L_t \langle \Delta n_e^2 \rangle}{\Gamma(n-3/2)\langle n_e \rangle^2 (1 + \mathbf{K}\cdot\mathbf{L}\cdot\mathbf{K})^n} \tag{249}$$

where

$$\mathbf{L} = \begin{bmatrix} L_x^2 & 0 & 0 \\ 0 & L_y^2 & L_{yz} \\ 0 & L_{yz} & L_z^2 \end{bmatrix} . \tag{250}$$

The scales $L_r$, $L_s$, $L_t$ and $L_x$, $L_y$, $L_z$, $L_{yz}$ are defined in Section 2.6 in terms of the penetration angle $\Phi$ and the axial ratio q. For $\mathbf{K}\cdot\mathbf{L}\cdot\mathbf{K} >> 1$, $S_\xi$ is proportional to $K^{-2n}$. Thus a $K^{-4}$ PSD for the three-dimensional electron density fluctuations corresponds to the n = 2 case.

The structure function $A_\xi(\rho)$ under the delta-layer approximation is given by Equation 71 which is reproduced here:

$$A_\xi(\rho) = \int_{-\infty}^{\infty} \exp(i\mathbf{K}_\perp\cdot\rho)\, S_\xi(\mathbf{K}_\perp, K_z=0)\, \frac{d^2\mathbf{K}_\perp}{(2\pi)^2} . \tag{71}$$

Using Equations 249 and 250 and performing the angular integral, Equation 71 reduces to

$$A_\xi(\rho) = \frac{4\sqrt{\pi}\Gamma(n)\, qL_x^2 \langle \Delta n_e^2 \rangle}{\Gamma(n-3/2)\, L_y \langle n_e \rangle^2} \int_0^\infty \frac{J_0\left(K\sqrt{\rho \cdot \mathbf{L}_\perp^{-1} \cdot \rho}\right)}{(1+K^2)^n} K\, dK \tag{251}$$

$$= \frac{\sqrt{\pi}(n-1)\, qL_x^2 \langle \Delta n_e^2 \rangle}{2^{n-3}\Gamma(n-3/2)\, L_y \langle n_e \rangle^2} (\rho \cdot \mathbf{L}_\perp^{-1} \cdot \rho)^{(n-1)/2} K_{n-1}\left(\sqrt{\rho \cdot \mathbf{L}_\perp^{-1} \cdot \rho}\right)$$

where $J_0$ is the Bessel function of order 0, $K_{n-1}$ is the modified Bessel function of order n-1, $\mathbf{L}_\perp$ is a 2–2 matrix containing the x-y components of $\mathbf{L}$, and $\mathbf{L}_\perp^{-1}$ is the inverse matrix of $\mathbf{L}_\perp$.

For all values of n except n equal to 2, $A_\xi(\rho)$ can be expanded in a power series of the form

$$A_\xi(\rho) = A_0 \left\{ 1 - A_2 \left[ \frac{x^2}{L_x^2} + \frac{y^2}{L_y^2} \right]^{\frac{m}{2}} \right\} \tag{252}$$

where $m = \min(2, 2n-2)$. For the n equal 2 case, $A_2$ does not exist unless an inner scale $\ell_i$ is imposed. This is accomplished by truncating the integral over K in Equation 251 at a cutoff $K = L_x/\ell_i$. For values of n greater than 2, the $J_0$ Bessel function in the integrand of Equation 252 can be expanded, and the resulting series can be integrated term-by-term. The first two terms of the expansion give

$$A_0 = \frac{2\sqrt{\pi}\Gamma(n)\, qL_x^2 \langle \Delta n_e^2 \rangle}{\Gamma(n-3/2)\, L_y \langle n_e \rangle^2} \left\{ 1 - \left[ 1 + \frac{L_x^2}{\ell_i^2} \right]^{1-n} \right\} \tag{253}$$

and

$$A_2 = \frac{\left[ 1 + \frac{L_x^2}{\ell_i^2} \right]^{n-1} - \left[ 1 + (n-1)\frac{L_x^2}{\ell_i^2} \right]}{4(n-2)\left[ 1 + \frac{L_x^2}{\ell_i^2} \right]^{n-1} - 1} . \tag{254}$$

In the limit that n equals 2, the $A_2$ coefficient becomes

$$A_2 = \frac{1}{4} \left\{ \left[ 1 + \frac{\ell_i^2}{L_x^2} \right] \ln \left[ 1 + \frac{L_x^2}{\ell_i^2} \right] - 1 \right\} . \tag{255}$$

This expression can be further reduced in the limit that the inner scale is much smaller than the outer scale (i.e. $\ell_i << L_x$) to give

$$A_2 \approx \frac{\ln (L_x/\ell_i)}{2} \quad . \tag{256}$$

Now the phase variance, decorrelation distances, and coherence bandwidth can be written in terms of geometrical parameters and electron density fluctuation parameters. Using Equation 52, the phase variance due to structured ionization is

$$\sigma_\phi^2 = \frac{2qL_x^2 L_\delta}{L_y} r_e^2 \lambda^2 \langle \Delta n_e^2 \rangle \tag{257}$$

where $L_\delta$ is the thickness of the delta layer. The decorrelation distances, decorrelation time, and coherence bandwidth are defined in Equations 79, 80 and 81 respectively. Using these definitions,

$$\ell_x = \left[\frac{2}{\ln(L_x/\ell_i)}\right]^{\frac{1}{2}} \frac{L_x}{\sigma_\phi} \frac{z_t + z_r}{z_t} \tag{258a}$$

$$\ell_y = \left[\frac{2}{\ln(L_x/\ell_i)}\right]^{\frac{1}{2}} \frac{L_y}{\sigma_\phi} \frac{z_t + z_r}{z_t} \tag{258b}$$

$$\tau_0 = \left[\frac{2}{\ln(L_x/\ell_i)}\right]^{\frac{1}{2}} \frac{T_0}{\sigma_\phi} \tag{259}$$

and

$$\omega_{coh} = \frac{\Lambda_y \omega_0^2}{2c \ln(L_x/\ell_i)} \frac{L_x^2}{\sigma_\phi^2} \frac{z_t + z_r}{z_t z_r} \quad . \tag{260}$$

These equations are only valid for the delta-layer approximation, for the quadratic phase structure approximation, and for a $K^{-4}$ three-dimensional electron density fluctuation PSD. It can be seen from the equations that the decorrelation distances and coherence bandwidth are only weakly dependent on the inner scale.

# APPENDIX C
# ACCURACY OF ANGULAR INTEGRATION TECHNIQUES

## C.1 INTRODUCTION.

The mean signal power in a $K_x$-$K_y$ grid cell at the output of an antenna is

$$E_A(k_x,k_y) = \int_{(k_x-1/2)\Delta K_x}^{(k_x+1/2)\Delta K_x} \frac{dK_x}{2\pi} \int_{(k_y-1/2)\Delta K_y}^{(k_y-1/2)\Delta K_y} \frac{dK_y}{2\pi} G(K_x,K_y)\, S_K(K_x,K_y) \quad . \tag{261}$$

Equation 261 is quite general, but it requires that the power in each angular bin be calculated and stored for each antenna. This latter requirement results in unacceptably large arrays. However, Equation 261 can be approximated by assuming that the antenna beam pattern varies slowly over the grid cells so $G(K_x,K_y)$ may be pulled out of the integral. There are several ways that this can be done. The purpose of this appendix is to calculate the accuracy of a few approximations to Equation 261.

In order to limit the scope of this calculation, isotropic scattering and a uniformly-weighted circular antenna will be assumed. Without further loss of generality, it can then be assumed that the antenna is pointed away from the line-of-sight in the x-direction, or equivalently, that the pointing azimuth is zero. For this case, the angular part of the GPSD is

$$S_K(K_x,K_y) = \pi \ell_0^2 \exp\left[ -\frac{(K_x^2 + K_y^2)\ell_0^2}{4} \right] , \tag{262}$$

and the antenna beam pattern is

$$G(K_x,K_y) = \exp\left[ -\frac{(Q-1)(K_x-K_0)^2\ell_0^2}{4} - \frac{(Q-1)K_y^2\ell_0^2}{4} \right] \tag{263}$$

where Q-1 is proportional to the square of the ratio of the antenna diameter D to the decorrelation distance:

$$Q = 1 + \frac{4\ln 2}{(1.02899\pi)^2} \frac{D^2}{\ell_0^2} \quad . \tag{264}$$

For this isotropic scattering and antenna case, the power at the output of the antenna reduces to

$$P_A = \frac{1}{Q} \exp\left[ -\frac{4\ln 2\, \Theta_0^2}{Q\ \theta_0^2} \right] \tag{265}$$

where $\Theta_0$ is the pointing direction elevation angle and $\theta_0$ is the beamwidth of the antenna.

The antenna-filtered decorrelation distance, which is the same in both the x- and y-directions, is

$$\ell_A = \ell_0 \sqrt{Q} \quad . \tag{266}$$

When the antenna is pointed in the $K_x$ direction, the $K_x$ angular grid size is then given by the expression

$$\Delta K_x = \frac{2}{N_x} \left[ \frac{(Q-1)K_0}{Q} + \frac{\kappa_{K,max}}{\ell_0 \sqrt{Q}} \right] \quad , \tag{267a}$$

and the $K_y$ angular grid size is

$$\Delta K_y = \frac{2}{N_y} \left[ \frac{\kappa_{K,max}}{\ell_0 \sqrt{Q}} \right] \tag{267b}$$

where $\kappa_{K,max}$ (Eqn. 217b) is determined by the condition that 99.9 percent of the signal energy be in the $K_x$-$K_y$ grid.

The exact expression for the received power will be compared to the total power in the grid,

$$P_{GK} = \sum_{k_x=-N_x/2}^{N_x/2-1} \sum_{k_y=-N_y/2}^{N_y/2-1} E_A(k_x,k_y) \quad , \tag{268}$$

to compute an error in the total power

$$P_E = \left| \frac{P_A - P_{GK}}{P_A} \right| \tag{269}$$

for each of the algorithms used to evaluate Equation 261.

## C.2 ALGORITHMS.

The first approximation to the exact result is just Equation 261. This expression will result in some error in the total power because of round-off errors in the summation of the contributions from each grid cell and because of the finite size of the angular grid. Additional error results when the beam is pointed near the edge of the grid so part of the beam is pointed out of the grid. The magnitude of this error will be apparent in the results of this analysis. With the assumptions of isotropic scattering and an isotropic Gaussian beam pattern, the integrals indicated in Equation 261 can be obtained in closed form with the result

$$E_1(k_x,k_y) = \frac{P_A}{4} \left\{ \operatorname{erfc}\left[ \frac{(k_x-1/2)\Delta K_x \ell_0 \sqrt{Q}}{2} - \frac{(Q-1)K_0\ell_0}{2\sqrt{Q}} \right] \right. - \operatorname{erfc}\left[ \frac{(k_x+1/2)\Delta K_x \ell_0 \sqrt{Q}}{2} - \frac{(Q-1)K_0\ell_0}{2\sqrt{Q}} \right] \Bigg\} \times \left\{ \operatorname{erfc}\left[ \frac{(k_y-1/2)\Delta K_y \ell_0 \sqrt{Q}}{2} \right] - \operatorname{erfc}\left[ \frac{(k_y+1/2)\Delta K_y \ell_0 \sqrt{Q}}{2} \right] \right\} \quad (270)$$

where erfc( ) is the complementary error function, and where

$$K_0\ell_0 = (1.02899\pi)\frac{\Theta_0}{\theta_0}\frac{\ell_0}{D} . \quad (271)$$

The second approximation, and the one that is used in channel modeling, is obtained by assuming that the antenna beam pattern is constant over an angular grid cell and can therefore be pulled out of the integral. The result is the product of the antenna beam pattern times a term that is equal to the incident power in a grid cell:

$$E_2(k_x,k_y) = G(K_x,K_y)\, E_I(k_x,k_y) \quad (272)$$

where the incident power in a grid cell is

$$E_I(k_x,k_y) = \int_{(k_x-1/2)\Delta K_x}^{(k_x+1/2)\Delta K_x} \frac{dK_x}{2\pi} \int_{(k_y-1/2)\Delta K_y}^{(k_y+1/2)\Delta K_y} \frac{dK_y}{2\pi} S_K(K_x,K_y) . \quad (273)$$

The indicated integrals can again be expressed in terms of error functions:

$$E_I(k_x,k_y) = \frac{1}{2}\left\{ \operatorname{erfc}\left[ \frac{(k_x-1/2)\Delta K_x \ell_0}{2} \right] - \operatorname{erfc}\left[ \frac{(k_x+1/2)\Delta K_x \ell_0}{2} \right] \right\} \times \frac{1}{2}\left\{ \operatorname{erfc}\left[ \frac{(k_y-1/2)\Delta K_y \ell_0}{2} \right] - \operatorname{erfc}\left[ \frac{(k_y+1/2)\Delta K_y \ell_0}{2} \right] \right\} . \quad (274)$$

The advantage of this approximation is that the error function terms depend only on the environment so they can be done once and used for all antennas thereby reducing the required processing time and array sizes.

A third approximation to Equation 261 is similar to the previous approximation. Rather than using the antenna gain at the center of each angular grid cell, the gain averaged over the grid cell is used:

$$E_3(k_x,k_y) = \frac{E_1(k_x,k_y)}{\Delta K_x \Delta K_y} \int_{(k_x-1/2)\Delta K_x}^{(k_x+1/2)\Delta K_x} \frac{dK_x}{2\pi} \int_{(k_y-1/2)\Delta K_y}^{(k_y+1/2)\Delta K_y} \frac{dK_y}{2\pi}\, G(K_x,K_y) \quad . \tag{275}$$

Writing the indicated integrals in terms of error functions gives the result:

$$E_3(k_x,k_y) = E_1(k_x,k_y) \frac{\pi}{\Delta K_x \Delta K_y (Q-1) \ell_0^2} \tag{276}$$

$$\times \left\{ \operatorname{erfc}\left[ \frac{\sqrt{Q-1}\,[(k_x-1/2)\Delta K_x - K_0]\,\ell_0}{2} \right] - \operatorname{erfc}\left[ \frac{\sqrt{Q-1}\,[(k_x+1/2)\Delta K_x - K_0]\,\ell_0}{2} \right] \right.$$

$$\left. \times \left\{ \operatorname{erfc}\left[ \frac{\sqrt{Q-1}\,(k_y-1/2)\Delta K_y\,\ell_0}{2} \right] - \operatorname{erfc}\left[ \frac{\sqrt{Q-1}\,(k_y+1/2)\Delta K_y\,\ell_0}{2} \right] \right\} \right. .$$

Finally, a simple way to eliminate the problem created by Equation 261 is to do away with the integral. This zeroth-order approximation is

$$E_4(k_x,k_y) = \frac{\Delta K_x \Delta K_y}{4\pi^2} G(k_x \Delta K_x, k_y \Delta K_y)\, S_K(k_x \Delta K_x, k_y \Delta K_y) \quad . \tag{277}$$

## C.3 RESULTS.

The relative error (Equation 269) of the four algorithms is calculated for a range of the ratio of the decorrelation distance to the antenna diameter. The scattering loss of the antenna for this range of $\ell_0/D$ is shown in Figure 9 for pointing angles of 0, $\theta_0/2$, and $\theta_0$. Figures 17, 18 and 19 show the relative errors of the four algorithms for the same set of pointing angles. For these calculations, a 32 by 32 angular grid is used (i.e. $N_x$ and $N_y$ are set equal to 32).

When the pointing angle is zero, Algorithm 1 (solid line) has a relatively constant error of about 0.0005. This error is due to the fact that the size of the angular and Doppler frequency grids are based on capturing 99.9 percent of the signal power. The amount of power outside of the rectangular $K_x$-$K_y$ grid is then $\sqrt{0.999}$ which is equal to 0.9995. Both Algorithms 2 (dashed line) and 3 (dotted line) for this case have peak errors of about 0.002 to 0.003 which occur when the angular spread of the incident power is about equal to the antenna beamwidth (i.e., $\ell_0$ is approximately equal to D). Algorithm 4 (dash-dot-dash line) has a maximum relative error for large values of $\ell_0/D$ of about 2, which is clearly too large.

As the pointing angle increases, the maximum error of Algorithm 1 remains constant because the angular grid is expanded in the direction the antenna is pointed. Algorithms 2 and 3 generally have errors which are close to or less than that of Algorithm 1. The maximum error of these algorithms is less than 0.0035 for pointing angles up to one beamwidth. When the pointing angle is equal to a beamwidth, the sign

of the errors of Algorithms 2 and 3 change over the range of $\ell_0/D$ resulting in errors that are smaller in magnitude than that of Algorithm 1.

Algorithm 2 generally has a slightly smaller error than Algorithm 3 over the ranges of $\ell_0/D$ and pointing angles considered in this analysis. Algorithm 2 is also simpler to implement than is Algorithm 3. Based on these results, the second algorithm is used in channel modelling.

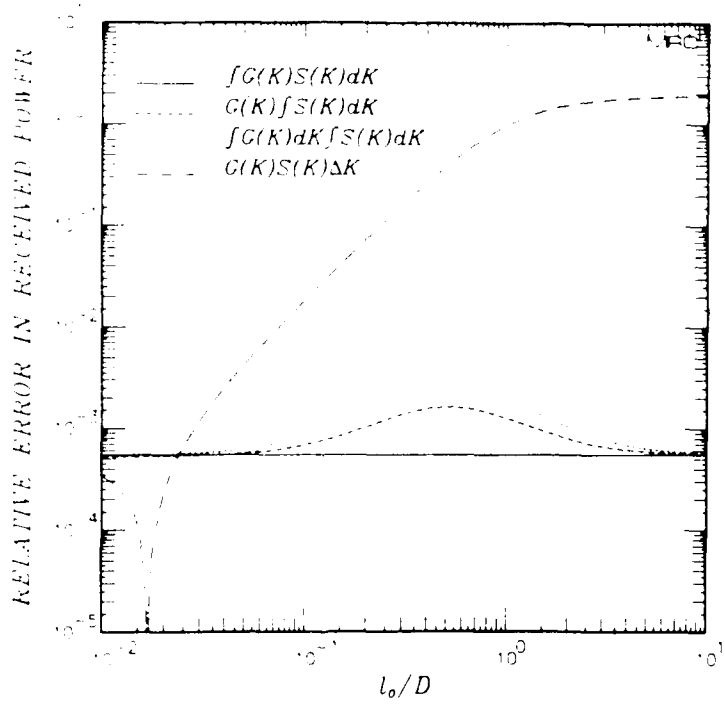


**Figure 17. Relative error for pointing angle of 0.**

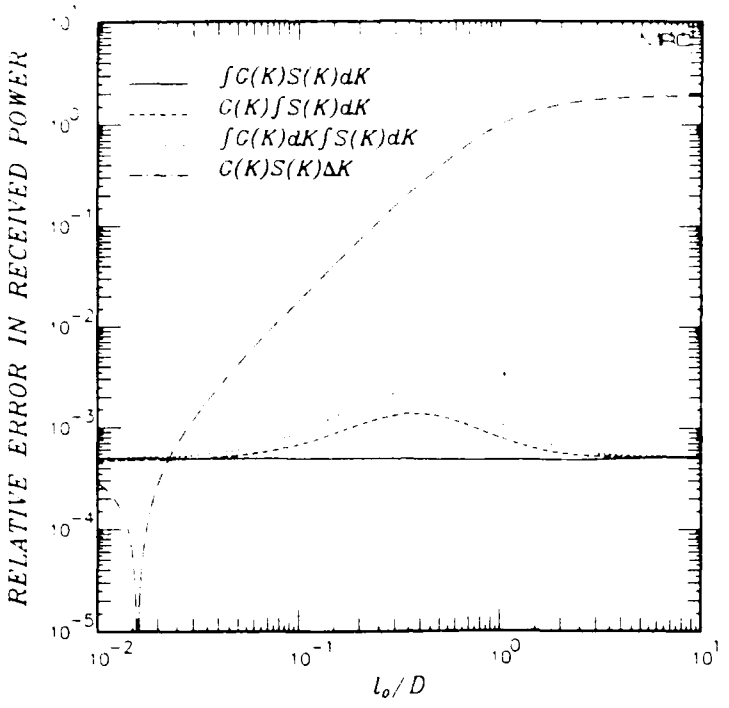


**Figure 18. Relative error for pointing angle of $\theta_0/2$.**

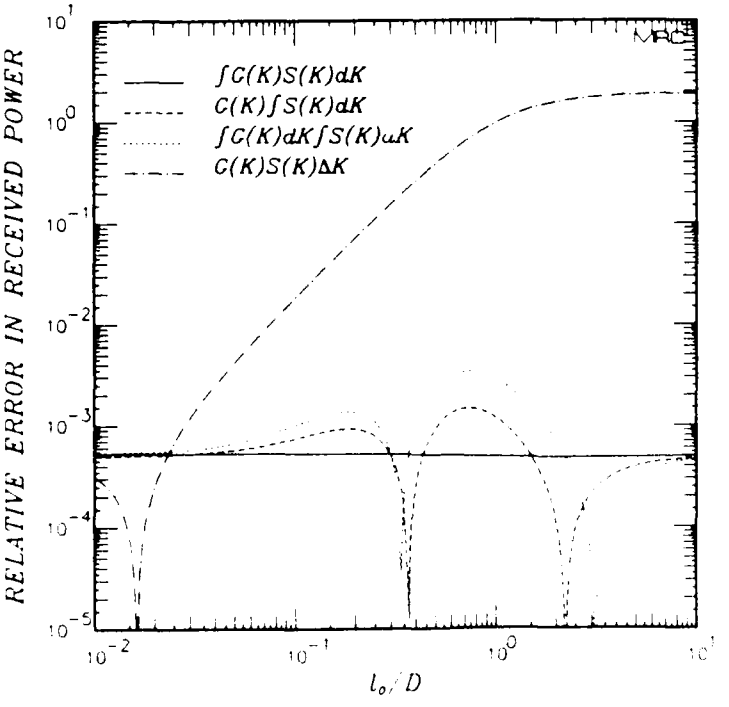


**Figure 19. Relative error for pointing angle of $\theta_0$.**

# APPENDIX D
# ANGLE-DOPPLER GRID CELL POWER

This appendix describes the algorithm used to compute the angle-Doppler grid cell power, $E(k_x,k_y,m)$, from the GPSD. This quantity is computed in the channel simulation on a grid which has a minimum of 32×32 angular cells and 150 Doppler cells. It is therefore necessary to have an efficient algorithm to compute the grid cell power in order to minimized the computation time of the channel simulation.

## D.1 CALCULATION OF GRID CELL POWER.

The first section of this appendix is primarily a review of material presented in Sections 2 and 4 of this report. Implementation details of the algorithms used to compute the angle-Doppler grid cell power are presented in the next section of this appendix.

### D.1.1 Separation of Angular and Doppler Frequency Variables.

Recall from Section 4 that the most general form for $E_{KD}(k_x,k_y,m_D)$ is given by the expression:

$$E_{KD}(k_x,k_y,m_D) = \int_{(k_x-1/2)\Delta K_x}^{(k_x+1/2)\Delta K_x} \frac{dK_x}{2\pi} \int_{(k_y-1/2)\Delta K_y}^{(k_y+1/2)\Delta K_y} \frac{dK_y}{2\pi} \int_{(m_D-1/2)\Delta\omega_D}^{(m_D+1/2)\Delta\omega_D} \frac{d\omega_D}{2\pi} S_{KD}(K_x,K_y,\omega_D) \; . \tag{278}$$

The integrand of this equation can be written in the form

$$S_{KD}(K_x,K_y,\omega_D) = S_D(\omega_D)\, S_{KC}(K_x - C_{xt}\tau_0\omega_D/\ell_x, K_y - C_{yt}\tau_0\omega_D/\ell_y) \tag{279}$$

where

$$S_D(\omega_D) = \sqrt{\pi}\tau_0 \exp\left[ - \frac{\tau_0^2\omega_D^2}{4} \right] \tag{280}$$

and

$$S_{KC}(K_x,K_y) = \frac{\pi \ell_x \ell_y}{\sqrt{1 - C_{xt}^2 - C_{yt}^2}} \times \exp\left[ - \frac{K_x^2\ell_x^2 (1 - C_{yt}^2) + K_y^2\ell_y^2 (1 - C_{xt}^2) + 2C_{xt}C_{yt} K_x \ell_x K_y \ell_y}{4(1 - C_{xt}^2 - C_{yt}^2)} \right] . \tag{281}$$

As described in Section 4.2.2, two tricks are used to efficiently evaluate the grid cell power. The first trick is to take advantage of the translational properties of the GPSD. The power in a $K_x$-$K_y$-$\omega_D$ grid cell is

$$E_{KD}(k_x,k_y,m_D) = \int_{(m_D-1/2)\Delta\omega_D}^{(m_D+1/2)\Delta\omega_D} \frac{d\omega_D}{2\pi} S_D(\omega_D) \tag{282}$$

$$\times \int_{(k_x-1/2)\Delta K_x}^{(k_x+1/2)\Delta K_x} \frac{dK_x}{2\pi} \int_{(k_y-1/2)\Delta K_y}^{(k_y+1/2)\Delta K_y} \frac{dK_y}{2\pi} S_{KC}(K_x - C_{xt}\tau_0\omega_D/\ell_x, K_y - C_{yt}\tau_0\omega_D/\ell_y) .$$

The key to simplifying this expression is to note that the Doppler grid cell size is relatively small because of the large number of Doppler samples that are required to produce a long time realization. Thus it can be assumed that $S_{KC}$ is constant over a Doppler cell, and Equation 281 reduces to a function of Doppler frequency times a shifted function of angle:

$$E_{KD}(k_x,k_y,m_D) = E_D(m_D)\, E_{KC}(k_x-m_x,k_y-m_y) \tag{283}$$

where

$$E_D(m_D) = \frac{1}{2}\left\{\text{erfc}\left[\frac{(m_D-1/2)\tau_0\Delta\omega_D}{2}\right] - \text{erfc}\left[\frac{(m_D+1/2)\tau_0\Delta\omega_D}{2}\right]\right\} . \tag{284}$$

The quantity $E_{KC}(k_x-m_x,k_y-m_y)$ is the power in a shifted $K_x$-$K_y$ grid cell where

$$E_{KC}(k_x,k_y) = \int_{(k_x-1/2)\Delta K_x}^{(k_x+1/2)\Delta K_x} \frac{dK_x}{2\pi} \int_{(k_y-1/2)\Delta K_y}^{(k_y+1/2)\Delta K_y} \frac{dK_y}{2\pi} S_{KC}(K_x,K_y) , \tag{285}$$

and the Doppler shift indices are given by

$$m_x = \text{int}\left[\frac{C_{xt}\tau_0\omega_D}{\ell_x\Delta K_x}\right] \tag{286a}$$

$$m_y = \text{int}\left[\frac{C_{yt}\tau_0\omega_D}{\ell_y\Delta K_y}\right] . \tag{286b}$$

Because of the $K_x$-$K_y$ cross terms in the expression for $S_{KC}$, an easily-evaluated closed-form result is still not obtainable for $E_{KC}$.

### D.1.2 Evaluation of Angular Grid Cell Power on a $K_p$-$K_q$ Grid.

The second trick used in the channel model technique is to note that a rotation by the angle $\vartheta$ (Eqn. 108) in the $K_x$-$K_y$ plane,

$$\vartheta = \frac{1}{2}\tan^{-1}\left[\frac{2C_{xt}C_{yt}\ell_x\ell_y}{\ell_x^2(1 - C_{xt}^2) - \ell_y^2(1 - C_{yt}^2)}\right] . \quad (287)$$

produces an orthogonal form of the GPSD which does not contain angular cross terms, and is therefore readily integrated. This orthogonalized GPSD is given by Equation 109 which has the following form for its angular part:

$$S_{KC}(K_p,K_q) = \frac{\pi\ell_p\ell_q}{\sqrt{(1 - C_{pt}^2)(1 - C_{qt}^2)}}\exp\left[-\frac{K_p^2\ell_p^2}{4(1 - C_{pt}^2)} - \frac{K_q^2\ell_q^2}{4(1 - C_{qt}^2)}\right] . \quad (288)$$

The quantities $\ell_p$, $\ell_q$, $C_{pt}$, and $C_{qt}$ are given by Equations 110 and 111 in terms of the corresponding quantities defined in the x-y coordinate system. The signal power in a $K_p$-$K_q$ grid cell is

$$E_{KC}(k_p,k_q) = E_p(k_p)\,E_q(k_q) \quad (289)$$

where

$$E_p(k_p) = \frac{1}{2}\left\{\mathrm{erfc}\left[\frac{(k_p-1/2)\Delta K_p\ell_p}{2\sqrt{1 - C_{pt}^2}}\right] - \mathrm{erfc}\left[\frac{(k_p+1/2)\Delta K_p\ell_p}{2\sqrt{1 - C_{pt}^2}}\right]\right\} . \quad (290)$$

A similar expression holds for $E_q(k_q)$.

Now, $E_{KC}(k_p,k_q)$ can be computed on a fine $K_p$-$K_q$ grid, and the values simply assigned to the $K_x$-$K_y$ grid cell in which they fall. The $K_x$-$K_y$ cell indices are computed as follows:

$$k_x = \mathrm{int}\left[\frac{k_p\Delta K_p\cos\vartheta - k_q\Delta K_q\sin\vartheta}{\Delta K_x}\right] \quad (291a)$$

$$k_y = \mathrm{int}\left[\frac{k_p\Delta K_p\sin\vartheta + k_q\Delta K_q\cos\vartheta}{\Delta K_y}\right] . \quad (291b)$$

The total power in a $K_x$-$K_y$ grid cell is then the sum of all $E_{KC}(k_p,k_q)$ values that fall within the $K_x$-$K_y$ cell. Roughly ten $K_p$-$K_q$ grid cells are required within each $K_x$-$K_y$ cell for this brute-force procedure to work. Thus the $K_p$-$K_q$ cell sizes are determined by the expressions:

$$\Delta K_p = \frac{0.1}{\left[\frac{\cos^2\vartheta}{(\Delta K_x)^2} + \frac{\sin^2\vartheta}{(\Delta K_y)^2}\right]^{\frac{1}{2}}} \quad (292a)$$

$$\Delta K_q = \frac{0.1}{\left[\frac{\sin^2\vartheta}{(\Delta K_x)^2} + \frac{\cos^2\vartheta}{(\Delta K_y)^2}\right]^{\frac{1}{2}}} . \quad (292b)$$

The size of the $K_p$-$K_q$ grid is also needed before $E_{KC}(k_p,k_q)$ can be computed. The one-dimensional form of $K_p$-$K_q$ angular power spectrum is

$$S_{KC}(K_p) = \frac{\sqrt{\pi}\ell_p}{\sqrt{1 - C_{pt}^2}} \exp\left[ - \frac{K_p^2 \ell_p^2}{4(1 - C_{pt}^2)} \right] . \tag{293}$$

In order that the $K_p$ grid contain a fraction $\zeta_0$ of the angular power, the grid must extend to $K_{p,max}$ where

$$\zeta_0 = \int_{-K_{p,max}}^{K_{p,max}} S_{KC}(K_p) \frac{dK_p}{2\pi} = \operatorname{erf}\left[ \frac{K_{p,max}\ell_p}{2\sqrt{1 - C_{pt}^2}} \right] . \tag{294}$$

Solving for $K_{p,max}$ gives the result:

$$K_{p,max} = \kappa_{K,max} \frac{\sqrt{1 - C_{pt}^2}}{\ell_p} \tag{295a}$$

where $\kappa_{K,max}$ is given by Equation 217b. A similar expression holds for $K_{q,max}$:

$$K_{q,max} = \kappa_{K,max} \frac{\sqrt{1 - C_{qt}^2}}{\ell_q} . \tag{295b}$$

## D.2 ALGORITHMS.

Implementation details of evaluation of $E_{KC}(k_x-m_x,k_y-m_y)$ are discussed in this section. This implementation minimizes the number of computations of $E_{KC}(k_x-m_x,k_y-m_y)$ by using the shifting property for non-zero Doppler frequencies, and minimizes the number of computations of $E_{KC}(k_p,k_q)$ by carefully defining the region of the $K_p$-$K_q$ grid where $E_{KC}(k_x-m_x,k_y-m_y)$ is required.

### D.2.1 Shifted Angular Grid Cell Power $E_{KC}(k_x-m_x,k_y-m_y)$.

In a computer implementation of the channel simulation, $E_{KC}(k_x,k_y)$ is an array with indices

$$k_x = -N_x/2, -N_x/2+1, \cdots, N_x/2-1 \tag{296a}$$

$$k_y = -N_y/2, -N_y/2+1, \cdots, N_y/2-1 . \tag{296b}$$

The shifting process is then just a matter of rearranging the data within the array. Before discussing the algorithms used to shift the $E_{KC}$ array, it is useful to understand the frequency at which this shifting process will occur.

D.2.1.1 Shifting Frequency. In evaluating the discrete impulse response function using Equation 211, the Doppler frequency discrete Fourier transform is performed last, after the two angular DFTs. The evaluation of the Doppler frequency

spectral components $\hat{h}_A(j\Delta\tau, m_D\Delta\omega_D)$ starts at zero Doppler frequency ($m_D=0$) and proceeds to the maximum positive Doppler frequency ($m_D=N_D/2-1$). Spectral components for negative values of Doppler frequency can be obtained by taking advantage in the symmetry of the power in an angle-Doppler grid cell, $E_D(m_D)E_{KC}(k_x-m_x,k_y-m_y)$. Both $E_D$ and $E_{KC}$ are even functions of their arguments. Thus $E_D(-m_D)$ is equal to $E_D(m_D)$, and $E_{KC}(k_x+|m_x|,k_y+|m_y|)$ is equal to $E_{KC}(-k_x-|m_x|,-k_y-|m_y|)$. Hence the Doppler frequency spectral components for negative Doppler frequencies can be evaluated using the angle-Doppler grid cell power calculated for the corresponding positive Doppler frequencies with $k_x\Delta K_x$ and $k_y\Delta K_y$ replaced by $-k_x\Delta K_x$ and $-k_y\Delta K_y$ in Equation 211. (The residual Doppler shifts, $\varepsilon_x$ and $\varepsilon_y$, in Equation 211 also change signs for negative Doppler frequencies.)

Now as each new Doppler frequency spectral component is computed (i.e. for each value of $m_D$, $m_D=1, 2, \cdots, N_D/2-1$), the incremental Doppler shift indices are

$$m_x = \text{int}\left[\frac{C_{xt}\tau_0 m_D\Delta\omega_D}{\ell_x\Delta K_x} - M_x(m_D-1)\right] \tag{297a}$$

$$m_y = \text{int}\left[\frac{C_{yt}\tau_0 m_D\Delta\omega_D}{\ell_y\Delta K_y} - M_y(m_D-1)\right] \tag{297b}$$

where $M_x(m_D)$ and $M_y(m_D)$ are the cumulative shift indices

$$M_x(m_D) = \sum_{m_D'=0}^{m_D} m_x(m_D') \ , \ M_x(-1) = 0 \tag{298a}$$

$$M_y(m_D) = \sum_{m_D'=0}^{m_D} m_y(m_D') \ , \ M_y(-1) = 0 \ . \tag{298b}$$

The corresponding residual shifts are

$$\varepsilon_x = \frac{C_{xt}\tau_0 m_D\Delta\omega_D}{\ell_x} - M_x(m_D)\Delta K_x \tag{299a}$$

$$\varepsilon_y = \frac{C_{yt}\tau_0 m_D\Delta\omega_D}{\ell_y} - M_y(m_D)\Delta K_x \ . \tag{299b}$$

Because the normalized Doppler frequency grid cell size ($\tau_0\Delta\omega_D$) is small compared to the normalized angular grid cell sizes ($\ell_x\Delta K_x$ and $\ell_y\Delta K_y$) due to the fact that there are generally more Doppler grid cells than angular grid cells (in one dimension), the incremental Doppler shift indices $m_x$ and $m_y$ may be zero for several sequential values of $m_D$. Thus, shifting of the $E_{KC}(k_x,k_y)$ array in the x-direction is necessary approximately every $\ell_x\Delta K_x/C_{xt}\tau_0\Delta\omega_D$ Doppler cells, and shifting in the y-

direction is necessary approximately every $\ell_y \Delta K_y / C_{yt} \tau_0 \Delta\omega_D$ Doppler cells. Note, however, that the residual shifts will change for every new value of $m_D$.

D.2.1.2 Shifting Algorithm. Assume for the moment that $E_{KC}(k_x,k_y)$ has been computed and that the shifted array $E_{KC}(k_x-m_x,k_y-m_y)$ is desired. The actual computation of $E_{KC}(k_x,k_y)$ for arbitrary $k_x$ and $k_y$ will be discussed in the next subsection.

For non-negative values of $C_{xt}$ and $C_{yt}$, the incremental Doppler shift indices $m_x$ and $m_y$ will also be non-negative. However, the general model puts no restrictions on the signs or the space-time correlation coefficients as long as the square root of the sum of the squares of these coefficients is between zero and one. Therefore, a completely general algorithm must include the possibility of positive and negative values of the incremental Doppler shifts.

Now assume that $E_{KC}(k_x-m_x,k_y)$ is desired where $m_x$ is positive. An algorithm that performs this shifting is

$$\begin{aligned}
E_{KC}(N_x/2-1,k_y) &\leftarrow E_{KC}(N_x/2-1-m_x,k_y) \\
E_{KC}(N_x/2-2,k_y) &\leftarrow E_{KC}(N_x/2-2-m_x,k_y) \\
&\vdots \\
E_{KC}(-N_x/2+m_x,k_y) &\leftarrow E_{KC}(-N_x/2,k_y) \ .
\end{aligned} \tag{300}$$

Note that after the shifting, $E_{KC}(-N_x/2,k_y)$ through $E_{KC}(-N_x/2+m_x-1,k_y)$ have not been defined. These grid cell powers will then need to be computed after the shifting is performed.

If $m_x$ is negative, a shifting algorithm is

$$\begin{aligned}
E_{KC}(-N_x/2,k_y) &\leftarrow E_{KC}(-N_x/2-m_x,k_y) \\
E_{KC}(-N_x/2+1,k_y) &\leftarrow E_{KC}(-N_x/2+1-m_x,k_y) \\
&\vdots \\
E_{KC}(N_x/2-1+m_x,k_y) &\leftarrow E_{KC}(N_x/2-1,k_y) \ .
\end{aligned} \tag{301}$$

Note that after the shifting, $E_{KC}(N_x/2+m_x,k_y)$ through $E_{KC}(N_x/2-1,k_y)$ have not been defined and will need to be computed.

Similar algorithms can be defined to shift $E_{KC}(N_x,k_y+m_y)$ by positive or negative $m_y$. The algorithm for computing $E_{KC}(k_x,k_y)$ is discussed next.

### D.2.2 Angular Grid Cell Power $E_{KC}(k_x,k_y)$.

Depending on the Doppler frequency, $E_{KC}$ may be computed over all or part of the $K_x$-$K_y$ grid. When the Doppler frequency is zero and $E_{KC}$ is computed for the first time, then $E_{KC}$ is computed over the entire angular grid. However, for positive values of the Doppler frequency, $E_{KC}$ is obtained by shifting and new values of $E_{KC}$ are required only in a small region of the $K_x$-$K_y$ grid. Angular grid cell power values for negative Doppler frequencies are obtained directly from the corresponding positive Doppler frequency values, and no new calculations of $E_{KC}$ are required.

This section describes an algorithm for computing $E_{KC}(k_x,k_y)$ with arbitrary limits on the indices. In general the limits on $k_x$ and $k_y$ are $k_{x,1}$ to $k_{x,2}$ and $k_{y,1}$ to $k_{y,2}$. When $E_{KC}$ is computed for the first time,

$$k_{x,1} = -N_x/2 \tag{302a}$$

$$k_{x,2} = N_x/2-1 \tag{302b}$$

$$k_{y,1} = -N_y/2 \tag{302c}$$

$$k_{y,2} = N_y/2-1 \ , \tag{302d}$$

and afterward,

$$k_{x,1} = \begin{cases} -N_x/2 & \text{if } m_x > 0 \\ N_x/2+m_x & \text{if } m_x < 0 \end{cases} \tag{303a}$$

$$k_{x,2} = \begin{cases} -N_x/2+m_x-1 & \text{if } m_x > 0 \\ N_x/2-1 & \text{if } m_x < 0 \end{cases} \tag{303b}$$

$$k_{y,1} = \begin{cases} -N_y/2 & \text{if } m_y > 0 \\ N_y/2+m_y & \text{if } m_y < 0 \end{cases} \tag{303c}$$

$$k_{y,2} = \begin{cases} -N_y/2+m_y-1 & \text{if } m_y > 0 \\ N_y/2-1 & \text{if } m_y < 0 \end{cases} \tag{303d}$$

D.2.2.1 <u>$K_p$-$K_q$ Regions.</u> Given these limits, the first task is to compute the $K_x$-$K_y$ region on the $K_p$-$K_q$ grid defined by the limits. This rectangular region is defined by the four points $(K_{x,1},K_{y,1})$, $(K_{x,1},K_{y,2})$, $(K_{x,2},K_{y,1})$, and $(K_{x,2},K_{y,2})$ where

$$K_{x,1} = \left[k_{x,1} - \frac{1}{2} - M_x(m_D)\right]\Delta K_x \tag{304a}$$

$$K_{x,2} = \left[k_{x,1} + \frac{1}{2} - M_x(m_D)\right]\Delta K_x \tag{304b}$$

$$K_{y,1} = \left[ k_{y,1} - \frac{1}{2} - M_y(m_D) \right] \Delta K_y \tag{304c}$$

$$K_{y,2} = \left[ k_{y,1} + \frac{1}{2} - M_y(m_D) \right] \Delta K_y \ . \tag{304d}$$

The corresponding $K_p$-$K_q$ coordinates are

$$K_{p,1} = K_{x,1} \cos \vartheta + K_{y,1} \sin \vartheta \tag{305a}$$

$$K_{p,2} = K_{x,1} \cos \vartheta + K_{y,2} \sin \vartheta \tag{305b}$$

$$K_{p,3} = K_{x,2} \cos \vartheta + K_{y,2} \sin \vartheta \tag{305c}$$

$$K_{p,4} = K_{x,2} \cos \vartheta + K_{y,1} \sin \vartheta \tag{305d}$$

$$K_{q,1} = K_{y,1} \cos \vartheta - K_{x,1} \sin \vartheta \tag{305e}$$

$$K_{q,2} = K_{y,2} \cos \vartheta - K_{x,1} \sin \vartheta \tag{305f}$$

$$K_{q,3} = K_{y,2} \cos \vartheta - K_{x,2} \sin \vartheta \tag{305g}$$

$$K_{q,4} = K_{y,1} \cos \vartheta - K_{x,2} \sin \vartheta \ . \tag{305h}$$

The algorithm that determines the region of the $K_p$-$K_q$ plane that is encompassed by the $K_x$-$K_y$ region and that contains signal energy depends on $K_{p,1}$ being the smallest $K_p$ value. If, in fact $K_{p,2}$ is less than $K_{p,1}$, then the $K_p$-$K_q$ coordinates must be renamed:

$$K_p = K_{p,1} \tag{306a}$$

$$K_q = K_{q,1} \tag{306b}$$

$$K_{p,1} = K_{p,2} \tag{306c}$$

$$K_{q,1} = K_{q,2} \tag{306d}$$

$$K_{p,2} = K_{p,3} \tag{306e}$$

$$K_{q,2} = K_{q,3} \tag{306f}$$

$$K_{p,3} = K_{p,4} \tag{306g}$$

$$K_{q,3} = K_{q,4} \tag{306h}$$

$$K_{p,4} = K_p \tag{306i}$$

$$K_{q,4} = K_q \ . \tag{306j}$$

With this ordering of the $K_p$-$K_q$ coordinates, the smallest value of $K_p$ is $K_{p,1}$ and the largest value is $K_{p,3}$. The smallest value of $K_q$ is $K_{q,4}$ and the largest value is $K_{q,2}$. Thus the $K_x$-$K_y$ region is outside of the limits of the $K_p$-$K_q$ grid if $K_{p,3} < -K_{p,max}$, $K_{p,1} > K_{p,max}$, $K_{q,2} < K_{q,max}$, or $K_{q,4} > K_{q,max}$. If none of these conditions are met, then there is signal energy within the $K_x$-$K_y$ region, and the calculation continues. If any of these conditions are met, then the $K_x$-$K_y$ region falls outside of the region in the $K_p$-$K_q$ plane where there is signal power, and there is no need to continue the calculation.

There are nine separate cases, illustrated in Figure 20, when the overlap between the $K_x$-$K_y$ region and the $K_p$-$K_q$ region containing 99.9 percent of the signal energy is considered. The rectangle for each case corresponds to the $K_x$-$K_y$ region over which the calculation of $E_{KC}$ is to be done. The numbered corners correspond to the $K_p$-$K_q$ coordinates of the $K_x$-$K_y$ rectangle given by Equation 305. The dashed lines illustrate the $\pm K_{q,max}$ limits of the $K_p$-$K_q$ grid. Case 1 configurations are determined by the condition that $-K_{q,max} < K_{q,1} < K_{q,max}$. Case 2 configurations occur when this condition is not met. The shaded areas in the figures illustrate the part of the $K_p$-$K_q$ plane bounded by the $K_x$-$K_y$ region that also meet the condition $-K_{q,max} < K_q < K_{q,max}$.

D.2.2.2 <u>$K_p$-$K_q$ Power Centroid Lines.</u> Once the $K_x$-$K_y$ region on the $K_p$-$K_q$ plane has been defined, an efficient method of computing the signal power is to draw a power centroid line across the region, as illustrated by the lines across the shaded areas in Figure 20. In two cases (2a-1 and 2b-1), this line is colinear with the $\pm K_{q,max}$ line. The power in $K_p$-$K_q$ grid cells is calculated for each value of $K_p$ in the shaded regions, by starting with the cell on the line and proceeding to larger values of $K_q$ until the upper $K_q$ boundary of the shaded region is encountered. Then the power in the first cell below the line is calculated and so on until the lower $K_q$ boundary of the shaded region is encountered.

The endpoints of the line depend on the case. For case 1:

$$K_{p,start} = K_{p,1} \tag{307a}$$

$$K_{p,stop} = K_{p,3} \tag{307b}$$

$$K_{q,start} = K_{q,1} \tag{307c}$$

$$K_{q,stop} = K_{q,3} \; . \tag{307d}$$

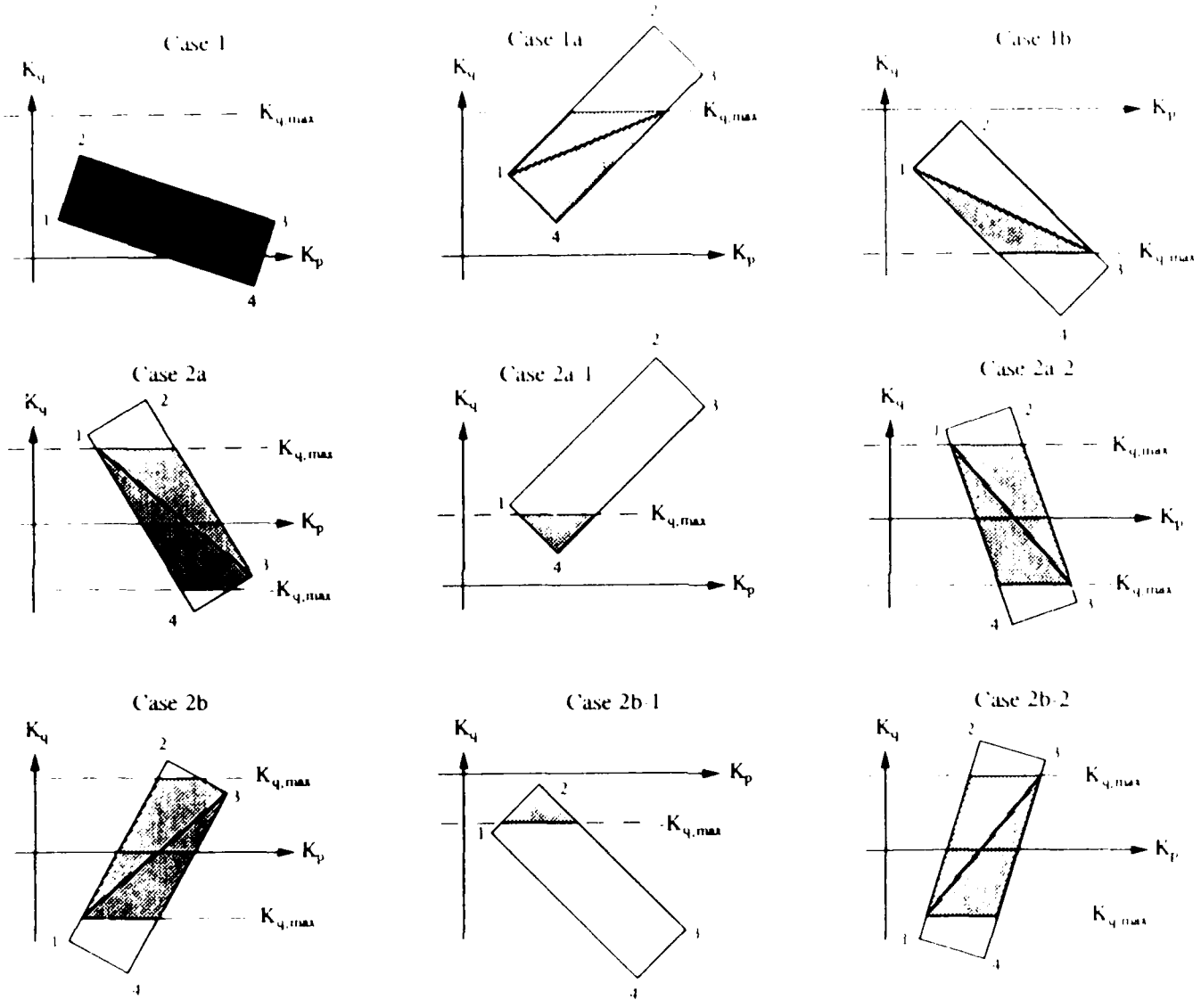


**Figure 20. $K_X$-$K_Y$ regions on the $K_P$-$K_Q$ plane.**

For case 1a:

$$K_{p,start} = K_{p,1} \tag{308a}$$

$$K_{p,stop} = K_{p,4} + (K_{q,max}-K_{q,4}) \frac{K_{p,3}-K_{p,4}}{K_{q,3}-K_{q,4}} \tag{308b}$$

$$K_{q,start} = K_{q,1} \tag{308c}$$

$$K_{q,stop} = K_{q,max} \ . \tag{308d}$$

For case 1b:

$$K_{p,start} = K_{p,1} \tag{309a}$$

$$K_{p,stop} = K_{p,2} - (K_{q,max}+K_{q,2}) \frac{K_{p,3}-K_{p,2}}{K_{q,3}-K_{q,2}} \tag{309b}$$

$$K_{q,start} = K_{q,1} \tag{309c}$$

$$K_{q,stop} = -K_{q,max} \ . \tag{309d}$$

For case 2a:

$$K_{p,start} = K_{p,1} + (K_{q,max}-K_{q,1}) \frac{K_{p,4}-K_{p,1}}{K_{q,4}-K_{q,1}} \tag{310a}$$

$$K_{p,stop} = K_{p,3} \tag{310b}$$

$$K_{q,start} = K_{q,max} \tag{310c}$$

$$K_{q,stop} = K_{q,3} \ . \tag{310d}$$

For case 2a-1:

$$K_{p,start} = K_{p,1} + (K_{q,max}-K_{q,1}) \frac{K_{p,4}-K_{p,1}}{K_{q,4}-K_{q,1}} \tag{311a}$$

$$K_{p,stop} = K_{p,4} + (K_{q,max}-K_{q,4}) \frac{K_{p,3}-K_{p,4}}{K_{q,3}-K_{q,4}} \tag{311b}$$

$$K_{q,start} = K_{q,max} \tag{311c}$$

$$K_{q,stop} = K_{q,max} \ . \tag{311d}$$

For case 2a-2:

$$K_{p,start} = K_{p,1} + (K_{q,max}-K_{q,1}) \frac{K_{p,4}-K_{p,1}}{K_{q,4}-K_{q,1}} \tag{312a}$$

$$K_{p,stop} = K_{p,2} - (K_{q,max}+K_{q,2}) \frac{K_{p,3}-K_{p,2}}{K_{q,3}-K_{q,2}} \tag{312b}$$

$$K_{q,start} = K_{q,max} \tag{312c}$$

$$K_{q,stop} = -K_{q,max} \ . \tag{312d}$$

For case 2b:

$$K_{p,start} = K_{p,1} - (K_{q,max}+K_{q,1}) \frac{K_{p,2}-K_{p,1}}{K_{q,2}-K_{q,1}} \tag{313a}$$

$$K_{p,stop} = K_{p,3} \tag{313b}$$

$$K_{q,start} = -K_{q,max} \tag{313c}$$

$$K_{q,stop} = K_{q,3} \ . \tag{313d}$$

For case 2b-1:

$$K_{p,start} = K_{p,1} - (K_{q,max}+K_{q,1}) \frac{K_{p,2}-K_{p,1}}{K_{q,2}-K_{q,1}} \tag{314a}$$

$$K_{p,stop} = K_{p,3} - (K_{q,max}+K_{q,3}) \frac{K_{p,2}-K_{p,3}}{K_{q,2}-K_{q,3}} \tag{314b}$$

$$K_{q,start} = -K_{q,max} \tag{314c}$$

$$K_{q,stop} = -K_{q,max} \ . \tag{314d}$$

Finally, for case 2b-2:

$$K_{p,start} = K_{p,1} - (K_{q,max}+K_{q,1}) \frac{K_{p,2}-K_{p,1}}{K_{q,2}-K_{q,1}} \tag{315a}$$

$$K_{p,stop} = K_{p,4} + (K_{q,max}-K_{q,4}) \frac{K_{p,3}-K_{p,4}}{K_{q,3}-K_{q,4}} \tag{315b}$$

$$K_{q,start} = -K_{q,max} \tag{315c}$$

$$K_{q,stop} = K_{q,max} \ . \tag{315d}$$

Once the endpoints of the line are defined, the slope of the line is

$$S_L = \frac{K_{q,stop}-K_{q,start}}{K_{p,stop}-K_{p,start}} \ . \tag{316}$$

D.2.2.3 <u>$K_p$-$K_q$ and $K_x$-$K_y$ Grid Power.</u> The final step is to compute the $K_p$-$K_q$ grid cell power and to assign that power to $K_x$-$K_y$ grid cells within the $K_x$-$K_y$ region.

The indices of the $K_p$ grid cells within the $K_x$-$K_y$ region are

$$k_{p,start} = \text{int}\left[\frac{\max(K_{p,start},-K_{p,max})}{\Delta K_p} + \frac{1}{2}\,\text{sign}\,(K_{p,start})\right] \tag{317a}$$

$$k_{p,stop} = \text{int}\left[\frac{\min(K_{p,stop},K_{p,max})}{\Delta K_p} + \frac{1}{2}\,\text{sign}\,(K_{p,stop})\right] , \tag{317b}$$

where sign (·) is the sign function (i.e. a function that is equal to +1 is the argument is positive and is equal to -1 otherwise), and the maximum $k_q$ index is

$$k_{q,max} = \text{int}\left[\frac{K_{q,max}}{\Delta K_q} + \frac{1}{2}\,\text{sign}\,(K_{q,max})\right] . \tag{318}$$

The minimum and maximum functions that appear in Equation 317 constrain $K_x$-$K_y$ region to also be within the $\pm K_{p,max}$ bounds where 99.9 percent of the signal energy lies. The 1/2 sign (K) terms cause the integer function to round its argument in the desired way.

Now a loop is executed over the $k_p$ index, starting at $k_{p,start}$ and ending at $k_{p,stop}$. For each value of $k_p$, the energy in a $\Delta K_p$ grid cell is given by Equation 290 which is reproduced here:

$$E_p(k_p) = \frac{1}{2}\left\{\text{erfc}\left[\frac{(k_p-1/2)\Delta K_p \ell_p}{2\sqrt{1 - C_{pt}^2}}\right] - \text{erfc}\left[\frac{(k_p+1/2)\Delta K_p \ell_p}{2\sqrt{1 - C_{pt}^2}}\right]\right\} . \tag{290}$$

Corresponding to each value of $k_p$ is a range of $k_q$ values. The loop over $K_q$ values starts at the power centroid line, which has a $K_q$ value of

$$K_{q,L} = K_{q,start} + (k_p\Delta K_p - K_{p,start})\, S_L \tag{319}$$

and an index of

$$k_{q,L} = \text{int}\left[\frac{K_{q,L}}{\Delta K_q} + \frac{1}{2}\,\text{sign}\,(K_{q,L})\right] . \tag{320}$$

The $K_q$ loop starts at the $k_q$ value of the line and proceeds to higher values of $k_q$ until the limits of the $K_x$-$K_y$ region are encountered, as described below. Then the calculation is restarted at the first $K_q$ cell below the line and $k_q$ is decremented until the $K_x$-$K_y$ region boundary is again reached. For each $K_q$ grid cell, the signal power is

$$E_q(k_q) = \frac{1}{2}\left\{\text{erfc}\left[\frac{(k_q-1/2)\Delta K_q \ell_q}{2\sqrt{1 - C_{qt}^2}}\right] - \text{erfc}\left[\frac{(k_q+1/2)\Delta K_q \ell_q}{2\sqrt{1 - C_{qt}^2}}\right]\right\} \tag{321}$$

and the total $K_p$-$K_q$ grid cell power is just $E_p(k_p)E_q(k_q)$.

Finally, the $K_p$-$K_q$ grid cell power is assigned to $K_x$-$K_y$ grid cells, and $E_p(k_p)E_q(k_q)$ is added to the power already assigned to each $K_x$-$K_y$ grid cell. The $K_x$-$K_y$ grid cell indices are computed as

$$k_x = \text{int}\left[\frac{k_p\Delta K_p\cos\vartheta - k_q\Delta K_q\sin\vartheta + M_x(m_D)\Delta K_x}{\Delta K_x}\right] \tag{322a}$$

$$k_y = \text{int}\left[\frac{k_p\Delta K_p\sin\vartheta + k_q\Delta K_q\cos\vartheta + M_y(m_D)\Delta K_y}{\Delta K_y}\right] . \tag{322b}$$

These indices are also used to stop the loop over $k_q$. This loop is terminated whenever $k_x$ or $k_y$ fall outside of the limits given by Equations 302 or 303. Thus when $k_q$ is being incremented for cells above the power centroid line, the $k_q$ loop is continued as long as $k_{x,1} \le k_x \le k_{x,2}$ and $k_{y,1} \le k_y \le k_{y,2}$. When either of these conditions are not met, the loop is reset to the first $k_q$ value below the line and $k_q$ is decremented as long as $k_{x,1} \le k_x \le k_{x,2}$ and $k_{y,1} \le k_y \le k_{y,2}$. When either of these conditions are not met, the next value in the $k_p$ loop is executed.

# APPENDIX E
# LIST OF ACRONYMS

| | | |
|---|---|---|
| ACIRF | - | Antenna/channel impulse response function |
| dB | - | Decibel |
| DFT | - | Discrete Fourier transform |
| DNA | - | Defense Nuclear Agency |
| FFT | - | Fast Fourier transform |
| FSK | - | Frequency-shift keying |
| GPSD | - | Generalized power spectral density |
| MHz | - | Million Hertz ($10^6$ cycles per second) |
| MRC | - | Mission Research Corporation |
| PSD | - | Power spectral density |
| PSK | - | Phase-shift keying |
| RF | - | Radio frequency |
| TEC | - | Total electron content |

## APPENDIX F
## LIST OF SYMBOLS

| Symbol | | | Page (where first used) |
|---|---|---|---|
| $A(\rho)$ | = | Aperture weighting function | 38 |
| a | = | Aperture weighting function normalization factor | 45 |
| $A_x$ | = | Antenna pointing factor | 70 |
| $A_y$ | = | Antenna pointing factor | 70 |
| $A\xi(\rho,t)$ | = | Structure function | 9 |
| $A_0$ | = | Structure function at zero offset, $A\xi(0,0)$ | 11 |
| $a_0$ | = | Beamwidth scale factor | 52 |
| $A_2$ | = | Quadratic coefficient of structure function expansion | 20 |
| $\mathbf{B}$ | = | Geomagnetic field | 19 |
| $B_\phi(\delta\rho,\delta t)$ | = | Autocorrelation of the phase of the RF wave | 87 |
| $B\xi(\delta\rho,\delta z,\delta t)$ | = | Three-dimensional structure function | 87 |
| c | = | Speed of light in vacuum ($2.997925\times10^8$ m/s) | 4 |
| C | = | Space-time correlation coefficient | 18 |
| $C_{pt}$ | = | P-direction space-time correlation coefficient | 34 |
| $C_{qt}$ | = | Q-direction space-time correlation coefficient | 34 |
| $C_{xt}$ | = | X-direction space-time correlation coefficient | 21 |
| $C_{yt}$ | = | Y-direction space-time correlation coefficient | 21 |
| D | = | Circular antenna diameter | 40 |
| d | = | Propagation distance difference | 26 |
| $D_u$ | = | Rectangular antenna size in u-direction | 47 |
| $D_v$ | = | Rectangular antenna size in v-direction | 47 |
| $d_x$ | = | Maximum x-direction separation of antennas | 71 |
| $d_y$ | = | Maximum y-direction separation of antennas | 71 |
| $\mathbf{E}(\mathbf{r},\omega,t)$ | = | Complex envelope of electric field | 4 |
| e | = | Base of natural logarithms (2.71828···) | 4 |
| $\mathfrak{E}(\mathbf{r},\omega,t)$ | = | Electric field of RF wave | 3 |
| $E_A(k_x,k_y)$ | = | Mean signal power in an angular grid cell at output of an antenna | 93 |
| $E_A(k_x,k_y,m_D)$ | = | Mean signal power in an angular-Doppler grid cell at output of an antenna | 64 |
| $E_I(k_x,k_y)$ | = | Mean incident power of angular grid cell | 95 |
| $E_{KC}(k_x,k_y)$ | = | Mean signal power in an angular grid cell | 65 |
| $E_{KD}(k_x,k_y,m_D)$ | = | Mean signal power in an angular-Doppler grid cell | 64 |
| $E_D(m_D)$ | = | Mean signal power in a Doppler grid cell | 65 |
| $E_p(k_p)$ | = | Mean signal power in a $K_p$ grid cell | 65 |
| $E_q(k_q)$ | = | Mean signal power in a $K_q$ grid cell | 65 |

## LIST OF SYMBOLS (Continued)

| Symbol | | | Page |
|---|---|---|---|
| $E_0$ | = | Complex envelope of electric field at transmitter | 11 |
| $E_1(k_x,k_y)$ | = | Mean power of angular grid cell for algorithm 1 | 95 |
| $E_2(k_x,k_y)$ | = | Mean power of angular grid cell for algorithm 2 | 95 |
| $E_3(k_x,k_y)$ | = | Mean power of angular grid cell for algorithm 3 | 96 |
| $E_4(k_x,k_y)$ | = | Mean power of angular grid cell for algorithm 4 | 96 |
| erf (x) | = | Error function | 70 |
| erfc (x) | = | Complementary error function | 30 |
| $erf^{-1}$ (x) | = | Inverse error function | 69 |
| F(z) | = | Wittwer's F function | 28 |
| $f_A$ | = | Antenna output frequency selective bandwidth | 50 |
| $f_D$ | = | Doppler frequency shift | 37 |
| $f_0$ | = | Channel frequency selective bandwidth | 23 |
| $f_1(\mathbf{R})$ | = | General function of n-dimensional vector **R** | 8 |
| $f_2(f_1)$ | = | General function of the function $f_1$ | 8 |
| $G(\mathbf{K}_\perp)$ | = | Antenna power beam pattern | 39 |
| $g(\mathbf{K}_\perp)$ | = | Antenna voltage beam pattern | 38 |
| $\mathbf{H}(\mathbf{r},\omega,t)$ | = | Complex envelope of magnetic field | 4 |
| $\mathcal{H}(\mathbf{r},\omega,t)$ | = | Magnetic field of RF wave | 4 |
| $H(\omega,t)$ | = | Channel transfer function | 75 |
| $h(\rho,\tau,t)$ | = | Channel impulse response function at position $\rho$ | 35 |
| $h(\tau,t)$ | = | Channel impulse response function | 75 |
| $\hat{h}(\mathbf{K}_\perp,\tau,\omega_D)$ | = | Fourier transform of the impulse response function | 60 |
| $h_A(\rho_0,\tau,t)$ | = | Impulse response function at antenna output | 59 |
| i | = | $\sqrt{-1}$ | 4 |
| int [x] | = | Integer function (integer part of argument) | 62 |
| j | = | Index of delay grid | 66 |
| $J_0(x)$ | = | Bessel function of zeroth order | 90 |
| $J_1(x)$ | = | Bessel function of first order | 46 |
| **K** | = | K-space vector | 19 |
| K | = | Magnitude of **K** | 21 |
| k | = | Wave number in vacuum ($k=\omega/c$) | 5 |
| $\langle k \rangle$ | = | Mean wave number in ionization | 6 |
| $\mathbf{K}'$ | = | Dummy $\mathbf{K}_\perp$ vector | 39 |
| $\mathbf{K}''$ | = | Dummy $\mathbf{K}_\perp$ vector | 3 |
| $k_d$ | = | Relative wave number $(k_1 - k_2)/2$ | 13 |
| $k_F$ | = | Frequency index | 76 |

## LIST OF SYMBOLS (Continued)

| Symbol | | | Page |
|---|---|---|---|
| $K_{n-1}(x)$ | = | Modified Bessel function of order n-1 | 90 |
| $K_p$ | = | Component of $\mathbf{K}_\perp$ in p-q-z coordinate system | 34 |
| $k_p$ | = | Index of $K_p$ grid | 65 |
| $K_{p,max}$ | = | Limit of $K_p$ grid | 102 |
| $K_{p,start}$ | = | Starting point of power centroid line | 107 |
| $k_{p,start}$ | = | Starting index of power centroid line | 111 |
| $K_{p,stop}$ | = | Stopping point of power centroid line | 107 |
| $k_{p,stop}$ | = | Stopping index of power centroid line | 111 |
| $K_{p,1}$ | = | Limit of the $K_p$-$K_q$ region for calculation of $E_{KC}$ | 106 |
| $K_{p,2}$ | = | Limit of the $K_p$-$K_q$ region for calculation of $E_{KC}$ | 106 |
| $K_{p,3}$ | = | Limit of the $K_p$-$K_q$ region for calculation of $E_{KC}$ | 106 |
| $K_{p,4}$ | = | Limit of the $K_p$-$K_q$ region for calculation of $E_{KC}$ | 106 |
| $K_q$ | = | Component of $\mathbf{K}_\perp$ in p-q-z coordinate system | 34 |
| $k_q$ | = | Index of $K_q$ grid | 65 |
| $K_{q,L}$ | = | Power centroid line $K_q$ value | 111 |
| $k_{q,L}$ | = | Power centroid line $K_q$ index | 111 |
| $K_{q,max}$ | = | Limit of $K_q$ grid | 102 |
| $k_{q,max}$ | = | Maximum $K_q$ index | 111 |
| $K_{q,start}$ | = | Starting point of power centroid line | 107 |
| $K_{q,stop}$ | = | Stopping point of power centroid line | 107 |
| $K_{q,1}$ | = | Limit of the $K_p$-$K_q$ region for calculation of $E_{KC}$ | 106 |
| $K_{q,2}$ | = | Limit of the $K_p$-$K_q$ region for calculation of $E_{KC}$ | 106 |
| $K_{q,3}$ | = | Limit of the $K_p$-$K_q$ region for calculation of $E_{KC}$ | 106 |
| $K_{q,4}$ | = | Limit of the $K_p$-$K_q$ region for calculation of $E_{KC}$ | 106 |
| $K_r$ | = | Component of $\mathbf{K}$ in r-s-t coordinate system (see Fig. 2) | 19 |
| $K_s$ | = | Component of $\mathbf{K}$ in r-s-t coordinate system (see Fig. 2) | 19 |
| $k_s$ | = | Mean wave number $(k_1 + k_2)/2$ | 13 |
| $K_t$ | = | Component of $\mathbf{K}$ in r-s-t coordinate system (see Fig. 2) | 19 |
| $K_u$ | = | Component of $\mathbf{K}_\perp$ in u-v-z coordinate system | 16 |
| $K_v$ | = | Component of $\mathbf{K}_\perp$ in u-v-z coordinate system | 16 |
| $K_x$ | = | Component of $\mathbf{K}_\perp$ in x-y-z coordinate system | 24 |
| $k_x$ | = | Index of $K_x$ grid | 63 |
| $K_x'$ | = | Dummy $K_x$ variable | 63 |
| $K_{x,max}$ | = | Limit of $K_x$ grid | 70 |
| $K_{x,1}$ | = | Limit of the $K_x$-$K_y$ region for calculation of $E_{KC}$ | 105 |
| $k_{x,1}$ | = | Lower limit of $K_x$ grid index | 105 |
| $K_{x,2}$ | = | Limit of the $K_x$-$K_y$ region for calculation of $E_{KC}$ | 105 |
| $k_{x,2}$ | = | Upper limit of $K_x$ grid index | 105 |
| $K_y$ | = | Component of $\mathbf{K}_\perp$ in x-y-z coordinate system | 24 |
| $k_y$ | = | Index of $K_y$ grid | 63 |
| $K_y'$ | = | Dummy $K_y$ variable | 63 |

## LIST OF SYMBOLS (Continued)

| Symbol | | | Page |
|---|---|---|---|
| $K_{y,max}$ | = | Limit of $K_y$ grid | 70 |
| $K_{y,1}$ | = | Limit of the $K_x$-$K_y$ region for calculation of $E_{KC}$ | 106 |
| $k_{y,1}$ | = | Lower limit of $K_y$ grid index | 105 |
| $K_{y,2}$ | = | Limit of the $K_x$-$K_y$ region for calculation of $E_{KC}$ | 106 |
| $k_{y,2}$ | = | Upper limit of $K_y$ grid index | 105 |
| $\mathbf{K}_0$ | = | Antenna pointing direction | 38 |
| $K_{0u}$ | = | Component of $\mathbf{K}_0$ in u-v-z coordinate system | 45 |
| $K_{0v}$ | = | Component of $\mathbf{K}_0$ in u-v-z coordinate system | 45 |
| $K_{0x}$ | = | Component of $\mathbf{K}_0$ in x-y-z coordinate system | 48 |
| $K_{0y}$ | = | Component of $\mathbf{K}_0$ in x-y-z coordinate system | 48 |
| $k_1$ | = | Mean wave number for frequency $\omega_1$ | 7 |
| $k_2$ | = | Mean wave number for frequency $\omega_2$ | 7 |
| $\mathbf{K}_\perp$ | = | **K** vector for position vectors in plane normal to line-of-sight | 16 |
| L | = | Scattering layer thickness (see Fig. 1) | 3 |
| **L** | = | Electron density fluctuation scale size matrix | 89 |
| $\ell$ | = | Path length along propagation direction | 14 |
| $\ell_A$ | = | Decorrelation distance at antenna output | 94 |
| $\ell_{Ax}$ | = | X-direction decorrelation distance at antenna output | 51 |
| $\ell_{Ay}$ | = | Y-direction decorrelation distance at antenna output | 51 |
| $\ell_i$ | = | Electron density fluctuation inner scale size | 90 |
| $\ell_p$ | = | P-direction decorrelation distance | 34 |
| $\ell_q$ | = | Q-direction decorrelation distance | 34 |
| $L_r$ | = | Striation scale size in r direction orthogonal to **B** | 19 |
| $L_S$ | = | Scattering loss | 49 |
| $L_s$ | = | Striation scale size in s direction orthogonal to **B** | 19 |
| $L_t$ | = | Striation scale size in t direction parallel to **B** | 19 |
| $L_x$ | = | Striation scale size in the x-y-z coordinate system | 20 |
| $\ell_x$ | = | Channel x-direction decorrelation distance | 22 |
| $L_y$ | = | Striation scale size in the x-y-z coordinate system | 20 |
| $\ell_y$ | = | Channel y-direction decorrelation distance | 22 |
| $L_{yz}$ | = | Striation scale size in the x-y-z coordinate system | 20 |
| $L_z$ | = | Striation scale size in the x-y-z coordinate system | 20 |
| $L_\delta$ | = | Delta layer thickness | 14 |
| $L_0$ | = | Scale size of electron density fluctuations | 6 |
| $\ell_0$ | = | Minimum channel decorrelation distance | 22 |
| $\mathbf{L}_\perp$ | = | **L** matrix in plane normal to line-of-sight | 90 |
| $\mathbf{L}_\perp^{-1}$ | = | Inverse of the matrix $\mathbf{L}_\perp$ | 90 |
| ln (x) | = | Natural logarithm | 5 |

## LIST OF SYMBOLS (Continued)

| Symbol | | | Page |
|---|---|---|---|
| $M(\omega)$ | = | Spectrum of transmitted modulation | 75 |
| m | = | One-dimensional electron density fluctuation spectral index | 90 |
| max [x,y] | = | Maximum function (equal to the larger of x and y) | 71 |
| $m_D$ | = | Index of Doppler frequency grid | 63 |
| $m_D'$ | = | Dummy Doppler frequency index | 103 |
| min [x,y] | = | Minimum function (equal to the smaller of x and y) | 111 |
| $m_t(t)$ | = | Transmitted modulation | 36 |
| $m_x$ | = | X-direction Doppler shift index | 62 |
| $M_x(m_D)$ | = | Cumulative x-direction Doppler shift index | 103 |
| $m_y$ | = | Y-direction Doppler shift index | 62 |
| $M_y(m_D)$ | = | Cumulative y-direction Doppler shift index | 103 |
| n | = | Spectral index of electron density fluctuations | 89 |
| $n_e(\mathbf{r},t)$ | = | Free electron density | 5 |
| $\langle n_e \rangle$ | = | Mean free electron density | 5 |
| $N_D$ | = | Number of Doppler frequency grid cells | 63 |
| $N_{D,min}$ | = | Minimum required number of Doppler frequency grid cells | 73 |
| $N_F$ | = | Number of frequency samples | 76 |
| $N_T$ | = | Total electron content (TEC) | 37 |
| $N_t$ | = | Number of time samples | 67 |
| $n_t$ | = | Index of time grid | 67 |
| $N_x$ | = | Number of $K_x$ grid cells | 63 |
| $N_y$ | = | Number of $K_y$ grid cells | 63 |
| $N_\tau$ | = | Number of delay samples | 67 |
| $N_0$ | = | Number of samples per decorrelation time | 69 |
| P | = | Antenna pointing effect term in filtered frequency selective bandwidth | 50 |
| $P_A$ | = | Mean power in the GPSD at the output of an antenna | 49 |
| $P_j$ | = | Mean power in the $j^{th}$ delay grid cell | 74 |
| $P_{GK}$ | = | Total power in angular grid | 94 |
| $P_{G\tau}$ | = | Total power in the delay grid | 74 |
| $P_x$ | = | $K_{0x}$ coefficient in antenna pointing effect term | 50 |
| $P_y$ | = | $K_{0y}$ coefficient in antenna pointing effect term | 50 |
| $P_{xy}$ | = | $K_{0x}K_{0y}$ coefficient in antenna pointing effect term | 50 |
| $P_0$ | = | Mean power in the GPSD | 27 |
| Q | = | Isotropic scattering and antenna filtering effect factor | 52 |
| q | = | Axial ratio of striations | 20 |
| $Q_x$ | = | Antenna filtering effect factor | 48 |
| $Q_y$ | = | Antenna filtering effect factor | 48 |
| $Q_{xy}$ | = | Antenna filtering effect factor | 48 |

## LIST OF SYMBOLS (Continued)

| Symbol | | | Page |
|---|---|---|---|
| $Q_0$ | = | Antenna filtering effect factor | 48 |
| R | = | Free space propagation distance from transmitter to receiver | 37 |
| $\mathbf{R}$ | = | General n-dimensional vector | 8 |
| $\mathbf{r}$ | = | Position vector | 3 |
| r | = | Magnitude of the vector $\rho$ | 46 |
| $\hat{r}$ | = | Unit vector in propagation coordinate system (see Fig. 2) | 19 |
| $R_c$ | = | Chip rate | 76 |
| $r_e$ | = | Classical radius of the electron ($2.8179\times10^{-15}$ m) | 5 |
| S | = | Transport equation source term | 12 |
| $S(\mathbf{K}_\perp,\tau,\omega_D)$ | = | Generalized power spectral density (GPSD) | 24 |
| $\hat{s}$ | = | Unit vector in propagation coordinate system (see Fig. 2) | 19 |
| $S_A(\mathbf{K}_\perp,\tau,\omega_D)$ | = | GPSD of signal at output of an antenna | 40 |
| $S_A(K_x)$ | = | Angular spectrum at antenna output | 70 |
| $S_A(\tau)$ | = | Delay spectrum at antenna output | 74 |
| $S_A(\omega_D)$ | = | Doppler frequency spectrum at antenna output | 72 |
| $S_D(\omega_D)$ | = | Doppler frequency spectrum of the GPSD | 24 |
| $S_K(\mathbf{K}_\perp)$ | = | Angular spectrum of the GPSD | 93 |
| $S_{KC}(\mathbf{K}_\perp)$ | = | Angular spectrum of the GPSD used in channel modelling | 62 |
| $S_{KC}(K_p)$ | = | One-dimensional angular spectrum of the GPSD used in channel modelling | 102 |
| $S_{KD}(\mathbf{K}_\perp,\omega_D)$ | = | Angular-Doppler spectrum of the GPSD | 34 |
| $S_{KS}(\mathbf{K}_\perp)$ | = | Doppler shifted version of $S_{KC}(\mathbf{K}_\perp)$ | 63 |
| $S_{K\tau}(\mathbf{K}_\perp,\tau)$ | = | Angular-delay spectrum of the GPSD | 24 |
| $S_L$ | = | Slope of power centroid line | 110 |
| $S_\xi(\mathbf{K})$ | = | PSD of electron density fluctuations | 19 |
| $S_\tau(\tau)$ | = | Delay distribution for fixed angle-of-arrival | 26 |
| $S_{\tau D}(\tau,\omega_D)$ | = | Delay-Doppler scattering function | 30 |
| $S_1$ | = | Transport equation source term 1 | 9 |
| $S_2$ | = | Transport equation source term 2 | 11 |
| sign (x) | = | Sign function (equal to the sign of argument) | 111 |
| t | = | Time | 3 |
| t' | = | Dummy time variable | 9 |
| $\hat{t}$ | = | Unit vector in propagation coordinate system (see Fig. 2) | 19 |
| $T_c$ | = | Chip duration | 75 |
| $t_p$ | = | Propagation time | 26 |
| $T_0$ | = | Decorrelation time of striations | 21 |
| $t_1$ | = | Time 1 | 7 |
| $t_2$ | = | Time 2 | 7 |

## LIST OF SYMBOLS (Continued)

| Symbol | | | Page |
|---|---|---|---|
| $U(\mathbf{r},\omega,t)$ | = | Scalar envelope of electric field | 6 |
| $u$ | = | Spatial coordinate in plane normal to line-of-sight | 16 |
| $\hat{u}$ | = | Unit vector in antenna coordinate system (see Fig. 8) | 43 |
| $u(\rho,t)$ | = | Received signal at position $\rho$ and time t | 36 |
| $u(\tau,t)$ | = | Received signal at delay $\tau$ and time t | 75 |
| $U_A(\rho_0,\omega,t)$ | = | Scalar envelope of electric field out of an antenna at $\rho_0$ | 38 |
| $U_0(\rho,t)$ | = | Transmitted signal | 10 |
| $v$ | = | Spatial coordinate in plane normal to line-of-sight | 16 |
| $\hat{v}$ | = | Unit vector in antenna coordinate system normal to $\hat{u}$ and $\hat{z}$ (see Fig. 8) | 43 |
| $\mathbf{v}$ | = | Velocity of scattering layer for frozen-in model | 18 |
| $X$ | = | Mean x-position in plane normal to line-of-sight | 12 |
| $x$ | = | X-coordinate in plane normal to line-of-sight | 6 |
| $x'$ | = | Dummy x variable | 10 |
| $\hat{x}$ | = | Unit vector in propagation coordinate system (see Fig. 2) | 19 |
| $x_0$ | = | X-component of vector $\rho_0$ | 62 |
| $x_1$ | = | X-coordinate of position 1 in plane normal to line-of-sight | 12 |
| $x_2$ | = | X-coordinate of position 2 in plane normal to line-of-sight | 12 |
| $Y$ | = | Mean y-position in plane normal to line-of-sight | 12 |
| $y$ | = | Y-coordinate in plane normal to line-of-sight | 6 |
| $\hat{y}$ | = | Unit vector in propagation coordinate system (see Fig. 2) | 19 |
| $y_0$ | = | Y-component of vector $\rho_0$ | 62 |
| $y_1$ | = | Y-coordinate of position 1 in plane normal to line-of-sight | 12 |
| $y_2$ | = | Y-coordinate of position 2 in plane normal to line-of-sight | 12 |
| $z$ | = | Distance along the line-of-sight | 3 |
| $z'$ | = | Dummy z-distance variable | 6 |
| $z''$ | = | Dummy z-distance variable | 10 |
| $\hat{z}$ | = | Unit vector in propagation coordinate system (see Fig. 2) | 19 |
| $z_r$ | = | Line-of-sight distance from scattering layer to receiver (see Fig. 1) | 3 |
| $z_t$ | = | Line-of-sight distance form transmitter to scattering layer (see Fig. 1) | 3 |
| $\alpha$ | = | Delay parameter in the GPSD | 24 |
| $\alpha_u$ | = | U-direction antenna beam pattern parameter | 45 |
| $\alpha_v$ | = | V-direction antenna beam pattern parameter | 45 |

## LIST OF SYMBOLS (Continued)

| Symbol | | | Page |
|---|---|---|---|
| $\beta(\omega)$ | = | Frequency dependence of index of refraction | 8 |
| $\beta_1$ | = | $\beta(\omega_1)$ | 9 |
| $\beta_2$ | = | $\beta(\omega_2)$ | 9 |
| $\Gamma(n)$ | = | Gamma function | 89 |
| $\Gamma(\delta\mathbf{r},\delta\omega,\delta t)$ | = | Two-position, two-frequency, two-time Mutual Coherence Function | 2 |
| $\Gamma(\rho)$ | = | Two-position mutual coherence function | 17 |
| $\Gamma(\omega)$ | = | Two-frequency mutual coherence function | 17 |
| $\Gamma(t)$ | = | Two-time mutual coherence function | 17 |
| $\hat{\Gamma}(\mathbf{K}_\perp)$ | = | Fourier transform of $\Gamma(\rho)$ | 17 |
| $\hat{\Gamma}(\tau)$ | = | Fourier transform of $\Gamma(\omega)$ | 17 |
| $\hat{\Gamma}(\omega_D)$ | = | Fourier transform of $\Gamma(t)$ | 17 |
| $\hat{\Gamma}(\mathbf{r},\tau,\omega_D)$ | = | Fourier transform of $\Gamma(\mathbf{r},\omega,t)$ | 40 |
| $\gamma$ | = | Distance parameter in solution for $\hat{\Gamma}_1$ | 17 |
| $\Gamma_A(\rho,\omega,t)$ | = | Mutual coherence function at antenna output | 38 |
| $\Gamma_A(t)$ | = | Temporal coherence function at antenna output | 50 |
| $\Gamma_A(x)$ | = | Spatial coherence function at antenna output | 51 |
| $\Gamma_0$ | = | Free space mutual coherence function | 11 |
| $\Gamma_1$ | = | Mutual coherence function without free space contribution | 11 |
| $\hat{\Gamma}_1$ | = | Fourier transform of $\Gamma_1$ | 17 |
| $\Gamma_2$ | = | Mutual coherence function factor, $\Gamma_1 = \Gamma_2\Gamma_3$ | 15 |
| $\Gamma_3$ | = | Mutual coherence function factor, $\Gamma_1 = \Gamma_2\Gamma_3$ | 15 |
| $\delta(x)$ | = | Dirac delta-function | 9 |
| $\delta_{m,n}$ | = | Kronecker delta symbol | 68 |
| $\Delta K_p$ | = | Angular grid $K_p$ cell size | 65 |
| $\Delta K_q$ | = | Angular grid $K_q$ cell size | 65 |
| $\Delta K_x$ | = | Angular grid $K_x$ cell size | 62 |
| $\Delta K_y$ | = | Angular grid $K_y$ cell size | 62 |
| $\Delta n_e(\mathbf{r},t)$ | = | Free electron density fluctuation | 5 |
| $\delta\mathbf{r}$ | = | Relative position | 2 |
| $\Delta t$ | = | Time sample size | 67 |
| $\delta t$ | = | Relative time | 2 |
| $\delta z$ | = | Relative distance along line-of-sight | 87 |
| $\delta\rho$ | = | Relative position vector in plane normal to line-of-sight | 87 |
| $\Delta\tau$ | = | Delay sample size | 66 |
| $\Delta\omega$ | = | Frequency grid sample size | 76 |
| $\delta\omega$ | = | Relative radian frequency | 2 |
| $\Delta\omega_D$ | = | Doppler frequency grid cell size | 63 |
| $\delta/\delta f$ | = | Functional derivative (differential with respect to function f) | 8 |

## LIST OF SYMBOLS (Continued)

| Symbol | | | Page |
|---|---|---|---|
| $\varepsilon$ | = | Dielectric constant | 4 |
| $\varepsilon_x$ | = | $K_x$ grid shift residual | 62 |
| $\varepsilon_y$ | = | $K_y$ grid shift residual | 62 |
| $\varepsilon_1$ | = | Dielectric constant fluctuation | 5 |
| $\zeta$ | = | Relative x-position in plane normal to line-of-sight | 12 |
| $\zeta_\omega$ | = | Fraction of signal power in a grid | 69 |
| $\eta$ | = | Relative y-position in plane normal to line-of-sight | 12 |
| $\theta$ | = | Elevation angle measured from line-of-sight | 45 |
| $\vartheta$ | = | Rotation angle between x-y-z and p-q-z coordinate systems | 34 |
| $\langle\theta_T(\omega)\rangle$ | = | Dispersive phase shift due to mean ionization | 35 |
| $\langle\theta'_T(\omega)\rangle$ | = | First derivative of phase shift due to mean ionization | 36 |
| $\langle\theta''_T(\omega)\rangle$ | = | Second derivative of phase shift due to mean ionization | 36 |
| $\theta_r$ | = | Scattering angle at the receiver | 26 |
| $\theta_t$ | = | Scattering angle at the transmitter | 26 |
| $\theta_u$ | = | Scattering angle about the antenna u-axis | 44 |
| $\theta_v$ | = | Scattering angle about the antenna v-axis | 44 |
| $\theta_x$ | = | Scattering angle about the propagation x-axis | 25 |
| $\theta_y$ | = | Scattering angle about the propagation y-axis | 25 |
| $\Theta_0$ | = | Pointing direction elevation angle (see Fig. 8) | 43 |
| $\theta_0$ | = | Antenna 3-dB beamwidth | 45 |
| $\theta_{0u}$ | = | Antenna 3-dB beamwidth about u-direction | 45 |
| $\theta_{0v}$ | = | Antenna 3-dB beamwidth about v-direction | 45 |
| $\kappa$ | = | Normalized grid variable $K_x \ell_x$, $K_y \ell_y$, or $\tau_0\omega_D$ | 69 |
| $\kappa_{max}$ | = | Maximum value of grid variable | 69 |
| $\kappa_{D,max}$ | = | Maximum value of $\kappa$ for Doppler frequency grid | 69 |
| $\kappa_{K,max}$ | = | Maximum value of $\kappa$ for angular grids | 69 |
| $\lambda$ | = | Wavelength of RF wave | 6 |
| $\Lambda_x$ | = | Asymmetry factor | 22 |
| $\Lambda_y$ | = | Asymmetry factor | 22 |
| $\xi(\rho,z,t)$ | = | Normalized electron density fluctuation | 8 |
| $\xi_N(\mathbf{K}_\perp,\omega_D)$ | = | Complex, normally-distributed, zero-mean, unity-power random number | 61 |
| $\xi_{U,x}$ | = | Uniformly distributed random number on the interval [0,1) | 67 |
| $\xi_{U,y}$ | = | Uniformly distributed random number on the interval [0,1) | 67 |
| $\xi_{U,1}$ | = | Uniformly distributed random number on the interval [0,1) | 68 |
| $\xi_{U,2}$ | = | Uniformly distributed random number on the interval [0,1) | 68 |

## LIST OF SYMBOLS (Continued)

| Symbol | | | Page |
|---|---|---|---|
| $\pi$ | = | Pi (3.141592654···) | 5 |
| $\rho$ | = | Two-dimensional position vector in the plane normal to line-of-sight | 7 |
| $\rho'$ | = | Dummy $\rho$ vector | 9 |
| $\rho''$ | = | Dummy $\rho$ vector | 38 |
| $\rho_0$ | = | Antenna position in plane normal to line-of-sight | 38 |
| $\rho_1$ | = | Position 1 in plane normal to line-of-sight | 7 |
| $\rho_2$ | = | Position 2 in plane normal to line-of-sight | 7 |
| $\sigma_\theta$ | = | Angle-of-arrival standard deviation | 48 |
| $\sigma^2_{\theta x}$ | = | Angle-of-arrival variance about the x-axis | 28 |
| $\sigma^2_{\theta y}$ | = | Angle-of-arrival variance about the y-axis | 28 |
| $\sigma^2_\tau$ | = | Time-of-arrival variance | 27 |
| $\sigma^2_\Phi$ | = | Phase variance imparted on RF wave | 13 |
| $\tau$ | = | Delay (relative time-of-arrival) | 16 |
| $\tau'$ | = | Dummy delay | 60 |
| $\langle\tau\rangle$ | = | Mean time-of-arrival | 27 |
| $\langle\tau^2\rangle$ | = | Mean squared time-of-arrival | 27 |
| $\tau_A$ | = | Antenna output decorrelation time | 50 |
| $\tau_{A,max}$ | = | Maximum $\tau_A$ for all antennas | 73 |
| $\tau_{A,min}$ | = | Minimum $\tau_A$ for all antennas | 73 |
| $\tau_0$ | = | Channel decorrelation time | 22 |
| $\Phi$ | = | Penetration angle (see Fig. 2) | 19 |
| $\phi$ | = | Phase of propagating wave | 14 |
| $\varphi$ | = | Azimuth angle | 46 |
| $\Phi_0$ | = | Azimuth angle of antenna pointing direction (see Fig. 8) | 43 |
| $\Psi$ | = | Rotation angle (see Fig. 8) | 43 |
| $\omega$ | = | Radian radio frequency | 3 |
| $\omega_A$ | = | Mean Doppler shift at antenna output | 51 |
| $\omega_{coh}$ | = | Coherence bandwidth | 22 |
| $\omega_D$ | = | Doppler radian frequency | 16 |
| $\omega'_D$ | = | Dummy Doppler radian frequency | 60 |
| $\omega_{D,max}$ | = | Limit of $\omega_D$ grid | 72 |
| $\omega_p$ | = | Radian plasma frequency | 5 |
| $\langle\omega^2_p\rangle$ | = | Square of radian plasma frequency evaluated at mean free electron density | 6 |

## LIST OF SYMBOLS (Continued)

| Symbol | | | Page |
|---|---|---|---|
| $\omega_0$ | = | Carrier radian frequency | 21 |
| $\omega_1$ | = | Radian radio frequency 1 | 7 |
| $\omega_2$ | = | Radian radio frequency 2 | 7 |
| $\partial/\partial x$ | = | Partial derivative | 6 |
| $\nabla$ | = | Gradient operator | 4 |
| $\nabla_d$ | = | Gradient operator for relative position coordinates | 13 |
| $\nabla_s$ | = | Gradient operator for mean position coordinates | 13 |
| $\nabla\times$ | = | Curl operator | 4 |
| $\nabla^2$ | = | Laplacian operator | 5 |
| $\nabla_s^2$ | = | Laplacian operator for mean position coordinates | 12 |
| $\nabla_d^2$ | = | Laplacian operator for relative position coordinates | 12 |
| $\nabla_\perp^2$ | = | Laplacian operator in plane normal to line-of-sight | 6 |
| $\nabla_{\perp 1}^2$ | = | Laplacian operator at position $\rho_1$ | 7 |
| $\nabla_{\perp 2}^2$ | = | Laplacian operator at position $\rho_2$ | 7 |

# DISTRIBUTION LIST

**DNA-TR-90-9**

**DEPARTMENT OF DEFENSE**

ASSISTANT TO THE SECRETARY OF DEFENSE
ATTN: EXECUTIVE ASSISTANT

DEFENSE ADVANCED RSCH PROJ AGENCY
ATTN: CHIEF SCIENTIST
ATTN: GSD R ALEWINE

DEFENSE COMMUNICATIONS AGENCY
ATTN: C4S/SSM, DR P CROWLEY
ATTN: SSS

DEFENSE COMMUNICATIONS ENGINEER CENTER
ATTN: CODE R410

DEFENSE INTELLIGENCE AGENCY
ATTN: DB-TPO
ATTN: DC-6
ATTN: DIR
ATTN: DT-1B
ATTN: RTS-2B

DEFENSE NUCLEAR AGENCY
ATTN: DFSP
ATTN: NANF
ATTN: NASF
ATTN: OPNA
ATTN: PRPD R YOHO
3 CYS ATTN: RAAE
ATTN: RAAE A CHESLEY
ATTN: RAAE G ULLRICH
ATTN: RAAE K SCHWARTZ
ATTN: RAAE M CRAWFORD
ATTN: RAAE S BERGGREN
ATTN: RAEE
2 CYS ATTN: TITL

DEFENSE NUCLEAR AGENCY
ATTN: FCPRA LC R HEDTKE
ATTN: TDNM
2 CYS ATTN: TDTT W SUMMA

DEFENSE TECHNICAL INFORMATION CENTER
2 CYS ATTN: DTIC/FDAB

JOINT DATA SYSTEM SUPPORT CTR
ATTN: JNSV

NATIONAL SECURITY AGENCY
ATTN: Q12 L PLUSWICK

STRATEGIC AND THEATER NUCLEAR FORCES
ATTN: DR E SEVIN
ATTN: DR SCHNEITER
ATTN: LC R DAWSON

STRATEGIC DEFENSE INITIATIVE ORGANIZATION
ATTN: EN
ATTN: EN LTC C JOHNSON
ATTN: PTP/L STOESSELL
ATTN: TN/DR M GRIFFIN

THE JOINT STAFF
ATTN: JKA
ATTN: JKC (ATTN: DNA REP)
ATTN: JKCS
ATTN: JLWT (THREAT ANALYSIS)
ATTN: JPEM

THE JOINT STAFF
ATTN: J6

U S NUCLEAR CMD & CENTRAL SYS SUPPORT STAFF
ATTN: SAB H SEQUINE

**DEPARTMENT OF THE ARMY**

ARMY LOGISTICS MANAGEMENT CTR
ATTN: DLSIE

HARRY DIAMOND LABORATORIES
ATTN: SLCIS-IM-TL (TECH LIB)

U S ARMY ATMOSPHERIC SCIENCES LAB
ATTN: SLCAS-AE (DR NILES)
ATTN: SLCAS-AR DR H HOLT

U S ARMY COMMUNICATIONS R&D COMMAND
ATTN: AMSEL-RD-ESA

U S ARMY ENGINEER DIV HUNTSVILLE
ATTN: PRESTON J KISS

U S ARMY FOREIGN SCIENCE & TECH CTR
ATTN: AIFRTA

U S ARMY MISSILE COMMAND
ATTN: AIAMS-S/B J GAMBLE

U S ARMY MISSILE COMMAND/AMSMI-RD-CS-R
ATTN: AMSMI-RD-CS-R (DOCS)

U S ARMY NUCLEAR & CHEMICAL AGENCY
ATTN: MONA-NU (D BASH)

U S ARMY NUCLEAR EFFECTS LABORATORY
ATTN: ATAA-PL
ATTN: ATAA-TDC
ATTN: ATRC-WCC (LUIS DOMINGUEZ)

U S ARMY STRATEGIC DEFENSE CMD
ATTN: CSSD-H-LS B CARRUTH
ATTN: CSSD-H-SA
ATTN: CSSD-H-SAV
ATTN: CSSD-IN-T M POPE
ATTN: CSSD-SA-EV (RON SMITH)

U S ARMY STRATEGIC DEFENSE COMMAND
ATTN: CSSD-GR-S W DICKINSON

USA SURVIVABILITY MANAGMENT OFFICE
ATTN: SLCSM-SE J BRAND

**DEPARTMENT OF THE NAVY**

COMMAND & CONTROL PROGRAMS
ATTN: OP 941

DEPARTMENT OF THE NAVY
ATTN: JCMG-707

NAVAL AIR SYSTEMS COMMAND
ATTN: PMA 271

NAVAL ELECTRONICS ENGRG ACTVY, PACIFIC
ATTN: CODE 250

NAVAL RESEARCH LABORATORY
ATTN: CODE 2000 J BROWN
ATTN: CODE 2627 (TECH LIB)
ATTN: CODE 4121.8 H HECKATHORN
ATTN: CODE 4183
ATTN: CODE 4701
ATTN: CODE 4720 J DAVIS
ATTN: CODE 4780 B RIPIN
ATTN: CODE 4780 DR P BERNHARDT
ATTN: CODE 4780 J HUBA
ATTN: CODE 4785 P RODRIGUEZ
ATTN: CODE 5300
ATTN: CODE 5326 G A ANDREWS
ATTN: CODE 5340 E MOKOLE
ATTN: CODE 8344 M KAPLAN

NAVAL SURFACE WARFARE CENTER
ATTN: CODE H-21

NAVAL TECHNICAL INTELLIGENCE CTR
ATTN: DA44

NAVAL UNDERWATER SYSTEMS CENTER
ATTN: CODE 3411, J KATAN

OFFICE OF CHIEF OF NAVAL OPERATIONS
ATTN: OP 654
ATTN: OP 941D

SPACE & NAVAL WARFARE SYSTEMS CMD
ATTN: CODE 3101 T HUGHES
ATTN: PD 50TD
ATTN: PD50TD1 G BRUNHART
ATTN: PME 106-4 S KEARNEY
ATTN: PME-106 F W DIEDERICH

THEATER NUCLEAR WARFARE PROGRAM OFC
ATTN: PMS-42331F (D SMITH)

**DEPARTMENT OF THE AIR FORCE**

AFIA/INIS
ATTN: AFIA/INKS MAJ SCHROCK

AIR FORCE CTR FOR STUDIES & ANALYSIS
ATTN: AFCSA/SASC LT RITTER

AIR FORCE ELECTRONIC WARFARE CENTER
ATTN: CPT J BREWER (SAZ)
ATTN: LT M MCNEELY

AIR FORCE GEOPHYSICS LABORATORY
ATTN: J KLOUBACHAR
ATTN: OP/W BLUMBERG
ATTN: SANTI BASU

AIR FORCE OFFICE OF SCIENTIFIC RSCH
ATTN: AFOSR/NP

AIR FORCE SYSTEMS COMMAND
ATTN: XTTW

AIR UNIVERSITY LIBRARY
ATTN: AUL-LSE

HQ AWS, DET 3 (CSTC/WE)
ATTN: WE

NATIONAL TEST FACILITY
ATTN: NTB/JPO DR C GIESE

STRATEGIC AIR COMMAND/XRFS
ATTN: XRFS

WEAPONS LABORATORY
ATTN: NTCA
ATTN: NTCTS LTC C ROYER
ATTN: NTN
ATTN: WL/SUL

**DEPARTMENT OF ENERGY**

EG&G, INC
*ATTN: D WRIGHT*

LAWRENCE LIVERMORE NATIONAL LAB
ATTN: L-97 T DONICH

SANDIA NATIONAL LABORATORIES
ATTN: P L MATTERN, 8300

SANDIA NATIONAL LABORATORIES
ATTN: A D THORNBROUGH
ATTN: CODE 9014 R BACKSTROM
ATTN: D DAHLGREN
ATTN: DIV 2344, ROBERT M AXLINE
ATTN: ORG 9110 G CABLE
ATTN: ORG 9110 W D BROWN
ATTN: TECH LIB 3141

**OTHER GOVERNMENT**

CENTRAL INTELLIGENCE AGENCY
ATTN: OSWR/NED
ATTN: OSWR/SSD FOR L BERG

DEPARTMENT OF COMMERCE
ATTN: G REEVE
ATTN: J HOFFMEYER
ATTN: W UTLAUT

U S DEPARTMENT OF STATE
ATTN: PM/TMP

**DEPARTMENT OF DEFENSE CONTRACTORS**

AEROJET ELECTRO-SYSTEMS
ATTN: A FYMAT

AEROSPACE CORP
ATTN: A MORSE
ATTN: BRIAN PURCELL
ATTN: C CREWS
ATTN: C RICE
ATTN: D RUDOLPH
ATTN: DR J M STRAUS
ATTN: G LIGHT
ATTN: I GARFUNKEL
ATTN: J KLUCK
ATTN: M ROLENZ

AT&T BELL LABORATORIES
ATTN: DENIS S LONGO
ATTN: JOSEPH A SCHOLL
ATTN: N BEAUCHAMP

ATLANTIC RESEARCH SERVICES CORP
ATTN: R MCMILLAN

ATMOSPHERIC AND ENVIRONMENTAL RESEARCH INC
ATTN: M KO

AUSTIN RESEARCH ASSOCIATES
ATTN: J THOMPSON

AUTOMETRIC, INC
ATTN: C LUCAS

BDM INTERNATIONAL INC
ATTN: W LARRY JOHNSON

BDM INTERNATIONAL INC
ATTN: L JACOBS

BERKELEY RSCH ASSOCIATES, INC
ATTN: J WORKMAN
ATTN: N T GLADD
ATTN: S BRECHT

BOEING CO
ATTN: G HALL

CALIFORNIA RESEARCH & TECHNOLOGY, INC
ATTN: M ROSENBLATT

CHARLES STARK DRAPER LAB, INC
ATTN: A TETEWSKI

COMMUNICATIONS SATELLITE CORP
ATTN: RICHARD A ARNDT

CONTEL FEDERAL SYSTEMS INC
ATTN: CHARLES BENNINGTON

CORNELL UNIVERSITY
ATTN: D FARLEY JR
ATTN: M KELLY

DYNETICS, INC
ATTN: WILLIAM D TEPPER

ELECTROSPACE SYSTEMS, INC
ATTN: LINDA CALDWELL/LIBRARIAN
ATTN: P PHILLIPS

EOS TECHNOLOGIES, INC
ATTN: B GABBARD
ATTN: R LELEVIER

FORD AEROSPACE CORPORATION
ATTN: PATRICIA BIRDWELL

GENERAL ELECTRIC COMPANY
ATTN: JOSEPH E STROSSER

GENERAL RESEARCH CORP INC
ATTN: J EOLL

GRUMMAN AEROSPACE CORP
ATTN: J DIGLIO

HARRIS CORPORATION
ATTN: LYMUEL MCRAE

HSS, INC
ATTN: D HANSEN

INFORMATION SCIENCE, INC
ATTN: W DUDZIAK

INSTITUTE FOR DEFENSE ANALYSES
ATTN: E BAUER
ATTN: H WOLFHARD

JAYCOR
ATTN: A GLASSMAN
ATTN: J SPERLING

JOHNS HOPKINS UNIVERSITY
ATTN: C MENG
ATTN: H G TORNATORE
ATTN: J D PHILLIPS
ATTN: R STOKES

KAMAN SCIENCES CORP
ATTN: DASIAC
ATTN: E CONRAD
ATTN: G DITTBERNER

KAMAN SCIENCES CORPORATION
ATTN: B GAMBILL
ATTN: DASIAC
ATTN: R RUTHERFORD

LOCKHEED MISSILES & SPACE CO, INC
ATTN: J HENLEY
ATTN: J KUMER
ATTN: R SEARS

LOCKHEED MISSILES & SPACE CO, INC
ATTN: CARL CRABILL
ATTN: D KREJCI

ATTN: D T RAMPTON
ATTN: E M DIMZCELI

LTV AEROSPACE & DEFENSE COMPANY
2 CYS ATTN: LIBRARY EM-08

M I T LINCOLN LAB
ATTN: D TOWLE L-230
ATTN: I KUPIEC L-100

MARTIN MARIETTA DENVER AEROSPACE
ATTN: J BENNETT
ATTN: H VON STRUVE III

MAXIM TECHNOLOGIES, INC
ATTN: B RIDGEWAY
ATTN: C HUA
ATTN: J SCHLOBOHM

MCDONNELL DOUGLAS CORPORATION
ATTN: J GROSSMAN
ATTN: R HALPRIN

METATECH CORPORATION
ATTN: W RADASKY

METEOR COMMUNICATIONS CORP
ATTN: R LEADER

MISSION RESEARCH CORP
ATTN: R ARMSTRONG
ATTN: W WHITE

MISSION RESEARCH CORP
ATTN: R L BOGUSCH

MISSION RESEARCH CORP
ATTN: DAVE GUICE

MISSION RESEARCH CORP
ATTN: B R MILNER
ATTN: C LONGMIRE
ATTN: D KNEPP
ATTN: D LANDMAN
ATTN: F FAJEN
ATTN: F GUIGLIANO
ATTN: G MCCARTOR
ATTN: K COSNER
ATTN: M FIRESTONE
ATTN: R BIGONI
2 CYS ATTN: R DANA
ATTN: R HENDRICK
ATTN: R KILB
ATTN: S GUTSCHE
ATTN: TECH LIBRARY

MITRE CORPORATION
ATTN: M HORROCKS
ATTN: R C PESCI
ATTN: W FOSTER

MITRE CORPORATION
ATTN: G CAMPARETTO

NORTHWEST RESEARCH ASSOC, INC
ATTN: E FREMOUW

PACIFIC-SIERRA RESEARCH CORP
ATTN: E FIELD JR
ATTN: F THOMAS
ATTN: H BRODE

PHOTOMETRICS, INC
ATTN: I L KOFSKY

PHOTON RESEARCH ASSOCIATES
ATTN: D BURWELL

PHYSICAL RESEARCH INC
ATTN: W SHIH

PHYSICAL RESEARCH INC
ATTN: A CECERE

PHYSICAL RESEARCH INC
ATTN: H FITZ

PHYSICAL RESEARCH, INC
ATTN: R DELIBERIS
ATTN: T STEPHENS

PHYSICAL RESEARCH, INC
ATTN: J DEVORE
ATTN: J THOMPSON
ATTN: R STOECKLEY
ATTN: W SCHLUETER

PHYSICS INTERNATIONAL CO
ATTN: C GILMAN

R & D ASSOCIATES
ATTN: G HOYT
ATTN: L DERAAB

R & D ASSOCIATES
ATTN: D CARLSON
ATTN: J THOMPSON

RAND CORP
ATTN: C CRAIN
ATTN: E BEDROSIAN

RAND CORP
ATTN: B BENNETT

RJO ENTERPRISES/POET FAC
ATTN: STEVEN KRAMER
ATTN: W BURNS

ROCKWELL INTERNATIONAL CORP
ATTN: R POTTER

SCIENCE APPLICATIONS INTL CORP
ATTN: C SMITH
ATTN: D HAMLIN
ATTN: D SACHS
ATTN: L LINSON

SCIENCE APPLICATIONS INTL CORP
ATTN: H SUNKENBERG
ATTN: LIBRARY

SCIENCE APPLICATIONS INTL CORP
ATTN: S ROSENCWEIG

SPARTA INC
ATTN: D DEAN

SRI INTERNATIONAL
ATTN: R LIVINGSTON
ATTN: R T TSUNODA
ATTN: W CHESNUT
ATTN: W JAYE

STEWART RADIANCE LABORATORY
ATTN: R HUPPI

TELECOMMUNICATION SCIENCE ASSOCIATES
ATTN: R BUCKNER

TELEDYNE BROWN ENGINEERING
ATTN: J FORD
ATTN: J WOLFSBERGER, JR
ATTN: N PASSINO

TOYON RESEARCH CORP
ATTN: J ISE

TRW INC
ATTN: ED SIMMONS

TRW SPACE & DEFENSE SECTOR SPACE
ATTN: D M LAYTON

USER SYSTEMS, INC
ATTN: S W MCCANDLESS, JR

UTAH STATE UNIVERSITY
ATTN: K BAKER, DIR ATMOS & SPACE SCI
ATTN: L JENSEN, ELEC ENG DEPT

VISIDYNE, INC
ATTN: J CARPENTER

**FOREIGN**

FOA 2
ATTN: B SJOHOLM

FOA 3
ATTN: T KARLSSON

**DIRECTORY OF OTHER**

BOSTON UNIVERSITY
ATTN: MICHAEL MENDILLO